Structural and Activity Relationship of Thienopyrimidines Analogs as Inhibitors of the Human Farnesyl Pyrophosphate Synthase

Chun Yuen (Carlos) Leung

A thesis submitted to McGill University in partial fulfillment of the requirement of the degree of

Master of Science

Department of Chemistry

McGill University, Montreal

January, 2016

TABLE OF CONTENTS

ABSTRACT

Human farnesyl pyrophosphate synthase (hFPPS) occupies the first branching point of the mevalonate pathway and plays an essential role in cell signalling, cell proliferation, and cell survival. It is responsible for the sequential condensation of dimethylallyl pyrophosphate (DMAPP) with two unit of isopentenyl pyrophosphate (IPP) to produce farnesyl pyrophosphate (FPP). Nitrogen containing bisphosphonates (*N*-BPs) are currently marketed as hFPPS inhibitors and used to treat osteoporosis and bone related cancers. The *N*-BPs have also been shown to improve survival of multiple myeloma patients and significantly reduces the disease progression of breast cancer in premenopausal women. However due to the highly charged nature of the bisphosphonate moiety and its high affinity for bone mineral, *N*-BPs have very poor biopharmaceutical properties. A new series of bisphosphonate inhibitors with increased overall lipophilicity containing the thienopyrimidine core have been designed and synthesized. Using differential scan fluorimetry (DSF), the thienopyrimidine bisphosphonates (ThPBPs) were also found to thermally stabilize hFPPS in the absence of magnesium, suggesting that the ThPBPs can bind to hFPPS away from the DMAPP/geranyl pyrophosphate (GPP) binding site. Further biophysical studies including ITC and X-ray crystallography confirmed that the ThPBPs can bind in an allosteric pocket of hFPPS in the absence of magnesium. A new series of non-bisphosphonate thienopyrimidine analogs was subsequently designed and synthesized to bind in the allosteric pocket with low micromolar potency.

RÉSUMÉ

La farnésyle pyrophosphate synthase humaine (FPPSh) occupe le premier point de dérivation de la voie du mévalonate et est essentiel pour la signalisation, la prolifération, et la survie cellulaire. Elle est responsable pour la condensation séquentielle du diméthylallyl-pyrophosphate (DMAPP) avec deux unité d'isopentényl-pyrophosphate (IPP) afin de produire le farnésyl-pyrophosphate (FPP). Les bisphosphonates contenants un atome d'azote (*N*-BPs) sont actuellement commercialisés come inhibiteur de FPPSh et utilisés pour traiter l'ostéoporose et les cancer liés aux os. Les *N*-BPs ont également été démontrés d'augmenter la survie des patients atteints de myélome multiple et réduit de manière significative la progression du cancer du sein pré ménopausique chez les patients. Cependant, en raison de la nature chargée du bisphosphonate et haute affinité pour l'hydroxyapatite, les *N*-BPs ont des propriétés pharmaceutiques très pauvres. Une nouvelle série d'inhibiteurs bisphosphonate plus lipophile dont la structure est basé sur le motif thiénopyrimidine ont été désignés et synthétisés. Utilisation d'analyse de fluorimétrie différentiel à balayage (DSF) ont démontré que les bisphosphonates thiénopyrimidine (ThPBPs) stabilisent thermiquement la FPPSh en absence de magnésium suggérant la possibilité que les ThPBPs s'engage à la FPPSh en l'absence de magnésium loin du site où DMAPP / géranyl pyrophosphate (GPP) se lie. D'autres études biophysiques y compris le titration calorimétrique (ITC) et la cristallographie aux rayons X ont confirmés que les ThPBPs peuvent s'engager en l'absence de magnésium à une poche allostérique connu. Une nouvelle série d'analogues de thiénopyrimidine non-bisphosphonates ont été conçus et synthétisés pour s'engager dans la poche allostérique.

ACKNOWLEDGMENTS

First and foremost, I would like to thank my supervisor Prof. Youla S. Tsantrizos for giving me the opportunity to pursue graduate level studies in her lab. I am very grateful for her time, effort, and patience she put into training me. While I was in her lab, she not only provided guidance over the course of my degree, she also gave me great advice to overcome a very difficult time of my life when I was affected by personal health issues. I am very grateful to have learned many interdisciplinary techniques which will help me prepare for my future.

I would also like to thank all the past and current members of the Tsantrizos lab whom helped me during my studies. They are Joris De Schuttter, Yih-Shyan Lin, Cyrus Lacbay, Alexios Matralis, John Mancuso, Demetrios Gritzalis, Shiguang Li, Alejandra Dominguez Huerta, Dimitris Xanthopoulous, Eleni Michail Ladopoulu, Weiling Chiu, Michail Tsakos, Cookie Cho, Vivian Ta, Kristina Wolf, Mark Sasson, and Charles Cole. They were always there to provide meaningful discussion and good advice when I needed. They also made my time in the Tsantrizos lab much more enjoyable.

Finally I would like to thank my family and friends for supporting me through the process of my graduate studies. Without my family's constant support and patience, I would have never been able to go through a very difficult period of my life when my personal health suffered a lot.

ABBREVIATIONS

ANT	Adenine nucleotide translocase
APC	Antigen presenting cells
DMAPP	Dimethylallyl pyrophosphate
FPP	Farnesyl pyrophosphate
FPPS	Farnesyl pyrophosphate synthase
FTase	Farnesyl transferease
GPP	Geranyl pyrophosphate
GGPP	Geranylgeranyl pyrophosphate
GGPPS	Geranylgeranyl pyrophosphate synthase
GGTase	Geranylgeranyltransferase
hFPPS	Human farnesyl pyrophosphate synthase
HMG-CoA	3-Hydroxy-3-methylglutaryl-coenzyme A
IC_{50}	Half maximal inhibitory concentration
INFγ	Interferon gamma
N-BP	Nitrogen-containing bisphosphonate
RIS	Risedronate
ThPBP	Thienopyrimidine bisphosphonate
ThPMP	Thienopyrimidine monophosphonate
TCR	T cell receptor
TNFα	Tumour necrosis factor alpha
ZOL	Zoledronate

LIST OF FIGURES

1. INTRODUCTION

1.1 The Mevalonate Pathway

The mevalonate pathway is an essential metabolic pathway responsible for the biosynthesis of isoprenoids in all mammalian cells (Fig. 1.1). The pathway begins with condensation of two molecules of acetyl-CoA to form acetoacetyl-CoA. Acetoacetyl-CoA is further converted to 3-hydroxy-3-methylglutaryl-CoA (HMG-CoA) and reduced to mevalonate by HMG-CoA reductase. Mevalonate is sequentially phosphorylated and decarboxylated to give isopentenyl pyrophosphate (IPP). IPP can be further isomerized to form dimethylallyl pyrophosphate (DMAPP). Both IPP and DMAPP are important intermediate building blocks for the biosynthesis of higher isoprenoids. The first branching point of the mevalonate pathway is catalyzed by the enzyme farnesyl pyrophosphate synthase (FPPS). FPPS performs the head-to-tail condensation of DMAPP and IPP to form geranyl pyrophosphate (GPP; Fig. 1.1). FPPS also catalyzes a second condensation step between GPP and IPP to form farnesyl pyrophosphate (FPP). The biosynthesis of FPP is the first branching point of the mevalonate pathway, because FPP can be funnelled into the biosynthesis of a wide variety of biomolecules such as steroids. FPP is further elongated into geranylgeranyl pyrophosphate (GGPP) by condensing with another IPP, this step is catalyzed by geranylgeranyl pyrophosphate synthase (GGPPS) (Fig. 1.1). Both FPP and GGPP are used for the post-translational modification of a large family of proteins known as the small GTPases. These prenylation events are commonly known as farnesylation and geranylgeranylation and they are catalyzed by farnesyltransferase (FTase), geranylgeranyltransferase I (GGTase-I) and Rab geranylgeranyltransferase (GGTase

II). Prenylation usually occurs at either one or two C-terminal cysteine residues of the target protein via a thioether linkage. Prenylation affects up to 4% of the proteins in the mammalian proteome.[1] This post-translational modification enables reversible association of the target protein with the intracellular membranes and modulates protein-protein interactions.

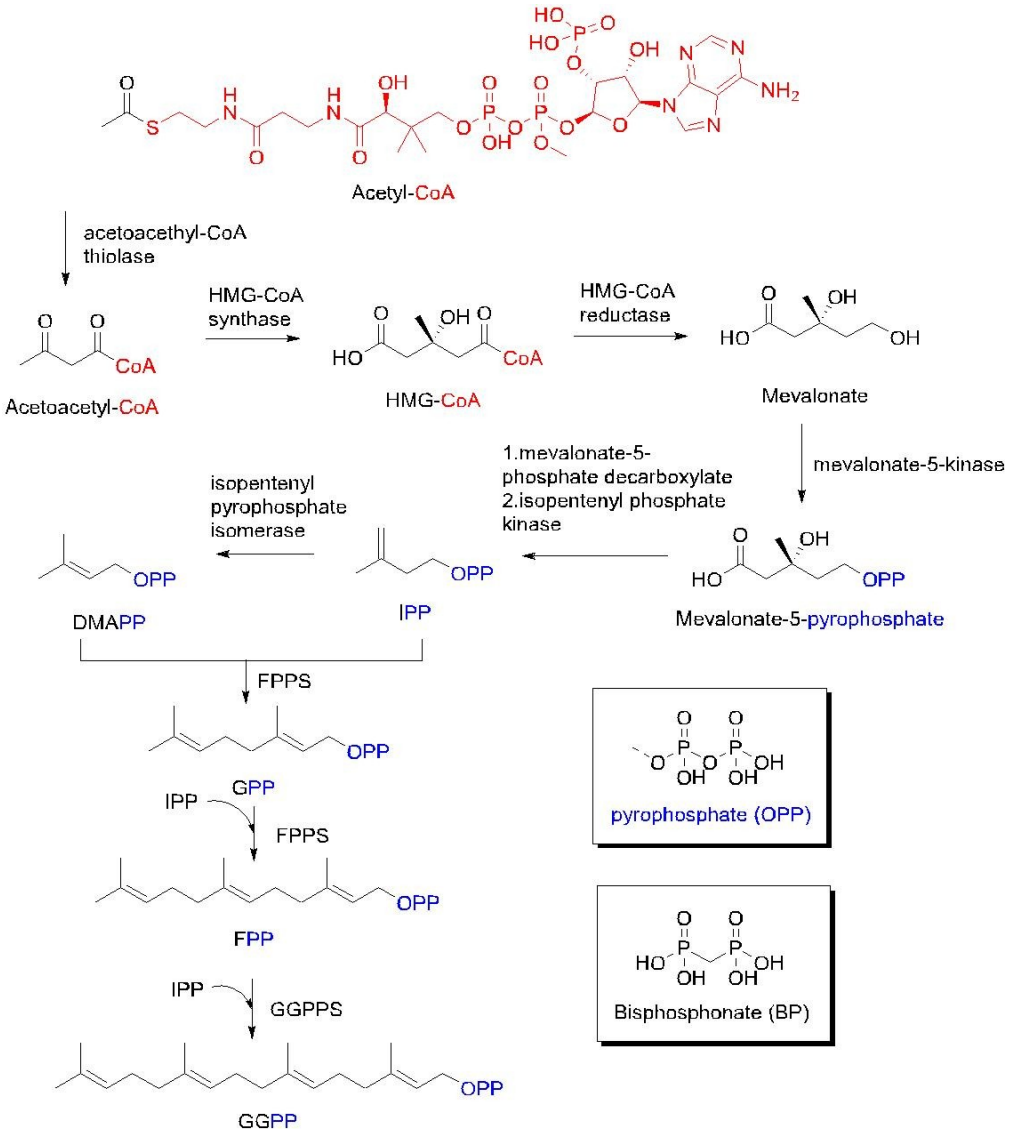

Figure 1.1 Mevalonate pathway. Structure of pyrophosphate (OPP) bioisostere and the bisphosphonate (BP) is shown for comparison

1.2 The Human FPPS and Cancer

The small GTPases are a family of proteins involved in cell signaling and are especially important for cell survival and proliferation. These proteins are all prenylated by FPP or GGPP in order to function. One of the most studied and well known GTPase is the Ras, which is especially important for cancer therapy. Among 500 validated cancer genes, three Ras genes (H-Ras, N-Ras, K-Ras) constitute the most frequently mutated oncogene family in human cancer. Among the most lethal cancers such as pancreatic (97% K-Ras mutation), colon (44.7% K-Ras mutation), and lung cancer (30.9% K-Ras mutation), the frequency of Ras mutation has been found to be very high.[2] Therefore many drug discovery efforts have focused on targeting the Ras protein. Initial effort at inhibiting Ras protein begun by looking for GTP-competitive inhibitor for Ras, however GTP binds to Ras protein with picomolar affinity; therefore directly targeting the Ras protein proved to be extremely challenging. Other efforts focused on the development of FTase inhibitor, which would inhibit the farnesylation of Ras and therefore preventing the association of Ras with the inner face of the plasma membrane. Pharmaceutical company such as Johnson and Johnson have developed potent small molecules inhibitor of FTase, which have been shown to effectively block the growth of H-Ras driven tumors. Two of these FTase inhibitors, Lonafarnib and Tipifarnib (Fig. 1.2), advanced to Phase III clinical trials. However both of these inhibitors showed no antitumor activity in clinical trials focused on pancreatic and colon cancer. It was later found that FTase inhibitors were indeed inhibiting the farnesylation of K-Ras and N-Ras, however these protein where still able to associate to the plasma membrane and function due to a

redundancy mechanism, where GGTase I adds GGPP to the Ras proteins as a biochemically equivalent replacement to FPP. Due to this redundancy mechanism, inhibitors that target FTase are not effective to down regulate Ras prenylation and activation. However other efforts toward developing FPPS inhibitors, as an alternative method of down regulating the biosynthesis of FPP and its downstream isoprenoid, have been proposed.

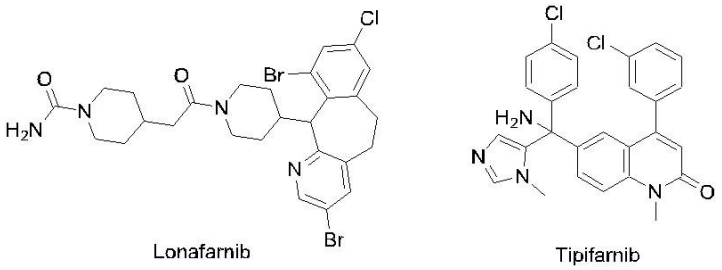

Figure 1.2 Structure of FTase inhibitiors: Lonafarnib and Tipifarnib

Inhibiting the human farnesyl pyrophosphate synthase (hFPPS) is not a novel concept. Pharmaceutical companies, such as Novartis, have developed very potent inhibitor of hFPPS known as bisphophosnates (BP), examples include the marketed drugs: Zoledronic acid (ZOL) and Risedronic acid (RIS) (Fig. 1.3). The main pharmacophore of these small molecules is a bisphosphonic acid moiety. The bisphosphonic acid moiety is a non-hydrolysable bioisostere of nature's pyrophosphate moiety; it is rendered non-hydrolysable by the central methylene carbon that has replaced the oxygen (Fig. 1.1). The bisphosphonic acid functional group is highly charged and highly water soluble making them only able to enter cells that possess fluid-phase endocytosis such as osteoclast and macrophages.[3] Furthermore the BP

possess high affinity to bone, causing them to rapidly accumulate to sites where there is high bone turnover. Due to these properties, the BP are suitable for treating bone disease and have been used to treat osteoporosis and to prevent bone fracture in patients with bone related cancers. Nitrogen containing BPs (*N*-BP) such as ZOL have been shown to be very potent inhibitors of hFPPS. Several *in vitro* and *in vivo* studies have been conducted to see whether *N*-BPs possess antitumor effects against non-skeletal cancer, including multiple myeloma, breast and prostate cancers.[4] Examples from clinical studies include investigations in patients suffering from multiple myeloma and breast cancer. In the first case, a recent clinical investigation by Morgan *et al.* showed evidence that ZOL improved the survival of patients with multiple myeloma via mechanisms that are both related as well as unrelated to the skeletal benefits.[5] In the latter case, Gnant *et al.* later showed that treating premenopausal women affected by endocrine-responsive early breast cancer using endocrine therapy and ZOL resulted in significant reduction of disease progression.[6]

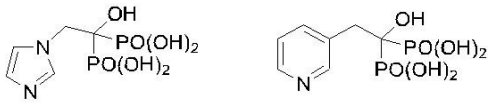

Figure 1.3 Structure of hFPPS inhibitor

Inhibition of hFPPS blocks the biosynthesis of FPP and all the downstream metabolite. It also leads to the accumulation of the natural substrate IPP inside the cells. The excess IPP becomes conjugated to AMP to form a toxic ATP analog (ApppI) (Figure 1.4). ApppI is cytotoxic due to its ability to inhibit mitochondrial

adenine nucleotide translocase (ANT) inside the cell. ANT is believed to be a regulatory component of mitochondrial permeability transition pore which controls mitochondrial permeability during apoptosis. Due to this regulation mechanism, excess intracellular IPP has been shown by Mitrofan *et al.* to directly induce apoptosis in cancer cells.[7] Wang *et al.* have also shown (through the transfection of antigen presenting cells (APC) using small interfering RNA to block the gene responsible for the expression of FPPS and of isopentenyl pyrophosphonate isomerase) that an artificially induced accumulation of IPP can lead to the stimulation of γδ T cells containing the antigen Vγ2Vδ2 T cell receptor (TCR).[8] The γδ T cells are a subset of T cells that functions as the innate and adaptive immune system by monitoring intermediates in the isoprenoid metabolism. Once activated, the Vγ2Vδ2 T cells produce high levels of inflammatory cytokines such as interferon gamma (INFγ) and tumor necrosis factor (TNFα) that are involved in killing tumor cells.[8]

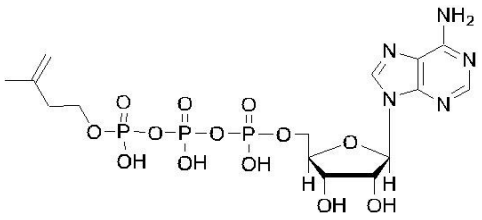

Figure 1.4 Structure of ApppI

1.3 Structure, Functions and Inhibitors of hFPPS

The human FPPS enzyme exists as a homodimer composed of 13 α-helices (Fig. 1.5). Initially, Hosfield *et al.* have proposed a mechanism for the catalytic cycle of hFPPS based on several X-ray crystal structure of *E. coli* FPPS complexes with its natural substrate and an inhibitor.[9] FPP is formed through a three-metal ion catalyzed three-step ionization-condensation-elimination mechanism (Fig. 1.6). The protein structure of hFPPS undergoes through three different conformational changes during the catalytic cycle: the fully open, partially closed, and fully closed conformations. When the enzyme is free of any ligand (apo-enzyme), the active site is fully open to solvent (i.e. binding sub-pockets for IPP, DMAPP, and GPP are not well defined). Once the allylic pocket of the enzyme is occupied with DMAPP, GPP, or a *N*-BP inhibitor and three magnesium cations (Mg^{2+}), the two ^{117}DDIMD^{121} and ^{257}DDYLD^{261} motifs come closer together and the two loops (H-I and D-E) close the entrance of the allylic pocket to form the partially closed conformation (Fig. 1.7).[10] Once this partially closed conformation is formed, the IPP sub-pocket becomes well defined and allows the binding of IPP. Upon binding of IPP, the basic ^{350}KRRK^{353} C-terminal tail of the enzyme folds over the pyrophosphate moiety of IPP and closes the IPP binding site to form the fully closed conformation. Lin *et al.* recently shown that the basic C-terminal tail is able to close the IPP binding site in the presence of *N*-BP containing an aryl substituted pyridine scaffold in the absence of IPP.[11]

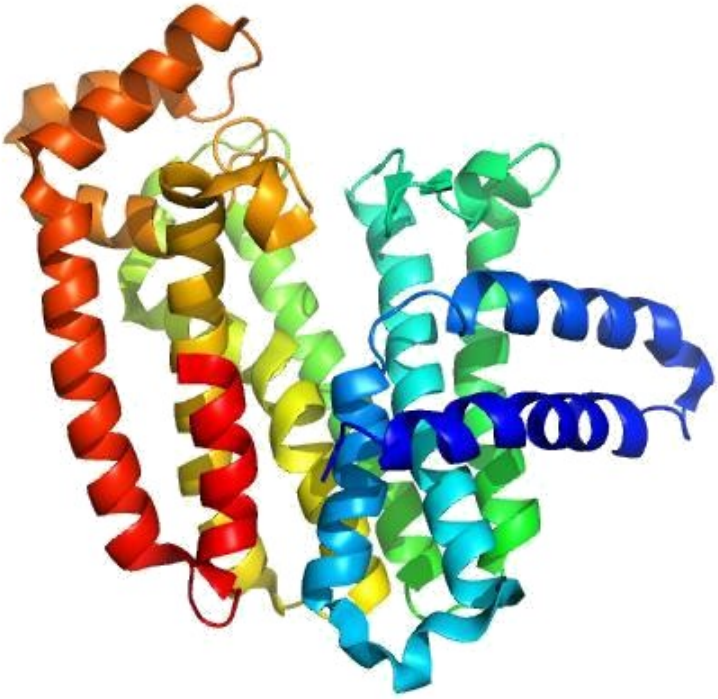

Figure 1.5 X-ray crystal structure of the unliganded hFPPS (PDB: 2F7M). The C-terminal tail of the enzyme is shown in red.

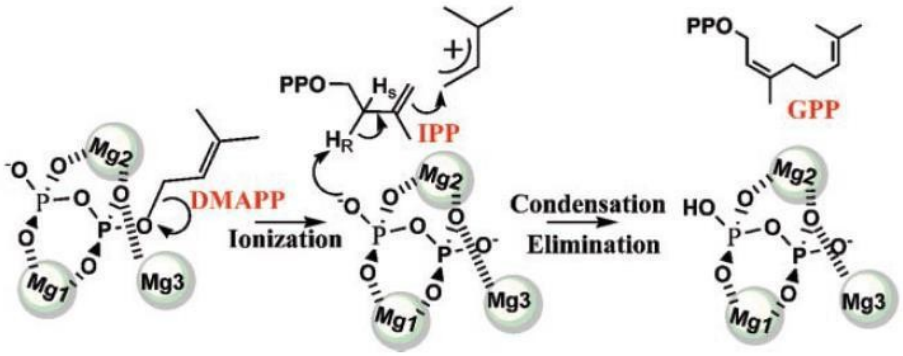

Figure 1.6 Proposed three-metal ion catalyzed three-step ionization-condesation-elimination mechanism.[9]

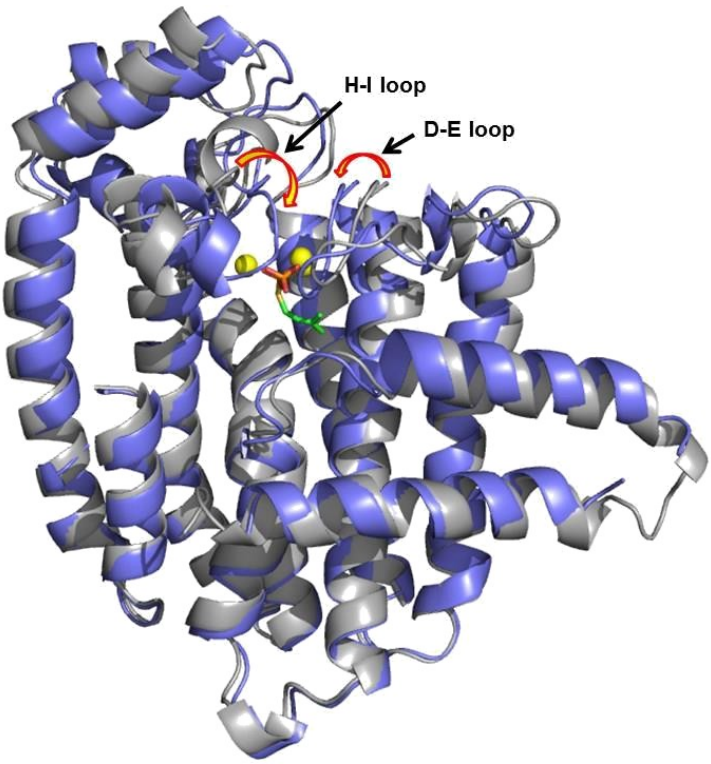

Figure 1.7 Superimposed X-ray crystal structures of hFPPS in the open conformation (grey, PDB: 2F7M) and semi-closed conformation (blue, PDB: 1YV5). The three magnesium ions are represented by yellow spheres. Figure made by Dr. Joris De Schutter (Tsantrizos Lab).

The current, clinically relevant *N*-BPs, such as ZOL and RIS are characterized by a bisphosphonic acid polar group mimicking the pyrophosphate of the natural substrate and a nitrogen containing heterocyclic side chain. The bisphosphonate moiety of the *N*-BPs is coordinated to a cluster of highly conserved aspartic acid residues, within the DMAPP/GPP sub-pocket of the active site, through three magnesium ions that are essential co-factor for the catalytic activity of the enxyme.[10] In addition, under physiological conditions, the nitrogen of the heterocyclic side chain is believed to be protonated, allowing for a bifurcated hydrogen bond with the

carbonyl oxygen of lysine 200 and the oxygen of threonine 201 and mimicking the carbocation intermediate formed during the catalytic cycle. Kavanagh *et al.* have shown (using isothermal titration calorimetry; ITC) that the ZOL and RIS exclusively binding to the allylic sub-pocket, which is the binding site of DMAPP and GPP.[12] Although these *N*-BPs are very potent inhibitor for hFPPS, they suffer from low soft-tissue exposure, rapid clearance from the systemic circulation and strong binding to bone minerals.

To overcome the poor pharmacokinetic properties of the bisphosphonates, Jahnke *et al.* screened a small library of 400 fragments using NMR spectroscopy for their binding affinity to human recombinant FPPS. In this fragment based screening, they discovered a series of non-bisphosphonate compounds (**1**-**2**) (Fig. 1.8) having weak affinity for FPPS.[13] Furthermore they confirmed that these compounds did not bind to the active site of the enzyme. Using X-ray crystallography, they showed that those compounds bind in an allosteric pocket near the C terminus of the enzyme adjacent to the IPP binding site (Fig. 1.9). This newly discovered allosteric binding site is composed of a small hydrophobic pocket next to a series of basic residues responsible for stabilizing the pyrophosphate moiety of IPP. Fragments **1** and **2** were further optimized into lead compound **3** (Fig 1.8) with low micromolar IC_{50} values (in our *in vitro* assay). The mechanism of inhibition is believed to be due to the allosteric inhibitor blocking the ^{350}KRRK^{353} C-terminal tail from clamping down to adopt the fully closed conformation in order for catalysis to happen. Furthermore the proximity

of the negative charge of the allosteric inhibitor would directly prevent IPP binding (due to charge-charge repulsion).[13]

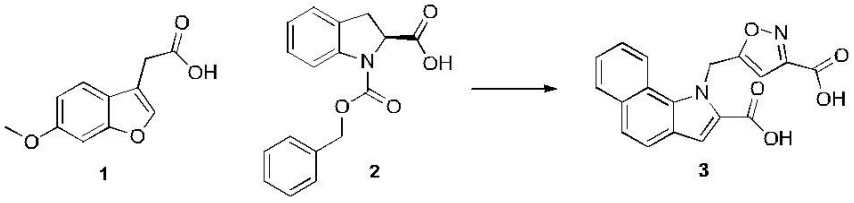

Figure 1.8 Allosteric inhibitors **1** and **2** of hFPPS found through fragment based screening and the final optimized low micromolar (in our in vitro assay, nanomolar in the Novartis MS-based assay) inhibitor **3**.[13]

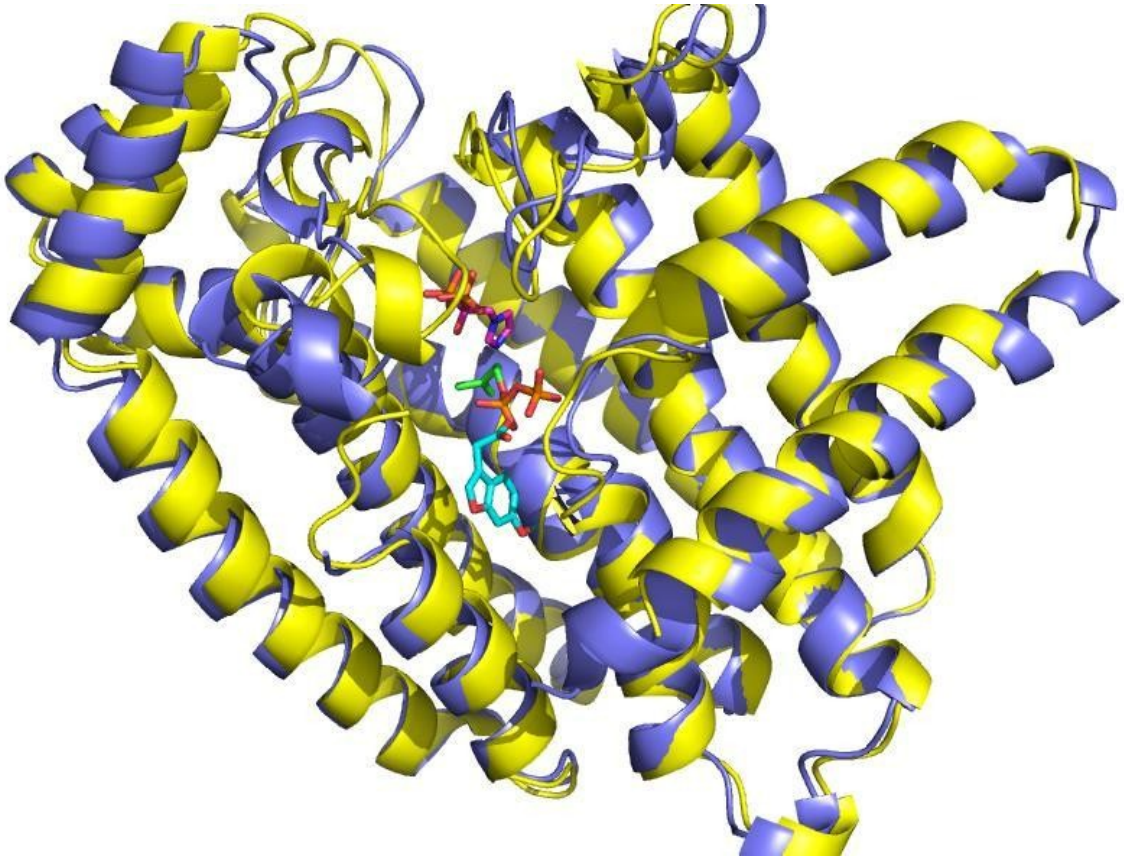

Figure 1.9 Superimposed X-ray crystal structures of ternary structure ZOL (magenta) /IPP(green) /hFPPS (blue, PDB: 1ZW5) and binary structure of the fragment **2** (cyan)/ hFPPS (yellow, PDB: 3N3L).[13]

1.4 Research Goals

Recent clinical investigations on *N*-BPs inhibitors such as ZOL have provided strong evidence that inhibiting hFPPS significantly reduces the disease progression of premenopausal women suffering from breast cancer and also improves the survival of patients with multiple myeloma. However due to their poor biopharmaceutical properties and their high affinity to bone, the current commercially available hFPPS inhibitors is only suitable to treat bone related cancer and osteoporosis.

The goal of my research project was to develop novel hFPPS inhibitors by exploring different chemical structure varying their size, shape, and electronic properties and comparing their inhibitory activity. Our structural activity relationship (SAR) studies included the evaluation of active site and allosteric inhibitors for hFPPS having a thienopyrimidine scaffold. The final inhibitors synthesized were evaluated in an enzymatic assay and several cell-based assay using human multiple myeloma cell lines. The research work of my MSc thesis has been published in the list of publication indicated below and my contributions to these publications is described in the following sections:

1) Leung, C.Y.; Langille, A.M.; Mancuso, J.; Tsantrizos, Y.S., Discovery of thienopyrimidine-based inhibitors of the human farnesyl pyrophosphate synthase - Parallel synthesis of analogs via a trimethylsilyl ylidene intermediate. *Bioorg. Med. Chem.,* **2013**, *21*, 2229-2240.

2) Leung, C.Y.; Park, J.; De Schutter, J. W.; Sebag, M.; Berghuis, A.M.; Tsantrizos, Y.S., Thienopyrimidine bisphosphonate (ThPBP) inhibitors of the human farnesyl pyrophosphate synthase: optimization and characterization of the mode of inhibition. *J. Med. Chem.,***2013**, *56*, 7939-7950.

3) De Schutter, J.W.; Park, J.; Leung, C.Y.; Gormley, P.; Lin, Y.-S.; Hu, Z.; Berghuis, A.M.; Poirier, J.; Tsantrizos, Y.S., Multistage screening reveals chameleon ligands of the human farnesyl pyrophosphate synthase: implications to drug discovery for neurodegenerative diseases. *J. Med. Chem.* **2014**, *57*, 5764-5776

1.5 References

1. Nguyen, U.T.T.; Guo, Z.; Delon, C.; Wu, Y.W.; Deraeve, C.; Fraenzel, B.; Bon, R.S.; Blankenfeldt, W.; Goody, R.S.; Waldmann, H.; Wolters, D.; Alexandrov, K., Analysis of the eukaryotic prenylome by isoprenoid affinity tagging. *Nat. Chem. Bio.*, **2009**, *5*, 227-235

2. Cox, A.D.; Fesik, S.W.; Kimmelman, A.C.; Luo, J.; Der, C.J., Drugging the undruggable RAS: mission possible? *Nat. Rev. Drug. Discov.*, **2014**, *13*, 828-851

3. Roelofs, A.J.; Thompson, K.; Gordon, S.; Rogers, M.J., Molecular mechanisms of action of bisphosphonates: current status. *Clin. Cancer Res.*, **2006**, *12*, 6222-6230

4. Senaratne, S.G.; Mansi, J.L.; Colston, K.W., The bisphosphonate zoledronic acid impairs membrane localization and induces cytochrome *c* release in breast cancer cells. *Br. J. Cancer*, **2002**, *86*, 1479-1486; Coleman, R. E.; Marshall, H.; Cameron, D.; Dodwell, D.; Burkinshaw, R.; Keane, M.; Gil, M.; Houston, S. J.; Grieve, R. J.; Barrett-Lee, P. J.; Ritchie, D.; Pugh, J.; Gaunt, C.; Rea, U.; Peterson, J.; Davies, C.; Hiley, V.; Gregory, W.; Bell, R. Breast-Cancer Adjuvant Therapy with Zoledronic Acid. *New Engl. J. Med.* **2011**, *365*, 1396−1405

5. Morgan, G. J.; Davies, F. E.; Gregory, W. M.; Cocks, K.; Bell, S.E.; Szubert, A. J.; Navarro-Coy, N.; Drayson, M. T.; Owen, R. G.; Feyler, S.; Ashcroft, A. J.; Ross, F.; Byrne, J.; Roddie, H.; Rudin, C.; Cook, G.; Jackson, G. H.; Child, J. A. First-line treatment with zoledronic acid as compared with clodronic acid in multiple myeloma (MRC Myeloma IX): a randomized controlled trial. *Lancet* **2010**, *376*, 1989 −1999

6. Gnant, M.; Mlineritsch, B.; Schippinger, W.; Luschin-Ebengreuth, G.; Pöstlberger, S.; Menzel, C.; Jakesz, R.; Seifert, M.; Hubalek, M.; Bjelic-Radisic, V.; Samonigg, H.; Tausch, C.; Eidtmann, H.; Steger, G.; Kwasny, W.; Dubsky, P.; Fridrik, M.; Fitzal, F.; Stierer, M.; Rücklinger, E.; Greil, R. Endocrine therapy plus zoledronic acid in premenopausal breast cancer. *N. Engl. J. Med.*, **2009**, *360*, 679–691

7. Mitrofan, L.M.; Pelkonen, J.; Mönkkönen, J., The level of ATP analog and isopentenyl pyrophosphate correlates with zoledronic acid-induced apoptosis in cancer cells in vitro. *Bone*, **2009**, *45*, 1153-1160

8. Wang, H.; Sarikonda, G.; Puan, K.-J.; Tanaka, Y.; Feng, J.; Giner, J.-L.; Cao, R.; Mönkkönen, J.; Oldfield, E.; Morita, C.T., Indirect stimulation of human Vγ2Vδ2 T cells through alterations in isoprenoid metabolism. *J. Immunol.*, **2011**, *187*, 5099-5113

9. Hosfield, D.J.; Zhang, Y.M.; Dougan, D.R.; Broun, A.; Tari, L.W.; Swanson, R.V.; Finn, J., Structural basis for bisphosphonate-mediated inhibition of isoprenoid biosynthesis. *J. Bio. Chem.*, **2004**,

10. Rondeau, J.-M.; Bitsch, F.; Bourgier, E.; Geiser, M.; Hemmig, R.; Kroemer, M.; Lehmann, S.; Ramage, P.; Rieffel, S.; Strauss, A.; Green, R.J.; Jahnke, W., Structural basis for the exceptional in vivo efficacy of bisphosphonate drugs. *ChemMedChem.*, **2006**, *1*, 267-273

11. Lin, Y.-S.; Park, J.; De Schutter, J.W.; Huang, X.F.; Berghuis, A.M.; Sebag, M.; Tsantrizos, Y.S., Design and synthesis of active site inhibitor of the human farnesyl pyrophosphate synthase: apoptosis and inhbition of ERK phosphorylation in multiple myeloma cells., *J. Med. Chem.*, **2012**, *55*, 3201-3215

12. Kavanagh, K.L.; Guo, K.; Dunford, J.E.; Wu, X.; Knapp, S.; Ebetino, F.H.; Rogers, M.J.; Russell, G.G.; Opperman, U., The molecular mechanism of nitrogen-containing bisphosphonates as antiosteoporosis drugs., *Proc. Natl. Acad. Sci.*, **2006**, *103*, 7829-7834

13. Jahnke, W.; Rondeau, J.-M.; Cotesta, S.; Marzinzik, A.; Pellé, X.; Geiser, M.; Strauss, A.; Götte, M.; Bitsch, F.; Hemmig, R.; Henry, C.; Lehmann, S.; Glickman, J. F.; Roddy, T. P.; Stout, S. J.; Green, J. R.; Allosteric non-bisphosphonate FPPS inhibitors identified by fragment-based discovery *Nat. Chem. Biol.* **2010**, *6*, 660-666.

2. Discovery of thienopyrimidine-based inhibitors of the human farnesyl pyrophosphate synthase - Parallel synthesis of analogs via a trimethylsilyl ylidene intermediate

Reference:

Leung, C.Y.; Langille, A.M.; Mancuso, J.; Tsantrizos, Y.S., Discovery of thienopyrimidine-based inhibitors of the human farnesyl pyrophosphate synthase - Parallel synthesis of analogs via a trimethylsilyl ylidene intermediate. *Bioorg. Med. Chem.,* **2013**, *21*, 2229-2240

In the above publication, the synthesis of the thienopyrimidine scaffold using the triemthylsilyl ylidene intermediate was explored by Dr. John Mancuso, Adrienne M. Langille and myself. The optimization of this synthetic method was performed by Adrienne and I and the C-5/C-6 disubstituted thienopyrimidine bisphosphonates were synthesized by Adrienne. I contributed to the synthesis of the mono-substituted thienopyrimidine bisphosphonates inhibitors. I also performed all of the *in vitro* inhibition assays of these compounds against both hFPPS and hGGPPS. The protein used to run the *in vitro* assays were produced by Dr. Yih-Shyan Lin from our research group.

Bioorganic & Medicinal Chemistry 21 (2013) 2229–2240

Contents lists available at SciVerse ScienceDirect

Bioorganic & Medicinal Chemistry

journal homepage: www . elsevier . com/locate/bmc

Discovery of thienopyrimidine-based inhibitors of the human farnesyl pyrophosphate synthase—Parallel synthesis of analogs via a trimethylsilyl ylidene intermediate

Chun-Yuen Leung [a], Adrienne M. Langille [a], John Mancuso [a,c], Youla S. Tsantrizos [a,b,⇑]

[a] Department of Chemistry, McGill University, 801 Sherbrooke Street West, Montreal, QC, Canada H3A 0B8
[b] Department of Biochemistry, McGill University, 3649 Promenade Sir William Osler, Montreal, QC, Canada H3G 0B1 [c] Tranzyme Pharma, 3001 12th Avenue North, Sherbrooke, QC, Canada J1H 5N4

a r t i c l e i n f o

Article history:
Received 4 January 2013
Revised 1 February 2013 Accepted
11 February 2013 Available online
18 February 2013

Keywords:
Thienopyrimidine bisphosphonates
Modified Gewald synthesis 2-(1-(Trimethylsilyl)ethylidene) malononitrile
Farnesyl pyrophosphate synthase

a b s t r a c t

Thienopyrimidine-based bisphosphonates were identified as a new class of nitrogen-containing bisphosphonate (N-BP) inhibitors of the human farnesyl pyrophosphate synthase (hFPPS). Analogs were prepared via cyclization of 2-(1-(trimethylsilyl)ethylidene)malononitrile to 2-amino-4-(trimethylsilyl) thiophene-3-carbonitrile in the presence of elemental sulfur. Direct ipso-iododesilylation of this interme-diate led to selective iodination at C_b of the sulfur atom in high efficiency. The synthetic protocols devel-oped were used in the parallel synthesis of structurally diverse thieno[2,3-d]pyrimidin-4-amine-based bisphosphonate inhibitors of hFPPS.

1. Introduction

The thienopyrimidine core is an integral part of numerous biologically active compounds, as evidenced by the plethora of literature and industrial patents disclosing the use of this heterocy-cle in agrochemicals[1–3] and human therapeutics (e.g., antifungal[4] and antiviral[5] agents). Thienopyrimidines are often used as bioisosteres of purine nucleobases (e.g., adenine),[5] and have been employed extensively in the design of various kinase inhibitors, including Aurora kinase,[6] tyrosine kinases,[7,8] cyclin-dependent kinase,[9] c-Jun N-terminal kinases,[10–12] PERK,[13] phosphoinositide 3-kinase a (PI3Ka),[14,15] and EGFR/ErbB-2.[16] Many of these inhibitors are currently under pre-clinical or clinical investigations for the treatment of cancer, inflammatory, autoimmune and neurodegenerative diseases. Thienopyrimidine-based compounds have also been reported as inhibitors of c-secretase[17] and antagonists of the adenosine A_{2A} receptor,[18–20] and implicated in the potential treatment or prevention of Alzheimer's disease.

In our own investigations, we focus on the identification of structurally diverse molecules that selectively inhibit mammalian prenyl synthase enzymes. Inspired by the privileged biopharmaceutical properties of the thienopyrimidine scaffold (1; Fig. 1), we decided to explore thienopyrimidine-based bisphosphonates (2; Fig. 1), as potential inhibitors of the human farnesyl pyrophosphate synthase (hFPPS) and/or geranylgeranyl pyrophosphate synthase (hGGPPS); these prenyl synthase enzymes are functionally closely related.

The development of synthetic methodologies amenable to parallel synthesis of structurally diverse libraries of thienopyrimi-

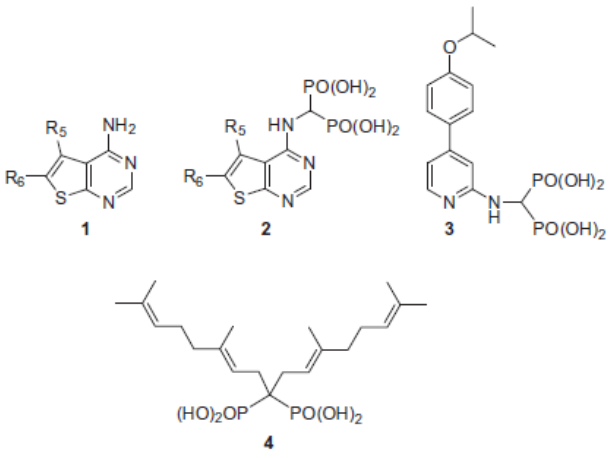

Figure 1. Structures of thieno[2,3-d]pyrimid-4-amines (general structure 1), thienopyrimidine-based bisphosphonate inhibitors of hFPPS/hGGPPS (general structure 2), hFPPS inhibitor 3 and hGGPPS inhibitor 4.

⇑ Corresponding author. Tel.: +1 514 398 3638; fax: +1 514 398 3797. E-mail address: youla.tsantrizos@mcgill.ca (Y.S. Tsantrizos).

0968-0896/$ - see front matter 2013 Elsevier Ltd. All rights reserved.
http://dx.doi.org/10.1016/j.bmc.2013.02.006

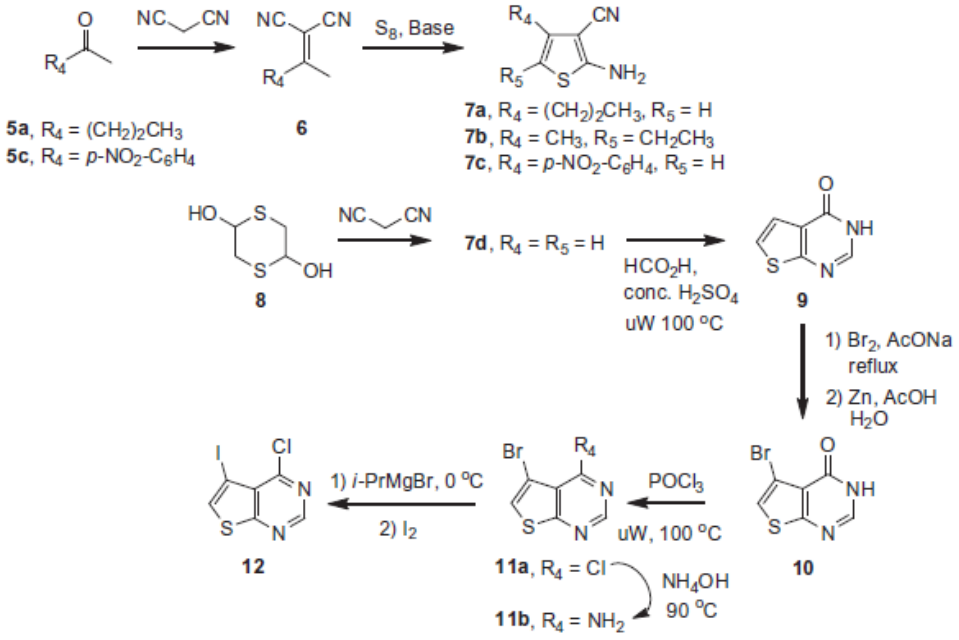

Scheme 1. Gewald synthesis of 2-aminothiophene-3-carbonitriles (7) and halo-substituted thienopyrimidines.

dine bisphosphonates (2) were required to support our medicinal chemistry efforts. We anticipated that the final compounds could be made from highly substituted thieno[2,3-d]pyrimidin-4-amine intermediates (1), after coupling of the exocyclic amine (at C-4) with the bisphosphonate moiety; the latter step could be easily achieved using previously developed procedures for the prepara-
tion of 2-aminopyridine bisphosphonates (e.g., hFPPS inhibitor 3; Fig. 1).[21,22]

Traditionally, thieno[2,3-d]pyrimid-4-amines (1) have been synthesized via a multistep process from 2-aminothiophenes (7; Scheme 1). However, preparation of highly substituted thienopyr-imidine libraries is usually hampered by limitations in selectively functionalizing the C_a and/or C_b positions of the thiophene core (7). Similarly, direct and selective substitution at those positions in the corresponding thieno[2,3-d]pyrimidine is very challenging (i.e., the C-5 and C-6 of 1).

The 2-aminothiophene core (7) can be easily prepared by the classical Gewald method (Scheme 1).[23] One-step and two-step procedures, under either thermal or microwave conditions, have been reported with various optimizations for the condensation of the Knoevenagel ylidene 6 with elemental sulfur to give the thio-phene 7. The drawbacks to this elegant protocol can be regioselec-tivity in the cyclization step, when non-symmetrical ketones (5) are used with an alkyl or a benzylic substituent, and the chemical stability of ylidene 6. For example, the one-pot condensation of pentane-2-one (5a) with malononitrile, sulfur and catalytic amounts of imidazole, was recently reported to produce a mixture of thiophenes 7a and 7b in 1:3.4 ratio and in modest yield (Scheme 1).[24] Furthermore, acetophenones bearing electron withdrawing substituents on the phenyl ring (e.g., 5c) often produce very low yields of the desired 2-aminothiophene (7c) under standard Ge-wald reaction conditions.[25] The low yields have been attributed, in part, to decomposition and dimerization of ylidene 6, under high temperatures and basic conditions.[25]

Alternatively, the unsubstituted 2-amino-thiophene-3-carboni-trile core (7d) has also been prepared from 2,5-dihydroxy-1,4-dithiane (8) and subsequently elaborated to substituted thie-no[2,3-d]pyrimidines.[26,27] Chlorination or bromination at C_a of the thiophene sulfur can be easily achieved with NCS or NBS, respectively. However, direct and regiospecific halogenation at the b-carbon, or the equivalent carbon on any thiophene-contain-ing bicyclic heterocycle, is unknown. Recent reports on the prepa-ration of 3-bromothiophenes usually describe the generation of the a-lithium-b-bromothiophene from the 2-bromothiophene using the (so-called) base-catalyzed halogen dance (BCHD) reaction.[28–32] This approach has also been used in the synthesis of 4-chloro-5-iodothieno[2,3-d]pyrimidine (12) from the LDA-medi-ated BCHD rearrangement of the 6-bromo-4-chlorothieno [2,3-d]pyrimidine first to the 5-bromo analog 11a, followed by treatment with a Grignard reagent and quenching of the anion with iodine (Scheme 1).[1,3] Several alternative approaches have been reported, most commonly involving 2,3-dibromination of 9, followed by reductive dehalogenation at the more reactive C_a po-
sition of the thiophene with Zn in acetic acid to give intermediate 10 (Scheme 1).[10,11] Two additional synthetic steps are required to convert 10–11b, which can then be used to prepare C-5 mono-substituted thienopyrimidines. Herein, we report an alternative protocol that allows selective disubstitution at either C_a or C_b of the thiophene core and is amenable to modular parallel synthesis of structurally diverse libraries of thieno[2,3-d]pyrimidin-4-amines (1). We also provide preliminary biological data which indicates that the thienopyrimidine-based bisphosphonates de-scribed herein are inhibitors of the human FPPS and new leads for drug discovery. Up-regulation of hFPPS has been linked to numerous human disorders,[33,34] including cancer[35] and neurode-generative diseases, thus inhibitors of this enzyme have the poten-tial of becoming valuable human therapeutics.

2. Results

2.1. Chemistry

As part of our continued interest in developing efficient, robust methodologies that are amenable to parallel synthesis of structur-ally diverse libraries of biologically active compounds,[21,22] we modified the classical Knoevenagel/Gewald approach by incorpo-rating the trimethylsilyl ylidine 14 as the precursor to the 2-ami-no-thiophene-3-carbonitrile scaffold (15; Scheme 2). The ylidine 2-(1-(trimethylsilyl)ethylidene)malononitrile (14) was prepared in nearly quantitative yield via condensation of acetyltrimethylsi-lane (13) with malononitrile under acidic conditions (Scheme 2). Ylidine 14 was found to be stable at _20 LC for several months

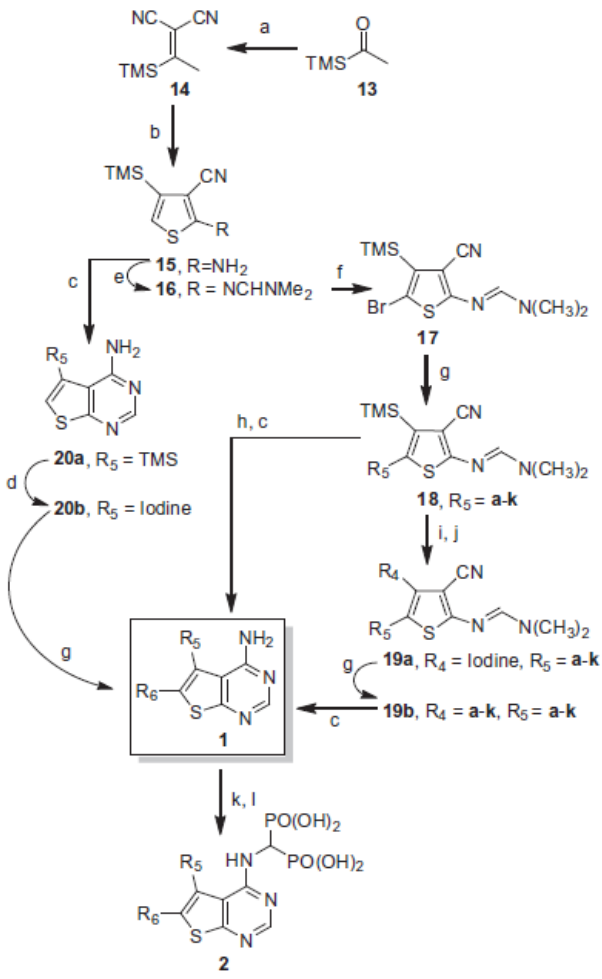

Scheme 2. Modular synthesis of highly substituted thieno[2,3-d]pyrimidin-4-amines; the stuctures of substituent a–k are shown in Table 1. Reagents and conditions: (a) $CH_2(CN)_2$, NH_4OAc, AcOH, C_6H_6, Dean–Stark trap, 95 LC, 24 h (90%); (b) S_8, Et_2NH, pyridine, rt, 18 h (85%); (c) $HCONH_2$, 130 LC, 48 h (75–85%); (d) ICl, DCM, _10 LC (>98%); (e) $(CH_3O)_2CHN(CH_3)_2$, DMF, rt, 4 h (90%); (f) NBS, DMF, rt, 13 h in the dark (80%); (g) various cross-coupling reactions under standard Suzuki, Buchwald–Hartwig, Sonogashira and Stille conditions, isolated yields varied from 50% to 95%, reactions were not individually optimized (for the conversion of 20b or 18 to 1, R_6 = H or R_5 = H, respectively); (h) TBAF, THF, 0 LC to rt, 3 h (>95%); (i) CF_3CO_2Ag, THF, _78 LC, 15 min; (j) I_2, THF, _78 LC, 3 h (>98%); (k) $CHOEt_3$, diethylphosphite, 130 LC, 24 h (50–75%); (l) TMSBr, MeOH, rt, 72 h (>85%).

and at RT for several weeks without any evidence of decomposi-tion. Condensation of 14 with elemental sulfur in pyridine provided the 2-amino-4-(trimethylsilyl)-thiophene-3-carbonitrile (15) as a dark orange/brown solid in >85% yield.

In order to explore direct cross-coupling reactions selectively at the C_b of the sulfur in the thiophene core (i.e., where intermediate 1 is mono-substituted at C-5), we initially focused on preparing the iodothiophene core, as a precursor to the 5-iodothienopyrimi-dine 20b (Scheme 2). Efforts to iodinate intermediate 15 at C_b, using silver trifluoroacetate and elemental iodine,[36,37] lead to decomposition of the starting material at temperatures ranging from 0 to _78 LC. Previous examples of ipso-iododesilylation of thiophenes under such conditions were reported to give poor yields when the TMS was adjacent to substituents with sp charac-ter.[37] Cyclization of 15 with formamide produced the 5-(trimethyl-silyl)thieno[2,3-d]pyrimidin-4-amine (20a) in 75–80% yield (Scheme 2; step c). Mindful of the facile decomposition of thiophenes upon exposure to light, this reaction was usually carried out in the dark. Subsequently, we reattempted to perform

Table 1
Mini-library of thieno[2,3-*d*]pyrimidin-4-amines (**1**) synthesized

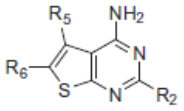

1a, R_2 = **a**, R_5 = R_6 = H
1b, R_2 = R_6 = H, R_5 = **a**
1c, R_2 = R_5 = H, R_6 = **Br**
1d, R_2 = R_5 = H, R_6 = **c**
1e, R_2 = R_5 = H, R_6 = **e**
1f, R_2 = R_5 = H, R_6 = **f**
1g, R_2 = R_5 = H, R_6 = **i**
1h, R_2 = R_6 = H, R_5 = **d**
1i, R_2 = R_6 = H, R_5 = **e**
1j, R_2 = R_6 = H, R_5 = **f**
1k, R_2 = H, R_5 = **g**, R_6 = **a**
1l, R_2 = H, R_5 = **h**, R_6 = **a**
1m, R_2 = H, R_5 = **j**, R_6 = **a**
1n, R_2 = H, R_5 = **k**, R_6 = **a**
1o, R_2 = H, R_5 = **b**, R_6 = **a**

R_2, R_5 and/or R_6 = H or a fragment from **a** to **k**

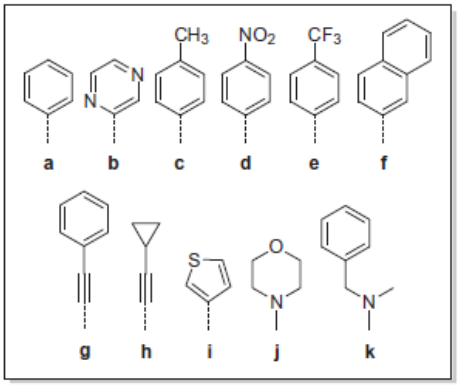

an ipso-iododesilylation reaction with silver trifluoroacetate and elemental iodine; however, this reaction resulted in mostly unre-acted starting material. Alternatively, excellent yields (>98%) of 20b were obtained when 20a was treated with ICl in DCM at _10 LC and the reaction was quenched at low temperatures (below 0 LC) with H_2O.[38,39] We noted that if the reaction mixture was allowed to warm-up above 0 LC, the isolated yield was significantly lower and mixtures of di-halogenated side products were observed by LC–MS. The iodo product 20b was found to be a useful building block for various cross-coupling reactions in the synthesis of C-5 mono-substituted thieno[2,3-d]pyrimidin-4-amines (e.g., 1b, 1h, 1i, 1j, Table 1). It is noteworthy that fragment 20b was obtained from 13 in four steps, with an average of 50–60% overall isolated yield, using our protocol (Scheme 2). This methodology is signifi-cantly more efficient in preparing analogs of 1 that are selectively mono-substituted at C-5 as compared to those reported previously (e.g., examples shown in Scheme 1).

In the course of these studies, we noted that thiophene 15 was somewhat chemically unstable. Interestingly, protection of the 2-amino moiety with N,N-dimethylformamide-dimethylacetal, provided intermediate 16, which is chemically stable and easy to prepare in high yield and purity (Scheme 2). Bromination of the protected thiophene 16 was also carried-out in >80% yield, provid-ing intermediate 17 (Scheme 2). Compound 17 is a suitable build-ing block for a variety of cross-coupling reactions. We explored selective cross-coupling with various boronic acids or boronate esters to obtain intermediates of general structure 18, which upon ipso-iododesilylation at C-4 (i.e., leading to 19a), followed by Suzuki, Buchwald–Hartwig, Sonogashira, Stille or other cross-cou-pling reactions, gave the disubstituted thiophenes 19b.

Finally, cyclization of 19b provided a library of novel and structurally diverse C-5/C-6 di-substituted thieno[2,3-d]pyrimi-

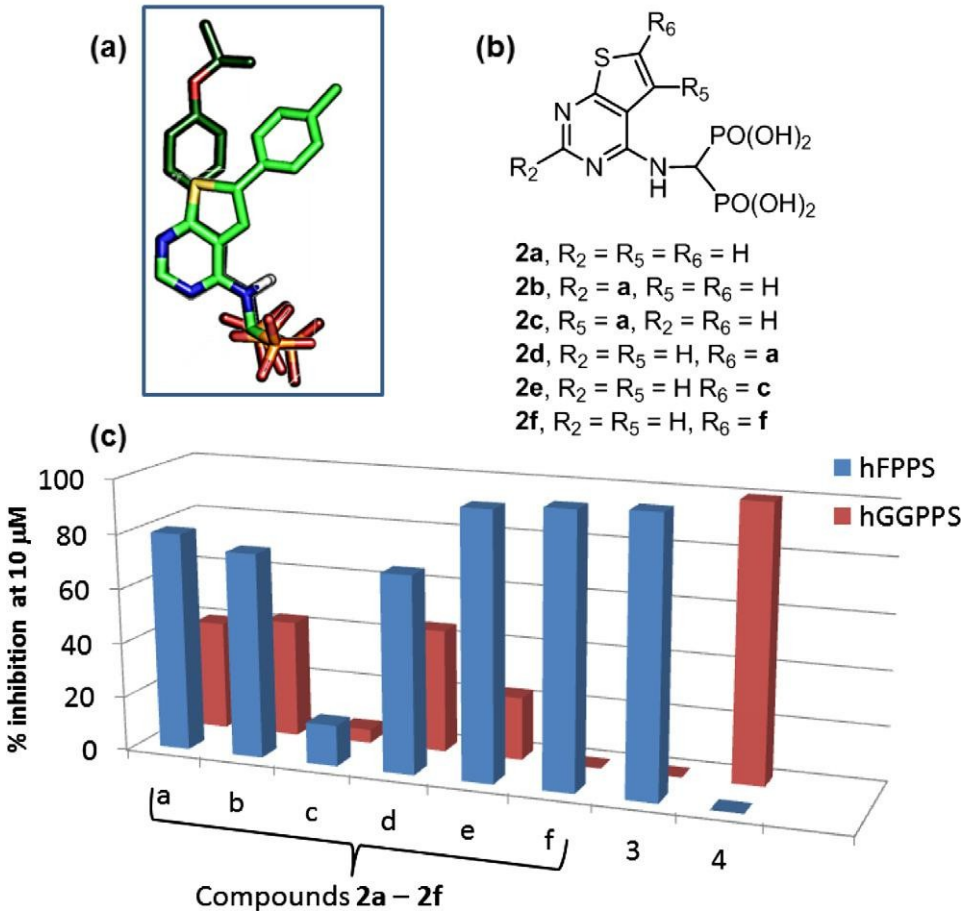

Figure 2. Inhibition data for human FPPS and GGPPS of select thienopyrimide-based bisphosphonates 2a–2f (R_2, R_5 and R_6 substituents are selected from those shown in Table 1). (a) Superposition of analog 2e with the bioactive conformation of inhibitor 3 (PDB: 4DEM). The carbon skeleton of 2e and 3 are highlighted in light and dark green colour, respectively; nitrogen, oxygen, sulphur and phosphorus atoms are indicated in blue, red, yellow and orange colour, respectively. (b) Structures of key thienopyrimide-based bisphosphonate compounds. (c) Inhibition data for hFPPS and hGGPPS at 10 lM of inhibitor; the hFPPS and hGGPPS inhibitors 3 and 4, respectively (Fig. 1) were used as +ve/_ve controls (% inhibition at 10 lM concentration of inhibitor; average values of three determinations; standard deviation ±10%).

din-4-amines (1k–o, Table 1) in good overall yield. For example, preparation of analogs 1l from 15 was achieved in seven steps (including cross coupling under typical Suzuki and Sonogashira conditions at C-5 and C-4, respectively) in an overall isolated yield of 50%. Similarly, analog 1m (involving Buchwald–Hartwig amina-tion in the conversion of 19a–19b) was prepared from 15 in 30% isolated overall yield. It should be noted that these reactions were not individually optimized during preparation of our library. Ana-log 1a (Table 1) was prepared by a different synthetic scheme, involving direct condensation of 2-aminothiophene-3-carbonitrile with benzonitrile under basic condition and at high temperature, as previously reported.[19]

To gain some insight as to the potential for developing favour-able structure–activity-relationship (SAR) for thienopyrimidine-based inhibitors of hFPPS and/or hGGPPS, a small cluster of analogs from this library were converted to the corresponding bisphospho-nates 2 (Scheme 2). Treatment of fragments 1 with triethyl ortho-formate and diethylphosphite, followed by hydrolysis of the tetraethyl bisphosphonate esters with TMSBr/MeOH resulted in the formation of bisphosphonic acids 2 (Scheme 2); details of this two-step protocol were previously described in the synthesis of the hFPPS inhibitor 3.[21]

2.2. Biological results and discussion

Initially, the bisphosphonic acid analogs 2a–f (Fig. 2b) were evaluated in our routine hFPPS and hGGPPS inhibition assays at a single concentration of 10 lM (as previously reported),[21] along with inhibitors 3 (IC_{50} = 28 nM in hFPPS; IC_{50} >100 lM in hGGPPS) and 4 (IC_{50} = 410 nM in our own hGGPPS assay;[21] IC_{50} >10 lM in hFPPS[40]) as the positive controls. The inhibition data observed are summarized in Figure 2c (% inhibition of hFPPS and hGGPPS at 10 lM of compound; average values of three determinations; standard deviation of approximately 10%). Significant inhibition of hFPPS was observed with the parent molecule 2a, as well as the C-2 and C-6 phenyl analogs 2b and 2d, respectively (75–80% inhibition at 10 lM). However, analog 2c exhibited <20% inhibi-tion at 10 lM (Fig. 2b and c). These preliminary data suggest that C-2 and C-6 derivatives of the thienopyrimidine core may be ben-eficial in developing inhibitors of hFPPS, whereas favourable sub-stitution at C-5 may be limited. In order to gain further insight as to the volume of space within the hFPPS binding pocket occu-pied by the substituents at C-6, the tolyl and naphthyl moieties (2e and 2f, respectively) were also investigated. These modifica-tions resulted in modest improvement in inhibiting hFPPS (Fig. 2c). The full dose response for hFPPS inhibition was subse-quently determined for analogs 2e and 2f and their IC_{50} values were calculated to be 390 and 250 nM, respectively. Interestingly, this modest SAR optimization (i.e., compounds 2e and 2f) also improved the selectivity in inhibiting hFPPS as compared to hGGPPS (Fig. 2c).

Superposition of the hFPPS-bound conformation of inhibitor 3 (IC_{50} = 28 nM; PDB: 4DEM),[21] with the thienopyrimidine analog 2e strongly suggests that these compounds cannot adopt the same

binding mode in the active site of hFPPS (Fig. 2a). Therefore, the thienopyrimidine-based bisphosphonates 2e and 2f represent novel leads for drug discovery into hFPPS inhibitors. To fully ex-plore the SAR potential of these compounds, synthesis of a larger and structurally diverse library of bisphosphonate analogs is cur-rently in progress. Concurrently, we are pursuing a number of structural investigations in order to determine the mechanism by which these compounds inhibit hFPPS.

3. Conclusion

Currently, nitrogen-containing bisphosphonates (N-BPs) are the only clinically validated drugs that target the human FPPS, thus blocking prenylation.[33,34] Although these drugs are mainly used for the treatment of bone-related diseases, recent clinical data pro-vides evidence that N-BPs are also disease modifying agents that improve the survival of cancer patients (particularly of patients with multiple myeloma[35]) via mechanisms unrelated to their ske-letal effects. In an effort to identify compounds with improved bio-pharmaceutical properties (as compared to those of the current drugs), we designed a new class of bisphosphonates based on the thienopyrimidine scaffold 1. Thienopyrimidines are usually pre-pared via the Gewald method. However, this approach is not easily amenable to parallel synthesis of highly substituted and structu-rally diverse analogs. In addition, structural diversity is typically dictated by the starting ketones 5 (Scheme 1); thus the synthesis is linear and does not allow preparation of permutation libraries. Furthermore, selective mono-substitution at the C_b of the thio-phene sulfur is challenging due to the inherent higher reactivity of the C_a carbon. We modified the classical Gewald methodology by employing 2-(1-(trimethylsilyl)-ethylidene)-malononitrile (14) as a novel synthon in the preparation of thieno[2,3-d]pyrimid-4-amine libraries (1; Scheme 2). Preparation of 5-iodothieno[2,3-d]pyrimidin-4-amine (20b) was achieved in high yields and signif-icantly fewer steps as compared to previous reports. This metho-dology was then used to prepare a small cluster of thienopyrimidine-based bisphosphonate compounds (2) and probe the ability to such N-BPs to inhibit the hFPPS. In depth SAR studies and structural investigations are currently in progress in order to evaluate the potential of these compounds for further optimization into potent and selective inhibitors of hFPPS.

4. Experimental

4.1. General procedures for characterization of compounds

All intermediate compounds were purified by normal phase flash column chromatography on silica gel using a CombiFlash in-strument and the solvent gradient indicated. Key thienopyrimidine building blocks, bisphosphonate esters and all final bisphosphonic acid inhibitors were analyzed by reverse-phase HPLC and fully characterized by ^{1}H, ^{13}C and ^{31}P NMR, and MS (HR-MS for key frag-ments and final inhibitors). Chemical shifts (d) are reported in ppm relative to the internal deuterated solvent (^{1}H, ^{13}C) or external H_3PO_4 (d 0.00 ^{31}P), unless indicated otherwise. High-resolution MS spectra were recorded using electrospray ionization (ESI+/_) and Fourier transform ion cyclotron resonance mass analyzer (FTMS). Melting points (when relevant) were determined using a conventional capillary melting point analyzer. The homogeneity of the bisphosphonate tetra esters and the final bisphosphonic acid inhibitors was confirmed by HPLC to >90% (using the conditions in-dicated below); IC_{50} values were determined only for samples with >95% homogeneity. HPLC analysis was performed using a Waters ALLIANCE instrument (e2695 with 2489 UV detector and 3100 mass spectrometer).

Method (homogeneity analysis using a Waters Atlantis T3 C18 5 lm column):

Solvent A: H_2O, 0.1% formic acid.
Solvent B: CH_3CN, 0.1% formic acid.
Mobile phase: linear gradient from 95% A and 5% B to 5% A and 95% B in 13 min, then 2 min at 100% B.
Flow rate: 1 mL/min.

4.2. Synthesis of key fragments

4.2.1. 2-(1-(Trimethylsilyl)ethyl)malononitrile (14)

Acetyltrimethylsilane (1.460 g, 12.56 mmol), malononitrile (1.140 g, 12.56 mmol) and ammonium acetate (262.1 mg, 2.386 mmol) were dissolved in acetic acid (0.58 mL, 10.05 mmol) and benzene (30 mL) in a 100 mL round bottom flask attached to a Dean–Stark trap and filled with benzene. The reaction mixture was stirred and heated to 95 LC for 24 h. The resulting orange solu-tion was cooled and diluted with ethyl acetate (20 mL). The organic layer was washed with saturated sodium bicarbonate solution (15 mL), water (45 mL), brine (15 mL) and dried over $MgSO_4$. The product was purified by column chromatography (25% ethyl acet-ate/hexanes) to give the desired product as clear pale yellow oil in 90% yield (1.973 g).

^{1}H NMR (400 MHz, $CDCl_3$) d 2.34 (s, 3H), 0.36 (s, 9H).
^{13}C NMR (126 MHz, $CDCl_3$) d 188.3, 113.2, 111.5, 94.4, 24.3, _2.2.

HRMS (ESI_) Calcd for $C_8H_{11}N_2Si$ m/z $[M\_H]^-$: 163.06970, found m/z 163.06875 and HRMS (ESI_) Calcd 327.14667 for $C_{16}H_{23}N_4Si_2$, found m/z 327.14695 $[2M\_H]^-$.

4.2.2. 2-Amino-4-(trimethylsilyl)thiophene-3-carbonitrile (15)

2-(1-(Trimethylsilyl)ethyl)malononitrile (1.21 g, 7.365 mmol) and sulfur (248.02 mg, 7.734 mmol) were dissolved in pyridine (25 mL) at room temperature. To this, diethylamine (0.762 mL, 7.365 mmol) was added dropwise. The reaction mixture stirred at room temperature for 18 h. Evaporation of pyridine afforded the crude thiophene, which was dissolved in ethyl acetate (20 mL) and washed with water (45 mL), brine (15 mL), and dried over $MgSO_4$. Purification by column chromatography (25% ethyl acetate/hexanes, R_f = 0.58) afforded the desired product as an or-ange oil in 85% yield (803.5 mg).

^{1}H NMR (300 MHz, $CDCl_3$) d 6.38 (s, 1H), 4.74 (br s, 2H), 0.30 (s, 9H).
^{13}C NMR (126 MHz, $CDCl_3$) d 164.3, 141.1, 116.8, 116.7, 92.3, _1.3.
HRMS (ESI+) Calcd 197.05632 for $C_8H_{13}N_2SSi$, found m/z 197.05615 $[M+H]^+$.

4.2.3. 5-(Trimethylsilyl)thieno[2,3-d]pyrimidin-4-amine (20a)

Fragment 20a was obtained in two different ways: (a) 2-Amino-4-(trimethylsilyl)thiophene-3-carbonitrile (15a, 400 mg, 2.04 mmol, 1 equiv) was added to formamide (8.1 mL, 200 mmol, 100 equiv) in a pressure vessel. The reaction mixture was sealed and stirred at 145 LC in the dark for 16 h. (b) 3-Cyano-4-(trimethyl-silyl)thiophen-2-yl)-N,N-dimethylformimidamide (79.3 mg, 0.315 mmol) was reacted with formamide (anhydrous, 2.5 mL, 63.08 mmol) in a dry 15 mL pressure vessel. The vessel was flushed with argon and the mixture stirred at 130 LC for 45 h. The dark red solution was diluted with ethyl acetate, washed with water (25 mL), brine (10 mL), and dried over Na_2SO_4. The crude mixture

was purified by flash column chromatography (5–30% EtOAc/hexanes, dry loading) to afford the desired product as a pink solid in 80% yield (59.0 mg).

^{1}H NMR (400 MHz, $CDCl_3$) d 8.47 (s, 1H), 7.43 (s, 1H), 5.36 (br s, 2H), 0.46 (s, 9H).
^{13}C NMR (126 MHz, $CDCl_3$) d 170.9, 158.8, 153.6, 133.2, 131.3, 119.8, 0.4.
HRMS (ESI+) Calcd 224.06722 for $C_8H_{13}N_2SSi$, found m/z 224.06705 $[M+H]^+$.

4.2.4. 5-Iodothieno[2,3-d]pyrimidin-4-amine (20b)

A solution of 5-(trimethylsilyl)thieno[2,3-d]pyrimidin-4-amine (220.4 mg, 0.987 mmol, 1 equiv) in dichloromethane (2 mL) was stirred at _10 LC ice slurry for 5 min. 1 M Iodine monochloride in dichloromethane (2.96 mL, 2.96 mmol, 3 equiv) was added to the reaction mixture dropwise and the reaction mixture was stirred at _10 LC for 30 min. Ice cooled water (30 mL) was directly added to the reaction mixture to quench the reaction. Dichloromethane (2 _ 20 mL) at room temperature was added to the mixture and the entire mixture was filtered through a Whatman #5 2.5 lm fil-ter paper. The yellowish solid was washed with dichloromethane (2 _ 10 mL) and recrystallized with methanol to give the desired product 5-iodothieno[2,3-d]pyrimidin-4-amine as a yellow colored solid (271.9 mg, >98% yield).

^{1}H NMR (300 MHz, CD_3CN): d 8.33 (1H, s), 7.79 (1H, s), 7.44 (br s, 2H).
^{13}C NMR (126 MHz, acetone-d_6) d 159.5, 154.7, 128.6, 116.4, 106.1, 70.5.
HRMS (ESI+) Calcd 277.92434 for $C_6H_4IN_3S$, found m/z 277.92353 $[M+H]^+$.
Melting point: 196 LC (dec).

4.2.5. 3-Cyano-4-(trimethylsilyl)thiophen-2-yl)-N,N-dimethylformimidamide (16)

To a solution of 2-amino-4-(trimethylsilyl)thiophene-3-carbo-nitrile (15, 372.40 mg, 1.90 mmol) in DMF (20 mL) was added DMF–DMA (2.5 mL, 18.97 mmol). After stirring at room tempera-ture for 4 h, the reaction mixture was diluted with ethyl acetate, washed with water (60 mL), brine (20 mL), and dried over $MgSO_4$. Solvent was removed in vacuo to afford the desired product as a brown-yellow solid in 90% yield (440.1 mg).

^{1}H NMR (500 MHz, $CDCl_3$) d 7.72 (s, 1H), 6.63 (s, 1H), 3.10 (s, 3H), 3.09 (s, 3H), 0.32 (s, 9H).
^{13}C NMR (126 MHz, $CDCl_3$) d 168.9, 154.8, 141.6, 120.7, 117.5, 101.2, 40.7, 35.2, _1.3.
^{29}Si NMR (99 MHz, $CDCl_3$) d _6.69.
HRMS (ESI+) Calcd 252.09852 for $C_{11}H_{18}N_3SSi$, found m/z 252.09781 $[M+H]^+$.

4.2.6. 5-Bromo-3-cyano-4-(trimethylsilyl)thiophen-2-yl-N,N-dimethylformimidamide (17)

N-Bromosuccinimide (121.2 mg, 0.68 mmol) was added to a solution of 3-cyano-4-(trimethylsilyl)thiophen-2-yl-N,N-dimethyl-formimidamide (163.0 mg, 0.648 mmol) in DMF (7 mL). The yellow solution was stirred in the absence of light at room tem-perature for 13 h. The mixture was diluted with ethyl acetate, washed with water (25 mL), brine (10 mL), and dried over $MgSO_4$. Solvent was removed in vacuo to afford the desired product as a brown-orange solid in 80% yield (177.1 mg).

^{1}H NMR (500 MHz, $CDCl_3$) d 7.63 (s, 1H), 3.09 (s, 6H), 0.44 (s, 9H).
^{13}C NMR (126 MHz, $CDCl_3$) d 168.4, 154.6, 138.9, 116.7, 106.2, 101.9, 40.8, 35.3, 0.2.
HRMS (ESI+) Calcd 330.00903 for $C_{11}H_{17}N_3BrSSi$, found m/z 330.00926 $[M+H]^+$.

4.2.7. 5-Bromo-3-cyanothiophen-2-yl-N,N-dimethylformimidamide

A 1 M solution of TBAF (5.13 mL) in THF was added dropwise to a solution of 5-bromo-3-cyano-4-(trimethylsilyl)thiophen-2-yl-N,N-dimethylformimidamide (17, 1.61 g, 4.89 mmol) in THF (100 mL) cooled to 0 LC. The reaction mixture was warmed to room temperature and stirred in the dark for 3 h. The volume of THF was reduced in vacuo and EtOAc was added, washed with water (3 _ 50 mL), brine (25 mL), and dried over Na_2SO_4. The desired crude product was obtained as a red oil in 95% yield (1.20 g) and used as such for the synthesis of analogs 1, where R_5 = H without any further purification.

^{1}H NMR (400 MHz, $CDCl_3$) d 7.64 (s, 1H), 6.86 (s, 1H), 3.11 (s, 6H).
^{13}C NMR (300 MHz, $CDCl_3$) d 167.0, 154.2, 128.3, 115.1, 99.4, 96.5, 40.8, 35.2.
MS (ESI+) m/z: 258.06 $[M+H]^+$.

4.2.8. N^0-(3-Cyano-4-iodo-5-phenylthiophen-2-yl)-N,N-dimethylformimidamide (19a, R_5 = a)

Silver trifluoroacetate (93.2 mg, 0.42 mmol) was added to a solution of N^0-(3-cyano-5-phenyl-4-(trimethylsilyl)thiophen-2-yl)-N,N-dimethylformimidamide (69.1 mg, 0.21 mmol) in THF (20 mL) cooled to _78 LC and stirred under argon for 15 min. Io-dine (214.2 mg, 0.84 mmol) dissolved in THF (10 mL) was added dropwise to the cold mixture and stirred in the dark at _78 LC for 4 h. Ethyl acetate was added and the mixture was filtered through Celite. The filtrate was washed with 2 M sodium thiosul-fate, brine, and dried over Na_2SO_4. The crude mixture was purified by flash column chromatography (5–30% EtOAc/hexanes, solid loading) to afford the desired product as an orange solid in >98% yield (80.0 mg).

^{1}H NMR (400 MHz, $CDCl_3$) d 7.77 (s, 1H), 7.58–7.51 (m, 2H), 7.40 (m, 3H), 3.13 (s, 6H).
^{13}C NMR (75 MHz, $CDCl_3$) d 167.2, 154.7, 134.1, 130.7, 129.5, 128.7, 128.6, 116.8, 105.7, 78.1, 40.9, 35.3.
HRMS (ESI+) Calcd 381.98694 for $C_{14}H_{13}N_3IS$, found m/z 381.98667 $[M+H]^+$.

4.3. Synthesis of thieno[2,3-d]pyrimidin-4-amines—general protocols

4.3.1. Suzuki coupling reactions using fragment 20b

Fragment 20b is not very soluble in non-polar solvents; consequently all reactions were carried out in MeOH. To an argon flushed microwave reactor vial, fragment 20b, the boronic acid or boronate ester (1.4 equiv) and $Pd(PPh_3)_4$ (0.1 equiv) and KF (2.5 equiv) were added and flushed again with argon. Argon flushed methanol was added to the reaction mixture and the reac-tion was stirred at 120 LC for 20 min (120 W). The crude mixture was filtered through celite and concentrated to dryness under va-cuum. The crude product was purified by normal phase flash col-umn chromatography on silica gel (silica gel was pre-washed

with hexanes) using a CombiFlash instrument and a solvent gradi-ent from 100% hexanes to 100% EtOAc.

4.3.2. General protocol for the Suzuki coupling reactions using fragment 17

In order to probe the versatility and stability of fragment 17, Suzu-ki coupling reactions were carried out using two different reaction conditions: (a) The boronic acid or boronate ester (1.5 equiv), $Pd(PPh_3)_4$ (0.1 equiv) and fragment 17 were dissolved in toluene/ethanol (3:1) (approximate concentration with respect to 17 of 0.1 M). The mixture was degassed and flushed with Argon. Aqueous 2 M Na_2CO_3 (2.5 equiv) was added and the mixture was again de-gassed and flushed with Argon. The reaction mixture was stirred at 85 LC overnight. The crude was filtered through a plug of celite, rinsed with 10 mL of solvent and concentrated under vacuum. The residue was purified on silica gel using a CombiFlash instrument to give the desired products (the common solvent gradient was from 2% EtOAc in hexanes to 100% EtOAc, unless otherwise indicated). (b) The proto-col described for the Suzuki reactions using fragment 20b was also used successfully; presumably the TMS group survives these condi-tions due to high solvation of the fluoride ion in methanol.

4.3.3. General protocol for Stille cross-coupling reactions using fragment 19a

Palladium acetate (1 equiv) and XPhos (2 equiv) in DME (2 mL) were heated under argon to 85 LC in a 2-dram vial for 10 min. To this mixture cesium carbonate (2 equiv), and fragment 19a (1 equiv 0.3 mmol) were added and stannane (1.77 equiv). The vial was flushed with argon and the reaction mixture was stirred at 80 LC for 15 h. The reaction mixture was diluted with EtOAc (10 mL), washed with water (3 _ 10 mL) and brine (10 mL), dried over Na_2SO_4, and concentrated under vacuum. The crude residue was purified by column chromatography on silica gel using a Com-biFlash instrument and a solvent gradient from% EtOAc in hexanes to 100% EtOAc, unless otherwise indicated.

4.3.4. General protocol for Sonogashira cross-coupling reactions using fragment 19a

Triethylamine (0.5 mL) was added to a vial of the iodide 19a (0.081 mmol), acetylene (0.018 mL, 0.16 mmol), copper(II) bro-mide (2.7 mg, 0.012 mmol), and $Pd(PPh_3)_4$ (9.4 mg, 0.008 mmol). The vial was purged with argon, capped, and heated to 90 LC for 13 h. Extracted with EtOAc (3 _ 10 mL) and washed with saturated sodium bicarbonate (5 mL), water (3 _ 5 mL), brine (5 mL), and dried over Na_2SO_4. The crude mixture was purified by flash column chromatography on silica gel (solid loading) using a solvent gradi-ent from 2% EtOAc in hexanes to 100% EtOAc (unless otherwise in-dicated) to afford the desired product.

4.3.5. General protocol for Buchwald–Hartwig amination reactions using fragment 19a

The amine (5 equiv) was added to a degassed solution of frag-ment 19a (usually on a 0.03 mmol scale), $Pd_2(dba)_3$ (5 mol %), XantPhos (11 mol %), and cesium carbonate (1.7 equiv) in toluene (1 mL). The vial was purged with argon and the reaction mixture stirred at 100 LC for 18 h. A second portion of $Pd_2(dba)_3$ (5 mol %) and XantPhos (11 mol %) were added and the reaction mixture was stirred at 100 LC for an additional 18 h. The reaction mixture was diluted with EtOAc (10 mL), washed with water (3 _ 10 mL) and brine (10 mL), dried over Na_2SO_4, and concentrated under va-cuum. The crude residue was purified by column chromatography on silica gel using a CombiFlash instrument and a solvent gradient from 2% EtOAc in hexanes to 100% EtOAc (unless otherwise indi-cated) to afford the desired product.

4.3.6. General protocol for the cyclization of C-4 and/or C-5 substituted fragments 18 or 19b to thieno[2,3-d]pyrimidin-4-amines 1

The mono-substituted or di-substituted fragments 18 or 19b, respectively, (0.04 mmol) and dry formamide (excess, >200 equiv) were added to a dry 15 mL pressure vessel. The vessel was flushed with argon and the mixture stirred at 130 LC for 48 h. The dark red solution was diluted with EtOAc, washed with water (25 mL), brine (10 mL), and dried over Na_2SO_4. The crude mixture was purified by flash column chromatography (5–100% EtOAc/hexanes, solid load-ing) to afford the desired product.

4.4. Spectral data of key synthetic intermediates 18

The R5 groups indicated are taken from the fragments shown in Table 1.

4.4.1. N^0-(3-Cyano-5-phenyl-4-(trimethylsilyl)thiophen-2-yl)-N,N-dimethylformimidamide (18, R_5 = a)

Isolated as a beige solid in 90% yield (179 mg).

^{1}H NMR (400 MHz, $CDCl_3$) d 7.71 (s, 1H), 7.36–7.33 (m, 5H), 3.12 (s, 3H), 3.08 (s, 3H), 0.12 (s, 9H).
^{13}C NMR (126 MHz, $CDCl_3$) d 167.8, 154.6, 139.1, 136.3, 135.9, 130.6, 128.5, 128.1, 118.0, 102.7, 40.7, 35.2, 0.4.
HRMS (ESI+) Calcd 328.12982 for $C_{17}H_{22}N_3SSi$, found m/z 328.12920 $[M+H]^+$.

4.4.2. N^0-(3-Cyano-5-(p-tolyl)-4-(trimethylsilyl)thiophen-2-yl)-N,N-dimethylformimidamide (18, R_5 = c)

Isolated as a pale yellow solid in 75% yield (115 mg).

^{1}H NMR (400 MHz, $CDCl_3$) d 7.79 (s, 1H), 7.21 (d, J = 8 Hz, 2H), 7.15 (d, J = 8 Hz, 2H), 3.32 (s, 3H), 3.20 (s, 3H), 2.38 (s, 3H), 0.14 (s, 9H).
^{13}C NMR (126 MHz, $CDCl_3$) d 167.6, 154.5, 139.3, 138.3, 135.9, 132.8, 130.4, 128.7, 117.9, 102.6, 40.6, 35.0, 21.4, 0.5.
HRMS (ESI+) Calcd 342.14547 for $C_{18}H_{24}N_3SSi$, found m/z 342.14458 $[M+H]^+$.

4.4.3. N^0-(3-Cyano-5-(4-(trifluoromethyl)phenyl)-4-(trimethylsilyl)thiophen-2-yl)-N,N-dimethylformimidamide (18, R_5 = e)

Isolated as a pale brown solid in 71% yield (49.6 mg).

^{1}H NMR (300 MHz, $CDCl_3$) d 7.72 (s, 1H), 7.61 (d, J = 8 Hz, 2H), 7.46 (d, J = 8 Hz, 2H), 3.12 (d, J = 12 Hz, 6H), 0.14 (s, 9H).
^{13}C NMR (75 MHz, $CDCl_3$) d 168.3, 154.7, 139.7, 137.4, 136.8, 130.5 (q, J_{CF} = 33 Hz), 125.0 (q, J_{CF} = 4 Hz), 124.1 (q, J_{CF} = 272 Hz), 117.7, 103.1, 40.8, 35.2, 0.5.
HRMS (ESI+) Calcd 396.11775 for $C_{18}H_{21}F_3N_3SSi$, found m/z 396.11519 $[M+H]^+$.

4.4.4. N^0-(3-Cyano-5-(naphthalen-2-yl)-4-(trimethylsilyl)thiophen-2-yl)-N,N-dimethylformimidamide (18, R_5 = f)

Isolated as an orange solid in 63% yield (72.1 mg).

^{1}H NMR (400 MHz, $CDCl_3$): d 7.87–7.81 (m, 5H), 7.74 (s, 1H), 7.53–7.51 (m, 2H), 7.46 (m, 1H), 3.15 (s, 3H), 3.10 (s, 3H) 0.13 (9H, s).
^{13}C NMR (75 MHz, $CDCl_3$): d 167.9, 154.6, 139.1, 136.6, 133.3, 133.0, 132.8, 129.6, 128.4, 128.1, 127.9, 127.7, 126.7, 126.6, 40.7, 35.2, 0.6.
HRMS (ESI+) Calcd 378.14547 for $C_{21}H_{24}N_3SSi$, found m/z 378.14412 $[M+H]^+$.

4.4.5. N^0-(4-Cyano-3-(trimethylsilyl)-[2,3^0-bithiophen]-5-yl)-N,N-dimethylformimidamide(18, R_5 = i)
Isolated as light brown solid in 75% yield (53.1 mg).

^{1}H NMR (400 MHz, $CDCl_3$): d 7.70 (s, 1H), 7.31–7.29 (m, 1H), 7.23 (m, 1H), 3.12 (3H, s), 3.09 (3H, s), 0.15 (s, 9H).
^{13}C NMR (75 MHz, $CDCl_3$): d 167.6, 154.7, 154.6, 137.3, 135.7, 132.9, 130.0, 125.5, 125.3, 117.8, 102.5, 40.7, 35.2, 0.2.
HRMS (ESI+) Calcd 334.08624 for $C_{15}H_{20}N_3S_2Si$, found m/z 334.08530 $[M+H]^+$.

4.4.6. N^0-(3-Cyano-4-(trimethylsilyl)-5-vinylthiophen-2-yl)-N,N-dimethylformimidamide (18, R_5 = h)
Isolated as beige solid in 75% yield (63 mg) and 95% purity (as determined by LC–MS). The impurity was determined to be the de-halogenated thiophene, however, this compound was eliminated from the library for the subsequent steps.

^{1}H NMR (400 MHz, $CDCl_3$) d 7.72 (s, 1H), 6.86 (dd, J = 16.9, 10.8 Hz, 1H), 5.36 (d, J = 17.0 Hz, 1H), 5.10 (d, J = 10.8 Hz, 1H), 3.12 (s, 3H), 3.10 (s, 3H), 0.41 (s, 9H).
^{13}C NMR (75 MHz, $CDCl_3$) d 166.3, 154.8, 138.1, 137.5, 130.7, 117.5, 113.6, 103.0, 40.7, 35.1, 0.8.
HRMS (ESI+) Calcd 278.11417 for $C_{13}H_{20}N_3SSi$, found m/z 278.11400 $[M+H]^+$.

4.5. Spectral data of key synthetic intermediates 19

The R_4 and/or R_5 groups indicated are taken from the fragments shown in Table 1.

4.5.1. N^0-(3-Cyano-5-phenyl-4-(pyrazin-2-yl)thiophen-2-yl)-N,N-dimethylformimidamide (19b, R_4 = b, R_5 = a)
Isolated as beige solid in 41% yield (8.0 mg) and 95% purity (as determined by LC–MS).

^{1}H NMR (400 MHz, $CDCl_3$): d 8.67 (dd, J = 2.6, 1.6 Hz, 1H), 8.46 (d, J = 2.6 Hz, 1H), 8.36 (d, J = 1.5 Hz, 1H), 7.85 (s, 1H), 7.28–7.25 (m, 3H), 7.17–7.14 (m, 2H), 3.15 (s, 3H), 3.15 (s, 3H).
^{13}C NMR (75 MHz, $CDCl_3$): d 166.9, 154.6, 149.3, 145.8, 144.5, 143.1, 132.7, 132.2, 131.1, 129.3, 129.0, 128.4, 115.9, 99.2, 40.9, 35.3.
HRMS (ESI+) Calcd 334.11209 for $C_{18}H_{16}N_5S$, found m/z 334.11144 $[M+H]^+$.

4.5.2. N^0-(3-Cyano-5-phenyl-4-(phenylethynyl)thiophen-2-yl)-N,N-dimethylformimidamide (19b, R_4 = g, R_5 = a)
Isolated as a red-orange solid in 95% yield (28.0 mg).

^{1}H NMR (400 MHz, $CDCl_3$) d 7.86–7.75 (d, J = 7.4 Hz, 3H), 7.83 (s, 1H), 7.57–7.51 (m, 2H), 7.42 (t, J = 7.5 Hz, 2H), 7.37–7.30 (m, 4H), 3.15 (s, 3H), 3.15 (s, 3H).
^{13}C NMR (126 MHz, $CDCl_3$) d 164.2, 154.6, 134.0, 133.3, 131.9, 128.8, 128.7, 128.5, 128.2, 127.5, 122.9, 116.6, 115.5, 100.9, 94.7, 83.3, 40.9, 35.3.
HRMS (ESI+) Calcd 356.12159 for $C_{22}H_{18}N_3S$, found m/z 356.12098 $[M+H]^+$.

4.5.3. N^0-(3-Cyano-4-(cyclopropylethynyl)-5-phenylthiophen-2-yl)-N,N-dimethylformimidamide (19b, R_4 = h, R_5 = a)
Isolated beige solid in 90% yield (15 mg, based on the recovery of some starting material).

^{1}H NMR (500 MHz, $CDCl_3$) d 7.78–7.75 (m, 3H), 7.38–7.35 (m, 2H), 7.30–7.26 (m, 1H), 3.10 (s, 6H), 1.52–1.46 (m, 1H), 0.91–0.87 (m, 2H), 0.87–0.83 (m, 2H).
^{13}C NMR (126 MHz, $CDCl_3$) d 163.8, 154.5, 133.30, 132.9, 128.6, 127.9, 127.1, 117.2, 115.6, 101.4, 99.6, 69.4, 40.9, 35.2, 9.1, 0.7.
HRMS (ESI+) Calcd 320.12159 for $C_{19}H_{18}N_3S$, found m/z 320.12139 $[M+H]^+$.

4.5.4. N^0-(3-Cyano-4-morpholino-5-phenylthiophen-2-yl)-N,N-dimethylformimidamide (19b, R_4 = j, R_5 = a)
Isolated as a beige solid in 90% yield (9.5 mg).

^{1}H NMR (400 MHz, $CDCl_3$) d 7.74 (s, 1H), 7.50 (d, J = 7.3 Hz, 2H), 7.35 (t, J = 7.5 Hz, 2H), 7.29 (t, J = 7.3 Hz, 1H), 3.75–3.71 (m, 4H), 3.12 (s, 3H), 3.10 (s, 3H), 3.10–3.07 (m, 4H).
^{13}C NMR (126 MHz, $CDCl_3$) d 164.4, 153.9, 143.8, 133.6, 129.3, 128.4, 127.6, 118.4, 116.3, 96.6, 67.5, 51.7, 40.9, 35.2.
HRMS (ESI+) Calcd 341.14306 for $C_{18}H_{21}ON_4S$, found m/z 341.14218 $[M+H]^+$.

4.5.5. N^0-(4-(Benzyl(methyl)amino)-3-cyano-5-phenylthiophen-2-yl)-N,N-dimethylformimidamide (19b, R_4 = k, R_5 = a)
The crude residue was purified by column chromatography on a CombiFlash instrument using a solvent gradient from 3% EtOAc/hexanes to 100% EtOAc with 0.1% triethylamine. The desired pro-duct was obtained in 45% yield (19 mg), 70% purity (as determined by ^{1}H NMR). The impurity was determined to be the dehaloge-nated thiophene and was eliminated in the following step.

^{1}H NMR (400 MHz, $CDCl_3$) d 7.76 (s, 1H), 7.50–7.44 (m, 1H), 7.38–7.27 (m, 5H), 7.25–7.21 (m, 4H), 4.16 (s, 2H), 3.14–3.07 (m, 8H), 2.74 (s, 3H).
^{13}C NMR (75 MHz, $CDCl_3$) d 164.2, 153.9, 144.6, 138.4, 133.7, 129.1, 128.9, 128.3, 128.2, 127.6, 127.3, 127.1, 125.3, 121.9, 120.1, 116.6, 96.9, 60.1, 41.1, 35.2.
HRMS (ESI+) Calcd 375.16379 for $C_{22}H_{23}N_4S$, found m/z 375.16296 $[M+H]^+$.

4.6. Spectral data of key thieno[2,3-d]pyrimidin-4-amines (1)

The yields indicated are for the isolated pure fragments after the cyclization step of 19b–1 from the library synthesis. For the key building blocks 5-(trimethylsilyl)thieno[2,3-d]pyrimidin-4-amine (20a) and 5-iodothieno[2,3-d]pyrimidin-4-amine (20b), refer to Sections 4.2.3 and 4.2.4, respectively.

4.6.1. 2-Phenylthieno[2,3-d]pyrimidin-4-amine (1a)
Synthesis of derivative 20c was achieved via direct condensa-tion of 2-aminothiophene-3-carbonitrile with benzonitrile, as previously reported.[12b] To an argon flushed pressure vessel, 2-

aminothiophene-3-carbonitrile (150 mg, 1.21 mmol, 1 equiv), benzonitrile (174.4 mg, 1.69 mmol, 1.4 equiv) and potassium tert-butoxide (135.3 mg, 1.21 mmol, 1 equiv) were added and the mixture was flushed again with argon. Anhydrous dioxane (1 mL) was added and the reaction mixture was stirred at 150 LC for 14 h. The crude mixture was concentrated to dryness under vacuum and was purified by flash column chromatogra-phy (0–50% EtOAc/hexanes, solid loading) to afford the final pro-duct in 27% yield (37.7 mg).

^{1}H NMR (500 MHz, $CDCl_3$): d 8.45–8.42 (m, 2H), 7.48–7.45 (m, 3H), 7.26 (d, J = 6.0 Hz, 1H), 7.14 (d, J = 6.0 Hz, 1H), 5.55 (s, 2H). ^{13}C NMR (126 MHz, $CDCl_3$): d 168.9, 160.3, 157.8, 137.9, 130.1, 128.4, 128.2, 123.3, 117.4, 114.3.
MS (ESI+) m/z: 228.1 $[M+H]^+$.

4.6.2. 5-Phenylthieno[2,3-d]pyrimidin-4-amine (1b)
Isolated as pale yellow solid in 22% yield (27 mg).

^{1}H NMR (500 MHz, CD_3OD): d 8.29 (s, 1H), 7.51–7.46 (m, 5H), 7.31 (s, 1H). ^{13}C NMR (126 MHz, CD_3OD) d 168.3, 160.0, 154.6, 137.2, 136.8, 130.2, 130.1, 129.8, 122.1, 114.9.
MS (ESI+) m/z: 228.4 $[M+H]^+$.

4.6.3. 6-Bromothieno[2,3-d]pyrimidin-4-amine (1c)
Isolated as a pale yellow solid in 35% yield (321 mg).

^{1}H NMR (300 MHz, DMSO-d_6): d 8.22 (1H, s), 7.72 (1H, s), 7.56 (2H, s). ^{13}C NMR (300 MHz, DMSO-d_6): d 167.5, 157.7, 154.8, 123.3, 116.7, 109.7.
MS (ESI+) m/z: 229.9 and 232.0 $[M+H]^+$.

4.6.4. 6-(p-Tolyl)thieno[2,3-d]pyrimidin-4-amine (1d)
Isolated as a beige solid in 65% yield (49.6 mg).

^{1}H NMR (400 MHz, DMSO-d_6): d 8.28 (s, 1H), 8.18 (s, 1H), 8.15 (s, 1H), 8.06–8.01 (m, 2H), 7.96–7.94 (m, 1H), 7.84–7.83 (m, 1H), 7.62–7.53 (m, 4H). ^{13}C NMR (75 MHz, DMSO-d_6) d 165.5, 162.9, 158.2, 154.0, 138.2, 130.5, 129.9, 125.5, 117.0, 114.9, 20.8.
HRMS (ESI+) Calcd for $C_{13}H_{12}N_3S$ m/z $[M+H]^+$: 242.07464, found m/z 242.07383.

4.6.5. 6-(4-(Trifluoromethyl)phenyl)thieno[2,3-d]pyrimidin-4-amine (1e)
Isolated as a pale yellow solid in 56% yield (18.6 mg).

^{1}H NMR (500 MHz, DMSO-d_6): d 8.29 (s, 1H), 8.14 (s, 1H), 7.86 (s, 4H), 7.66 (s, 2H). ^{13}C NMR (126 MHz, DMSO-d_6) d 166.3, 158.5, 154.6, 137.1, 135.7, 128.31 (q, J = 32.0 Hz), 126.3 (q, J = 3.7 Hz), 124.09 (q, J = 272.0 Hz), 117.8, 116.9.
HRMS (ESI+) Calcd 296.04638 for $C_{13}H_9F_3N_3S$, found m/z 296.04552 $[M+H]^+$.

4.6.6. 6-(Naphthalen-2-yl)thieno[2,3-d]pyrimidin-4-amine (1f)
Isolated as a brown solid in 35% yield (15.4 mg).

^{1}H NMR (500 MHz, DMSO-d_6): d 8.28 (s, 1H), 8.18 (s, 1H), 8.15 (s, 1H), 8.06–8.01 (m, 2H), 7.96–7.94 (m, 1H), 7.84–7.83 (m, 1H), 7.62–7.53 (m, 4H). ^{13}C NMR (126 MHz, DMSO-d_6) d 165.9, 158.3, 154.3, 133.0, 132.6, 130.7, 129.0, 128.1, 127.7, 127.0, 126.7, 124.4, 123.4, 117.1, 116.3, 104.6.
HRMS (ESI+) Calcd 278.07464 for $C_{16}H_{11}N_3S$, found m/z 278.07371 $[M+H]^+$.

4.6.7. 6-(Thiophen-3-yl)thieno[2,3-d]pyrimidin-4-amine (1g)
Isolated as a brown solid in 28% yield (9.6 mg).

^{1}H NMR (400 MHz, DMSO-d_6): d 8.24 (s, 1H), 7.78 (m, 2H), 7.73 (dd, J = 5.0, 2.9 Hz, 1H), 7.50 (br s, 2H), 7.41 (dd, J = 5.0, 1.4 Hz, 1H). ^{13}C NMR (126 MHz, DMSO-d_6) d 165.3, 158.1, 154.0, 134.6, 133.1, 128.3, 125.4, 121.9, 116.6, 115.3.
HRMS (ESI+) Calcd 234.01542 for $C_{10}H_7N_3S_2$, found m/z 234.01433 $[M+H]^+$.

4.6.8. 5-(4-Nitrophenyl)thieno[2,3-d]pyrimidin-4-amine (1h)
Isolated as orange solid in 40% yield (14.2 mg); all NMR data was consistent with previous reports.[24]

^{1}H NMR (500 MHz, DMSO-d_6): d 8.37 (s, 1H), 8.34 (d, J = 8.2 Hz, 2H), 7.73 (d, J = 8.2 Hz, 2H), 7.69 (s, 1H), 7.06 (s, 2H).
^{13}C NMR (75 MHz, $CDCl_3$) d 167.7, 158.3, 154.0, 147.1, 142.0, 133.2, 130.1, 123.9, 122.9, 112.2.
MS (ESI+) m/z: 273.1 $[M+H]^+$.

4.6.9. 5-(4-(Trifluoromethyl)phenyl)thieno[2,3-d]pyrimidin-4-amine (1i)
Isolated as a pale yellow solid in 57% yield (28.2 mg).

^{1}H NMR (400 MHz, DMSO-d_6): d 8.36 (s, 1H), 7.87 (d, J = 8.0 Hz), 7.70 (d, J = 8.0 Hz), 7.62 (s, 1H).
^{13}C NMR (126 MHz, DMSO-d_6) d 167.5, 158.3, 153.9, 139.6, 133.6, 129.1, 128.5 (q, J = 32.1 Hz), 125.7 (q, J = 3.8 Hz), 124.3 (q, J = 272.1 Hz), 122.2, 112.4.
HRMS (ESI+) Calcd 296.04638 for $C_{13}H_8F_3N_3S$, found m/z 294.04552 $[M+H]^+$.

4.6.10. 5-(Naphthalen-2-yl)thieno[2,3-d]pyrimidin-4-amine (1j)
Isolated as a pale yellow solid in 54% yield (27.0 mg).

^{1}H NMR (500 MHz, DMSO-d_6): d 8.37 (s, 1H), 8.08–8.00 (m, 4H), 7.62–7.59 (m, 4H).
^{13}C NMR (75 MHz, DMSO-d_6) d 167.3, 158.4, 153.8, 134.9, 133.0, 132.8, 132.4, 128.5, 128.0, 127.8, 127.7, 126.8, 126.7, 126.6, 121.1, 113.0.
HRMS (ESI+) Calcd 278.07464 for $C_{16}H_{11}N_3S$, found m/z 278.07371 $[M+H]^+$.

4.6.11. 6-Phenyl-5-(phenylethynyl)thieno[2,3-d]pyrimidin-4-amine (1k)
Isolated as a brown solid in 85% yield (12 mg).

^{1}H NMR (500 MHz, $CDCl_3$) d 8.45 (s, 1H), 7.96–7.94 (m, 1H), 7.94–7.93 (m, 1H), 7.51–7.47 (m, 4H), 7.45–7.37 (m, 4H), _6.30 (br s, 2H).

^{13}C NMR (126 MHz, $CDCl_3$) d 165.3, 158.4, 154.6, 143.9, 133.0, 131.4, 129.4, 129.3, 129.0, 128.9, 128.6, 122.0, 116.5, 108.8, 94.8, 85.2.
HRMS (ESI+) Calcd 328.09029 for $C_{20}H_{14}N_3S$, found m/z 328.09015 $[M+H]^+$.

4.6.12. 5-(Cyclopropylethynyl)-6-phenylthieno[2,3-d]pyrimidin-4-amine (1l)

Isolated as a beige solid in 85% yield (11 mg).

^{1}H NMR (500 MHz, $CDCl_3$): d 8.39 (s, 1H), 7.88–7.81 (m, 2H), 7.49–7.35 (m, 3H), 1.52 (m, 1H), 0.98–0.92 (m, 2H), 0.84 (m, 2H).

^{13}C NMR (126 MHz, $CDCl_3$): d 164.9, 158.4, 154.4, 143.0, 133.1, 129.1, 128.8, 128.4, 116.7, 109.3, 99.5, 71.6, 8.8, 0.55.
HRMS (ESI+) Calcd 292.09029 for $C_{17}H_{14}N_3S$, found m/z 292.09030 $[M+H]^+$.

4.6.13. 5-Morpholino-6-phenylthieno[2,3-d]pyrimidin-4-amine (1m)

The crude mixture was purified by flash column chromatogra-phy (5–100% EtOAc/hexanes with 0.1% Et_3N, solid loading) to af-ford the desired product as a beige solid in 50% yield (20.5 mg).

^{1}H NMR (400 MHz, $CDCl_3$) d 8.42 (s, 1H), 7.49–7.41 (m, 5H), 3.84 (d, J = 10.6 Hz, 2H), 3.60 (td, J = 11.5, 2.3 Hz, 2H), 3.03 (td, J = 11.6, 2.8 Hz, 2H), 2.95 (d, J = 11.8 Hz, 2H), 1.60 (s, 1H).
^{13}C NMR (75 MHz, $CDCl_3$) d 164.5, 158.8, 154.3, 138.3, 133.4, 131.2, 131.0, 129.2, 128.6, 113.9, 67.8, 53.2.
HRMS (ESI+) Calcd 313.11176 for $C_{16}H_{17}ON_4S$, found m/z 313.11125 $[M+H]^+$.

4.6.14. N^5-Benzyl-N^5-methyl-6-phenylthieno[2,3-d]pyrimidine-4,5-diamine (1n)

The crude mixture was purified by flash column chromatogra-phy (5–100% EtOAc/hexanes with 0.1% Et_3N, solid loading) to af-ford the desired product as a pale orange solid in 53% yield (9.0 mg).

^{1}H NMR (500 MHz, $CDCl_3$) d 8.41 (s, 1H), 7.47–7.36 (m, 5H), 7.29–7.21 (m, 3H), 7.12–7.06 (m, 2H), 3.99 (d, J = 13.3 Hz, 1H), 3.66 (d, J = 13.3 Hz, 1H), 2.77 (s, 3H).
^{13}C NMR (126 MHz, $CDCl_3$) d 164.4, 158.6, 154.3, 139.3, 138.1, 133.6, 130.8, 130.6, 128.9, 128.9, 128.7, 128.46, 127.7, 114.2, 60.7, 43.4.
HRMS (ESI+) Calcd 347.13249 for $C_{20}H_{19}N_4S$, found m/z 347.13188 $[M+H]^+$.

4.6.15. 6-Phenyl-5-(pyrazin-2-yl)thieno[2,3-d]pyrimidin-4-amine (1o)

Isolated as a beige solid in 95% yield (7.0 mg).

^{1}H NMR (500 MHz, $CDCl_3$) d 8.68 (dd, J = 2.6, 1.5 Hz, 1H), 8.50 (d, J = 2.6 Hz, 1H), 8.48 (s, 1H), 8.29 (d, J = 1.4 Hz, 1H), 7.36–7.30 (m, 3H), 7.22–7.19 (m, 2H).
^{13}C NMR (126 MHz, $CDCl_3$) d 167.3, 159.1, 154.1, 150.8, 149.0, 143.1, 143.0, 141.9, 132.9, 130.2, _129.4 (3 _ C), 126.1, 115.9.
HRMS: Calcd 306.08079 for $C_{16}H_{12}N_5S$, found m/z 306.08165 $[M+H]^+$.

4.7. Synthesis of bisphosphonic acids 2

4.7.1. Standard 2-step procedure for the conversion of thienopyrimidin-4-amines 1 to inhibitors 2

The R_2, R_5 and R_6 groups indicated are taken from the fragments shown in Table 1.

Step (a): A solution of the thienopyrimidin-4-amine 1 (0.2 mmol) in anhydrous toluene (10 mL) was flushed with argon. Triethyl orthoformate (1.5 equiv) and diethylphosphite (7 equiv) was added to the reaction mixture via syringe and the reaction mixture was flushed again with argon, sealed, and stirred for 130 LC in the dark for 48 h. The crude mixture was concentrated to dryness under vacuum and purified by flash column chromato-graphy (20–100% EtOAc/hexanes to 0–20% MeOH/EtOAc, solid loading) to afford the desired tetraethyl bisphosphonate ester.

Step (b): A solution of the tetraethyl bisphosphonate ester (1 equiv) in CH_2Cl_2 was cooled to 0 LC and trimethylsilyl bromide (15 equiv) was added via syringe. The reaction mixture was stirred at room temperature for 3–5 days; completion of conversion was monitored by ^{31}P NMR. The mixture was then concentrated under vacuum, diluted with HPLC grade MeOH (_5 mL), and the solvent was evaporated to dryness; this step was repeated four times. The organic solvents were evaporated under vacuum, the residue was suspended in 0.5 mL MeOH, excess water (_5 mL Milli-Q grade) was added to induce full precipitation of the final bisphosphonic acid. The amorphous powder was collected by filtration, washed with de-ionized water (2_), with HPLC-grade CH_3CN (2_), with distilled Et_2O or toluene (2_) and dried under vacuum to give the final compound as a white solid.

4.7.2. (Thieno[2,3-d]pyrimidin-4-ylamino)methylene bisphosphonic acid (2a)

The tetraethyl ((5-(trimethylsilyl)thieno[2,3-d]pyrimidin-4-yl)amino)methylene bisphosphonate was prepared from inter-mediate 20a; isolated in 60% yield (36.7 mg).

^{1}H NMR (400 MHz, CD_3OD): d 8.50 (s, 1H), 7.45 (s, 1H), 5.98 (td, J = 22.0, 9.9 Hz, 1H), 5.78 (d, J = 10.3 Hz, 1H), 4.28–4.12 (m, 8H), 1.26 (td, J = 7.1, 1.7 Hz, 12H), 0.52 (s, 9H).
^{13}C NMR (126 MHz, CD_3OD): d 170.1, 156.2, 152.7, 133.0, 131.3, 120.3, 63.4 (d, J_{CP} = 122.5 Hz), 44.2 (t, J_{CP} = 583 Hz), 16.3, 0.09.
^{31}P NMR (81 MHz, CD_3OD): d 14.81.
MS (ESI) m/z 532.15 $[M+Na]^+$.

A solution of the bisphosphonate tetraester (47.4 mg, 0.093 mmol) in THF (2 mL) was then cooled to 0 LC and 0.1 mL (23.6 mg of a 1 M solution, 0.1 mmol) of TBAF in THF was added. After stirring for 20 min at 0 LC, the mixture was warmed to ambi-ent temperature and stirred for and additional 4 h in the dark. THF was removed under vacuum and the crude mixture was dissolved in 10 mL of EtOAc, washed with water (1 _ 5 mL) and brine (1 _ 5 mL), and dried over anhydrous sodium sulfate. The desily-lated product was obtained quantitatively as a pale yellow solid (41.2 mg).

^{1}H NMR (500 MHz, CD_3OD): d 8.47 (s, 1H), 7.72 (d, J = 6.0 Hz, 1H), 7.57 (d, J = 6.0 Hz 1H), 6.00 (t, J = 23.7 Hz, 1H), 4.20 (m, 8H), 1.26 (m, 12H).
^{13}C NMR (126 MHz, CD_3OD): d 167.6, 157.6, 154.1, 125.1, 119.8, 118.5, 65.16, 45.6 (t, J_{CP} = 150.1 Hz), 16.6.
^{31}P NMR (81 MHz, CD_3OD): d 18.52.
HRMS (ESI+) Calcd 460.08370 for $C_{15}H_{25}N_3NaO_6P_2S$, found 461.08320 $[M+Na]^+$.

The final inhibitor, thieno[2,3-d]pyrimidin-4-ylamino methy-lene bisphosphonic acid (2a) was isolated as a white solid in 70% yield (20.8 mg).

^{1}H NMR (400 MHz, D_2O, 10% ND_4OD, 10% DMSO internal standard): d 8.284 (s, 1H), 7.549 (d, J = 5.9 Hz, 1H), 7.427 (d, J = 6.1 Hz, 1H), 4.594 (t, J = 19.1 Hz, 1H).
^{13}C NMR (126 MHz, D_2O, 20% ND_4OD, 10% DMSO internal standard): d 164.3, 157.3, 154.2, 123.4, 119.8, 117.9, 51.7 (t, J_{CP} = 125.6 Hz).
^{31}P NMR (81 MHz, D_2O, 20% ND_4OD): d 13.308.
HRMS (ESI_) Calcd 323.96873 for $C_7H_8SN_3O_6P_2$, found 323.96125 $[M\_H]^-$.

4.7.3. (((2-Phenylthieno[2,3-d]pyrimidin-4-yl)amino)methylene)diphosphonic acid (2b)

The tetraethyl (((2-phenylthieno[2,3-d]pyrimidin-4-yl)amino)-methylene)bis(phosphonate) was isolated as an orange oil 61% (52.0 mg).

^{1}H NMR (500 MHz, MeOD-d_4): d 8.43–8.41 (m, 2H), 7.71 (d, J = 6.0 Hz, 1H), 7.51 (d, J = 6.0 Hz, 1H), 7.49–7.47 (m, 4H), 6.21 (t, J = 23.7 Hz, 1H), 4.22–4.19 (m, 8H), 1.25–1.22 (m, 12H).
^{13}C NMR (126 MHz, MeOD-d_4): d 169.5, 160.5, 157.3, 139.0, 131.5, 129.5, 129.1, 124.8, 119.7, 116.8, 65.1 (m), 45.5 (t, J = 150.1 Hz), 16.7.
^{31}P NMR (81 MHz, MeOD-d_4): d 17.6.
MS (ESI+) m/z: 514.7 $[M+H]^+$.

The final product (((2-phenylthieno[2,3-d]pyrimidin-4-yl)amino)methylene)diphosphonic acid (2b) was isolated as a pale yellow solid in 66% yield (22.0 mg).

^{1}H NMR (300 MHz, D_2O): d 8.15–8.12 (m, 2H), 7.44–7.40 (m, 4H), 7.28 (d, J = 6.0 Hz, 1H), 4.86 (t, J = 19.0 Hz, 1H).
^{13}C NMR (126 MHz, D_2O): d 166.3, 161.5, 157.8, 138.4, 131.4, 129.6, 129.1, 128.8, 123.6, 119.9, 116.6, 105.9, 50.6 (t, J = 123.6).
^{31}P NMR (81 MHz, D_2O): d 14.2.
HRMS (ESI_) Calcd 399.9928 for $C_{13}H_{12}N_3P_2O_6S$, found m/z 399.9922 $[M\_H]^-$.

4.7.4. (((5-Phenylthieno[2,3-d]pyrimidin-4-yl)amino)methylene)diphosphonic acid (2c)

The tetraethyl (((5-phenylthieno[2,3-d]pyrimidin-4-yl)amino)-methylene)bis(phosphonate) was isolated as a pale yellow solid 24% yield (61 mg).

^{1}H NMR (500 MHz, MeOD-d_4): d 8.52 (s, 1H), 7.60–7.55 (m, 3H), 7.52–7.50 (m, 2H), 7.45 (s, 1H), 5.80 (t, J = 22.4 Hz, 1H), 4.11–4.03 (m, 8H), 1.22–1.19 (m, 12H).
^{13}C NMR (75 MHz, MeOD-d_4): d 166.9, 152.8, 135.4, 134.4, 129.2, 128.9, 128.8, 122.0, 63.7 (m), 43.6 (t, J = 150.1 Hz), 15.2. ^{31}P NMR (81 MHz, MeOD-d_4): d 16.1.
MS (ESI+) m/z: 515.3 $[M+H]^+$.

The final inhibitor (((5-phenylthieno[2,3-d]pyrimidin-4-yl)amino)methylene)diphosphonic acid (2c) was isolated as a white solid in 54% yield (5.1 mg)

^{1}H NMR (500 MHz, D_2O): d 8.17 (s, 1H), 7.68 (s, 1H), 7.54 (d, J = 7.0 Hz, 2H), 7.43 (t, J = 7.6 Hz, 2H), 7.35 (d, J = 7.4 Hz, 1H), 7.12 (s, 1H).
^{13}C NMR (126 MHz, D_2O): d 165.0, 153.2, 135.3, 129.4, 129.1, 128.3, 120.7, 113.9, 50.6 (t, J = 123.6).
^{31}P NMR (81 MHz, D_2O): d 13.4.
HRMS (ESI_) Calcd 399.9928 for $C_{13}H_{12}N_3P_2O_6S$, found m/z 399.9918 $[M\_H]^-$.

4.7.5. (6-Phenylthieno[2,3-d]pyrimidin-4-ylamino)methylene bisphosphonic acid (2d)

The tetraethyl ((6-phenylthieno[2,3-d]pyrimidin-4-yl)amino)-methylene bisphosphonate was isolated in 65% yield (38.0 mg).

^{1}H NMR (500 MHz, CD_3OD) d 8.45 (s, 1H), 8.04 (s, 1H), 7.75 (d, J = 7.3 Hz, 2H), 7.48 (t, J = 7.6 Hz, 2H), 7.41 (d, J = 7.3 Hz, 1H), 6.00 (t, J = 23.6 Hz, 1H), 4.22 (dd, J = 7.7, 3.2 Hz, 8H), 1.45–1.09 (m, 12H).
^{13}C NMR (126 MHz, CD_3OD) d 167.0, 157.2, 154.1, 142.7, 134.6, 130.4, 130.1, 127.2, 119.8, 115.2, 65.2, 45.6, 16.7.
^{31}P NMR (81 MHz, CD_3OD) d 17.004.
MS (ESI) m/z 536.15 $[M+Na]^+$.

The final inhibitor (6-phenylthieno[2,3-d]pyrimidin-4-ylamino)methylene bisphosphonic acid (2d) was isolated as a white so-lid in 63% yield (18.8 mg).

^{1}H NMR (400 MHz, D_2O, 10% ND_4OD): d 8.18 (s, 1H), 7.80 (s, 1H), 7.71 (d, J = 7.4 Hz, 2H), 7.42 (t, J = 7.6 Hz, 2H), 7.33 (t, J = 7.4 Hz, 1H).
^{13}C NMR (126 MHz, D_2O, 10% ND_4OD): d 163.1, 156.2, 153.6, 139.2, 133.2, 129.3, 128.6, 125.9, 118.64, 114.8.
^{31}P NMR (81 MHz, D_2O, ND_4OD) d 13.29.
HRMS (ESI_) Calcd 399.99166 for $C_{13}H_{12}SN_3O_6P_2$, found 399.99268 $[M\_H]^-$.

4.7.6. (((6-(p-Tolyl)thieno[2,3-d]pyrimidin-4-yl)amino)methylene)diphosphonic acid (2e)

The tetraethyl (((6-(p-tolyl)thieno[2,3-d]pyrimidin-4-yl)amino)methylene)bis(phosphonate) was isolated as a light brown powder 94% (27.3 mg).

^{1}H NMR (500 MHz, MeOD-d_4): d 8.43 (s, 1H), 7.97 (s, 1H), 7.60 (d, J = 8.1 Hz, 2H), 7.27 (d, J = 7.8 Hz, 1H), 6.00 (t, J = 23.6 Hz, 1H), 4.24–4.21 (m, 8H), 2.37 (s, 3H), 1.31–1.24 (m, 12H).
^{13}C NMR (126 MHz, MeOD-d_4): d 166.8, 157.0, 153.9, 142.9, 140.4, 131.8, 130.9, 127.1, 119.8, 114.4, 65.10 (m), 45.6 (t, J = 150 Hz), 21.3, 16.7 (m).
^{31}P NMR (81 MHz, MeOD-d_4): d 17.4.
MS (ESI+) m/z: 528.2 $[M+H]^+$.

The final inhibitor (((6-(p-tolyl)thieno[2,3-d]pyrimidin-4-yl)amino)methylene)diphosphonic acid (2e) was isolated as a white solid in 94% yield (27.3 mg).

^{1}H NMR (500 MHz, D_2O): d 8.22 (s, 1H), 7.80 (s, 1H), 7.66 (d, J = 8.2 Hz, 2H), 7.30 (d, J = 8.0 Hz, 2H), 2.33 (s, 3H).

^{13}C NMR (126 MHz, D_2O): d 164.3, 157.6, 155.0, 140.8, 140.7, 131.9, 127.5, 120.2, 115.7, 21.8.
^{31}P NMR (81 MHz, D_2O): d 13.72.
HRMS (ESI_) Calcd 414.00840 for $C_{14}H_{14}N_3P_2O_6S$, found m/z 414.00863 $[M\_H]^-$.

4.7.7. (((6-(Naphthalen-2-yl)thieno[2,3-d]pyrimidin-4-yl)amino)methylene)diphosphonic acid (2f)

The tetraethyl (((6-(naphthalen-2-yl)thieno[2,3-d]pyrimidin-4-yl)amino)methylene)bis(phosphonate) was isolated as a white powder 71% (30.8 mg)

^{1}H NMR (500 MHz, MeOD-d_4): d 8.45 (s, 1H), 8.14 (s, 2H), 7.94–7.83 (m, 4H), 7.53–7.47 (m, 2H), 6.02 (t, J = 23.6 Hz, 1H), 4.24–4.21 (m, 8H), 1.31–1.24 (m, 12H).
^{13}C NMR (126 MHz, MeOD-d_4): d 167.1, 157.1, 154.2, 142.6, 135.0, 134.8, 131.9, 130.0, 129.3, 128.8, 128.0, 127.9, 126.3, 124.6, 119.9, 115.6, 65.1 (m), 45.7 (t, J = 150 Hz), 16.7 (m).
^{31}P NMR (81 MHz, MeOD-d_4): d 17.4.
MS (ESI+) m/z: 564.3 $[M+H]^+$.

The final inhibitor (((6-(naphthalen-2-yl)thieno[2,3-d]pyrimi-din-4-yl)amino)methylene)diphosphonic acid (2f) was isolated as a white solid in 86% yield (29.5 mg).

^{1}H NMR (500 MHz, D_2O): d 8.19 (s, 1H), 8.13 (s, 1H), 7.91–7.83 (m, 5H), 7.50–7.44 (m, 2H).
^{13}C NMR (126 MHz, D_2O): d 164.8, 157.8, 155.1, 140.7, 134.7, 134.3, 132.2, 130.4, 129.6, 129.3, 128.6, 128.3, 126.2, 125.3, 120.3, 116.8.
^{31}P NMR (81 MHz, D_2O): d 13.74.
HRMS (ESI_) Calcd 450.0084 for $C_{17}H_{14}N_3P_2O_6S$, found m/z 450.0085 $[M\_H]^-$.

Acknowledgments

Financial support for this work was provided by NSERC and FQRNT (research Grants to Y.S.T). A.L. is grateful to NSERC for graduate scholarship.

Supplementary data

Supplementary data associated with this article can be found, in the online version, at http://dx.doi.org/10.1016/j.bmc.2013.02.006.

References and notes

1. Marugan, J. J.; Zheng, W.; Southall, N.; Huang, W.; McCoy, J. G.; Titus, S.; Patnaik, S. WO 2012/044993.
2. Brewster, W. K.; Demeter, D. A.; Erickson, W. R.; Klittich, C. J. R.; Lowe, C. T.; Rieder, B. J.; Nugent, J. S.; Yerkes, C. N.; Zhu, Y. WO 2007/046809.
3. Brewster, W. K.; Klittich, C. J. R.; Balko, T.W.; Breax, N. T.; Erickson, W. R.; Hunter, J. E.; Lowe, C. T.; Ricks, M. J.; Siddall, T. L.; Yerkes, C. N.; Zhu, Y. U.S. Patent Application 2006/0089370.
4. Tani, N.; Rahnasto-Rilla, M.; Wittekindt, C.; Salminen, K. A.; Ritvanen, A.; Ollakka, R.; Koskiranta, J.; Raunio, H.; Juvonen, R. O. Eur. J. Med. Chem. 2012, 47, 270.
5. Babu, Y.; Chand, P.; Wu, M.; Kotian, P. L.; Kumar, V. S.; Lin, T.-H.; El-Kattan, Y.; Ghosh, A. K. WO 2006/050161.
6. McClellan, W. J.; Dai, Y.; Abad-Zapatero, C.; Albert, D. H.; Bouska, J. J.; Glaser, K. B.; Magoc, T. J.; Marcotte, P. A.; Osterling, D. J.; Stewart, K. D.; Davidsen, S. K.; Michaelides, M. R. Bioorg. Med. Chem. Lett. 2011, 21, 5620.
7. Dai, Y.; Guo, Y.; Frey, R. R.; Ji, Z.; Curtin, M. L.; Ahmed, A. A.; Albert, D. H.; Arnold, L.; Arries, S. S.; Barlozzari, T.; Bauch, J. L.; Bouska, J. J.; Bousquet, P. F.; Cunha, G. A.; Glaser, K. B.; Guo, J.; Li, J.; Marcotte, P. A.; Marsh, K. C.; Moskey, M. D.; Pease, L. J.; Stewart, K. D.; Stoll, V. S.; Tapang, P.; Wishart, N.; Davidsen, S. K.; Michaelides, M. R. J. Med. Chem. 2005, 48, 6066.
8. Luke, R. W.; Ballard, P.; Buttar, D.; Campbell, L.; Curwen, J.; Emery, S. C.; Griffen, A. M.; Hassall, L.; Hayter, B. R.; Jones, C. D.; McCoull, W.; Mellor, M.; Swain, M. L.; Tucker, J. A. Bioorg. Med. Chem. Lett. 2009, 19, 6670.
9. Horiuchi, T.; Chiba, J.; Uoto, K.; Soga, T. Bioorg. Med. Chem. Lett. 2009, 19, 305.
10. Sham, H. L.; Konradi, A. W.; Hom, R. K.; Probst, G. D.; Bowers, S.; Truong, A.; Neitz, R. J.; Sealy, J.; Toth, G. WO 2010/091310.
11. Bowers, S.; Truong, A. P.; Neitz, R. J.; Hom, R. K.; Sealy, J. M.; Probst, G. D., et al Bioorg. Med. Chem. Lett. 2011, 21, 5521.
12. Angell, R. M.; Atkinson, F. L.; Brown, M. J.; Chuang, T. T.; Christopher, J. A.; Cichy-Knight, M.; Dunn, A. K.; Hightower, K. E.; Malkakorpi, S.; Musgrave, J. R.; Neu, M.; Rowland, P.; Shea, R. L.; Smith, J. L.; Somers, D. O.; Thomas, S. A.; Thompson, G.; Wang, R. Bioorg. Med. Chem. Lett. 2007, 17, 1296.
13. Axten, J. M.; Grant, S. W.; Heerding, D. A.; Medina, J. R.; Romeril, S. P.; Tang, J. WO 2011/119663.
14. Edgar, K. A.; Wallin, J. J.; Berry, M.; Lee, L. B.; Prior, W. W.; Sampath, D.; Friedman, L. S.; Belvin, M. Cancer Res. 2010, 70, 1164.
15. Heffron, T. P.; Wei, B. Q.; Olivero, A.; Staben, S. T.; Tsui, V.; Do, S.; Dotson, J.; Folkes, A. J.; Goldsmith, P.; Goldsmith, R.; Gunzner, J.; Lesnick, J.; Lewis, C.; Mathieu, S.; Nonomiya, J.; Shuttleworth, S.; Sutherlin, D. P.; Wan, N. C.; Wang, S.; Wiesmann, C.; Zhu, B.-Y. J. Med. Chem. 2011, 54, 7815.
16. Rheault, T. R.; Ceferro, T. R.; Dickerson, S. H.; Donaldson, K. H.; Gaul, M. D.; Goetz, A. S.; Mullin, R. J.; McDonald, O. B.; Petrov, K. G.; Rusnak, D. W.; Shewchuk, L. M.; Spehar, G. M.; Truesdale, A. T.; Vanderwall, D. E.; Wood, E. R.; Uehling, D. E. Bioorg. Med. Chem. Lett. 2009, 19, 817.
17. Fischer, C.; Shah, S.; Hughes, B. L.; Nikov, G. N.; Crispino, J. L.; Middleton, R. E.; Szewczak, A. A.; Munoz, B.; Shearman, M. S. Bioorg. Med. Chem. Lett. 2011, 21, 773.
18. Barbay, J. K.; Leonard, K.; Chakravarty, D.; Shook, B. C.; Wang, A. WO 2010/045009.
19. Chakravarty, D.; Shook, B. C. WO 2010/045017.
20. Barbay, J. K.; Chakravarty, D.; Shook, B. C.; Wang, A. WO 2010/045006.
21. Lin, Y.-S.; Park, J.; De Schutter, J. W.; Huang, X. F.; Berghuis, A. M.; Sebag, M.; Tsantrizos, Y. S. J. Med. Chem. 2012, 55, 3201.
22. De Schutter, J. W.; Zaretsky, S.; Welbourn, S.; Pause, A.; Tsantrizos, Y. S. Biorg. Med. Chem. Lett. 2010, 20, 5781.
23. Gewald, K.; Schinke, E.; Boettcher, H. Chem. Ber. 1966, 99, 94.
24. Huang, X.-G.; Liu, J.; Ren, J.; Wang, T.; Chen, W.; Zeng, B.-B. Tetrahedron 2011, 67, 6202.
25. Barnes, D. M.; Haight, A. R.; Hameury, T.; McLaughlin, M. A.; Mei, J.; Tedrow, J. S.; Toma, J. D. R. Terahedron 2006, 62, 11311.
26. Hesse, S.; Perspicace, E.; Kirsch, G. Tetrahedron Lett. 2007, 48, 5261.
27. Tranberg, C. E.; Zickgraf, A.; Giunta, B. N.; Luetjens, H.; Figler, H.; Murphree, L. J.; Falke, R.; Fleischer, H.; Linden, J.; Scammells, P. J.; Olsson, R. A. J. Med. Chem. 2002, 45, 382.
28. Miller, R. E.; Rantanen, T.; Ogilvie, K. A.; Groth, U.; Snieckus, V. Org. Lett. 2010, 12, 2198.
29. Getmanenko, Y.; Tongwa, P.; Timofeeva, T. V.; Marder, S. R. Org. Lett. 2010, 12, 2136.
30. Schmürch, M.; Spina, M.; Khan, A. F.; Mihoviloviv, M. D.; Stanetty, P. Chem. Soc. Rev. 2007, 36, 1046.
31. Schlosser, M. Angew. Chem., Int. Ed. 2005, 44, 376.
32. Lukevics, E.; Arsenyan, P.; Belyakov, S.; Popelis, J.; Pudova, O. Tetrahedron Lett. 2001, 42, 2039.
33. Rondeau, J.-M.; Bitsch, F.; Bourgier, E.; Geiser, M.; Hemmig, R.; Kroemer, M.; Lehmann, S.; Ramage, P.; Rieffel, S.; Strauss, A.; Green, J. R.; Jahnke, W. ChemMedChem 2006, 1, 267.
34. Kavanagh, K. L.; Guo, K.; Dunford, J. E.; Wu, X.; Knapp, S.; Ebetino, F. H.; Rogers, M. J.; Russell, R. G. G.; Oppermann, U. Proc. Natl. Acad. Sci. U.S.A. 2006, 103, 7829.
35. Morgan, G. J.; Davies, F. E.; Gregory, W. M.; Cocks, K.; Bell, S. E.; Szubert, A. J.; Navarro-Coy, N.; Drayson, M. T.; Owen, R. G.; Feyler, S.; Ashcroft, A. J.; Ross, F.; Byrne, J.; Roddie, H.; Rudin, C.; Cook, G.; Jackson, G. H.; Child, J. A. Lancet 2010, 376, 1989.
36. Feng, X. J.; Wu, P. L.; Tam, H. L.; Li, K. F.; Wong, M. S.; Cheah, K. W. Chem. Eur. J. 2009, 15, 11681.
37. Ye, X.-S.; Wong, H. N. C. J. Org. Chem. 1997, 62, 1940.
38. Bair, J. S.; Palchaudhuri, R.; Hergenrother, P. J. J. Am. Chem. Soc. 2010, 132, 5469.
39. Wilhelms, W. Synthesis 2006, 10, 1578.
40. Wiemer, A. J.; Tong, H.; Swanson, K. M.; Hohl, R. J. Biochem. Biophys. Res. Commun. 2007, 353, 921.

3. Thienopyrimidine bisphosphonate (ThPBP) inhibitors of the human farnesyl pyrophosphate synthase: optimization and characterization of the mode of inhibition

Reference:

Leung, C.Y.; Park, J.; De Schutter, J. W.; Sebag, M.; Berghuis, A.M.; Tsantrizos, Y.S., Thienopyrimidine bisphosphonate (ThPBP) inhibitors of the human farnesyl pyrophosphate synthase: optimization and characterization of the mode of inhibition. *J. Med. Chem.* **2013**, *56*, 7939-7950

In the above publication, Dr. Jaeok Park from Dr. Albert M. Berghuis' lab performed all the X-ray diffraction acquisition and analysis work. Dr. Joris W. De Schutter performed the differential scan fluorimetry experiments. The anti-proliferation assay on multiple myeloma cells where performed by Ms. Xian Fang Huang (a research assistant in Dr. Sebag's laboratory). I contributed to the synthesis and the determination of the *in vitro* hFPPS inhibitory activity of all the thienopyrimidine bisphosphonates. I also performed the relative binding affinity for bone of the thienopyrimidine bisphosphonate compared to risedronic acid.

Journal of Medicinal Chemistry

Article

pubs.acs.org/jmc

Thienopyrimidine Bisphosphonate (ThPBP) Inhibitors of the Human Farnesyl Pyrophosphate Synthase: Optimization and Characterization of the Mode of Inhibition

Chun Yuen Leung,[†] Jaeok Park,[‡] Joris W. De Schutter,[†] Michael Sebag,[⊥] Albert M. Berghuis,[‡,§,†] and Youla S. Tsantrizos*[,∥,‡,†]

[†]Department of Chemistry, McGill University, 801 Sherbrooke Street West, Montreal, Quebec, Canada H3A 0B8

[‡]Department of Biochemistry, McGill University, 3649 Promenade Sir William Osler, Montreal, Quebec, Canada H3G 0B1

[§]Department of Microbiology and Immunology, McGill University, 801 Sherbrooke Street West, Montreal, Quebec, Canada H3A 0B8

[∥]Groupe de Recherche Axé sur la Structure des Proteines, McGill University, 3649 Promenade Sir William Osler, Montreal, Quebec, Canada H3G 0B1

[⊥]Division of Haematology, McGill University Health Center, Royal Victoria Hospital, C6.80, 687 Pine Avenue West, Montreal, Quebec, Canada H3A 1A1

*Supporting Information

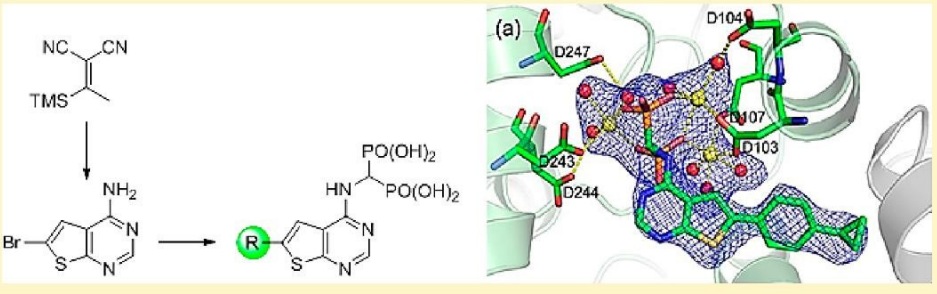

ABSTRACT: Human farnesyl pyrophosphate synthase (hFPPS) controls the post-translational prenylation of small GTPase proteins that are essential for cell signaling, cell proliferation, and osteoclast-mediated bone resorption. Inhibition of hFPPS is a clinically validated mechanism for the treatment of lytic bone diseases, including osteoporosis and cancer related bone metastases. A new series of thienopyrimidine-based bisphosphonates (ThP-BPs) were identified that inhibit hFPPS with low nanomolar potency. Crystallographic evidence revealed binding of ThP-BP inhibitors in the allylic subpocket of hFPPS. Simultaneous binding of inorganic pyrophosphate in the IPP subpocket leads to conformational closing of the active site cavity. The ThP-BP analogues are significantly less hydrophilic yet exhibit higher affinity for the bone mineral hydroxyapatite than the current N-BP drug risedronic acid. The antiproliferation properties of a potent ThB-BP analogue was assessed in a multiple myeloma cell line and found to be equipotent to the best current N-BP drugs. Consequently, these compounds represent a new structural class of hFPPS inhibitors and a novel scaffold for the development of human therapeutics.

INTRODUCTION

Human farnesyl pyrophosphate synthase (hFPPS) controls the first branching point of the mevalonate pathway and catalyzes the biosynthesis of farnesyl pyrophosphate (FPP). FPP is the key precursor for the biosynthesis of many metabolites, including geranylgeranyl pyrophosphate (GGPP), squalene, and cholesterol. FPP and GGPP are essential for the post-translational prenylation of all small GTPase proteins that play a crucial role in cell signaling, cell proliferation, and osteoclast-mediated bone resorption.[1,2] Inhibition of hFPPS can down-regulate the activity of mutated H-Ras, K-Ras, and N-Ras proteins that function as major drivers of tumor growth in many cancers. For example, whole genome sequencing of human multiple myeloma (MM) tumors has revealed that 50% of MM patients harbored either K-Ras or N-Ras activating mutations, underscoring the importance of hFPPS in this disease.[3] Metastatic bone disease is highly prevalent in patients with MM, breast, and prostate cancers. It is estimated that approximately 70% of all patients with advanced forms of these three types of cancers will at some point develop bone metastases.[4] Thus, the clinical benefits of hFPPS inhibition include both decrease of prenylation of mutated Ras proteins, leading to a decrease in cellular growth and/or survival as well as alleviation of tumor-associated bone destruction via inhibition of osteoclast activity.[5] It is noteworthy that inhibitors

Received: June 25, 2013
Published: September 2, 2013

dx.doi.org/10.1021/jm400946f | J. Med. Chem. 2013, 56, 7939−7950

of the farnesyltransferase enzyme (FTase), which catalyze the prenylation of Ras (e.g., tipifarnib[70]), have also been extensively investigated as an alternative mechanism for downregulating oncogenesis but failed to demonstrate significant clinical efficacy. It was subsequently realized that the substrate specificity of the transferase enzymes (FTase and GGTase I and II) is not absolutely stringent and cross-prenylation can occur, restoring the biological function of the mutated Ras proteins.[71] However, this redundancy mechanism cannot compromise the clinical effects of drugs that directly down-regulates the biosynthesis of FPP by inhibiting hFPPS.

Additionally, blocking the catalytic activity of hFPPS impacts both the downstream and upstream levels of isoprenoids in the mevalonate pathway, leading to numerous cellular changes. Intracellular accumulation of the substrate isopentenyl pyrophosphate (IPP), as a consequence of hFPPS inhibition, leads to accumulation of an ATP derivative (ApppI), which induces cell apoptosis by inhibiting the mitochondrial adenine nucleotide translocase (ANT).[6,7] IPP is also a natural antigen that directly stimulates γδ T cells that carry the Vγ2Vδ2 T cell receptors and is strongly implicated in the human innate immune response against tumors.[8] Interestingly, treatment of different types of cancer cells with the same hFPPS inhibitor may result in dramatically different intracellular levels of IPP (from ~10-fold to nearly 1000-fold increase in intracellular concentrations have been reported),[9] highlighting the varia-bility in regulating/disregulating metabolic pathways in differ-ent cells. These observations suggest that selectivity in biochemical interventions may be possible, even when targeting a critical step in an important metabolic pathway.

Currently, nitrogen-containing bisphosphonate drugs (N-BPs) are the only clinically relevant compounds that inhibit hFPPS.[10,11] Bisphosphonates are chemically stable bioisosteres of pyrophosphates and structurally characterized by two phosphonate groups attached to a central carbon (Cα) instead of an oxygen atom. Additionally, one of the Cα substituents (i.e., the N-BP side chain) is usually characterized by a basic nitrogen atom, presumed to be protonated under physiological conditions and mimicking the interactions of the putative allylic carbocation transition state that forms during the hFPPS catalytic cycle.[12] The structure of the most potent N-BP drugs, such as zoledronic acid (1) and risedronic acid (2a), is also characterized by a Cα-hydroxyl moiety, which maximizes their affinity for the bone mineral hydroxyapatite (HAP).[13,62] The Cα-hydroxyl moiety also participates in additional interaction with the active site of the enzyme, thus contributing to the potency of these compounds.[10,13]

N-BP drugs are routinely used to treat osteoporosis and other lytic bone diseases, including bone cancer metastasis and multiple myeloma (MM).[14−16] N-BPs bind so strongly to bone that their half-life (in bone) can be months to several years, depending on the type of drug and the degree of bone turnover.[17,18] In chronic diseases (e.g., osteoporosis), concerns that prolonged use of N-BPs can lead to side effects, such as osteonecrosis of the jaw and atypical femoral fractures, have led to the recommendation by physicians of a "drug holiday". However, this treatment can lead to uncertainty with respect to the type of drug that should be used and the duration of treatment for different patients.[19] Furthermore, the systemic half-life of current N-BPs is extremely low; for example, after iv administration of 1, 50% of the dose gets trapped in the bone mineral and the rest is rapidly cleared by the kidneys (the dose-limiting toxicity of 1 is based on nephrotoxicity).[20,21]

In spite of their poor drug-like properties (including extremely low cell membrane permeability and oral bioavail-ability), recent clinical investigations provide evidence that some N-BP drugs (e.g., 1) are disease modifying agents that improve the survival of patients with multiple myeloma (MM) via mechanisms that are both related as well as unrelated to the skeletal benefits.[22,23] Similar results were reported for patients with premenopausal breast cancer,[24] although these findings seem to be more controversial.[25] Nonetheless, the identification of hFPPS inhibitors with superior oral bioavailability, half-life in plasma (i.e., slower rates of elimination from the blood circulation), and higher nonskeletal tissue distribution may provide effective antiresorptive agents that are also more effective in cancer chemotherapy than the current N-BP drugs. In this report, we describe our structure−activity relationship (SAR) studies on thienopyrimidine-based bisphosphonate (ThP-BP) inhibitors of hFPPS and the identification of analogues with low nanomolar potency. Co-crystal structures of two ThP-BP analogues bound to the allylic subpocket of hFPPS (i.e., the DMAPP/GPP binding subpocket of the active site) revealed details of the protein − inhibitor interactions and conformational changes to the C-terminal region that lead to closing of the active site cavity. These ThP-BP molecules are significantly less hydrophilic than the current N-BP drugs but exhibit high affinity for the bone mineral hydroxyapatite. The in vitro affinity of bisphosphonates for hydroxyapatite is known to correlate well with the in vivo affinity of the N-BP drugs for bone.[13,62] Thus, the ThP-BP compounds are promising new leads for medicinal chemistry studies that aim to identify new inhibitors of hFPPS with better biopharmaceutical properties than those of the current N-BP drugs.

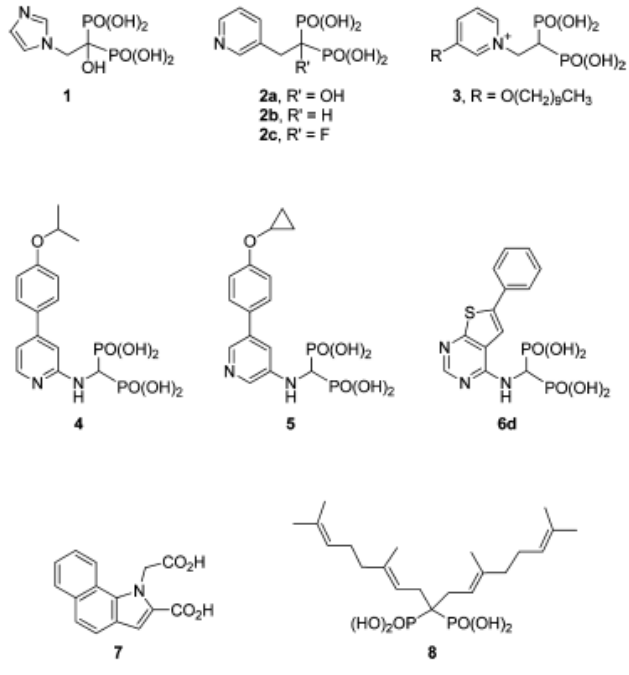

CHEMISTRY

In our search of new structural classes of hFPPS inhibitors, we recently identified thienopyrimidine-based bisphosphonates (ThP-BPs; e.g., 6d) with modest in vitro potency in inhibiting hFPPS.[26] The thienopyrimidine scaffold is considered to be

dx.doi.org/10.1021/jm400946f | J. Med. Chem. 2013, 56, 7939−7950

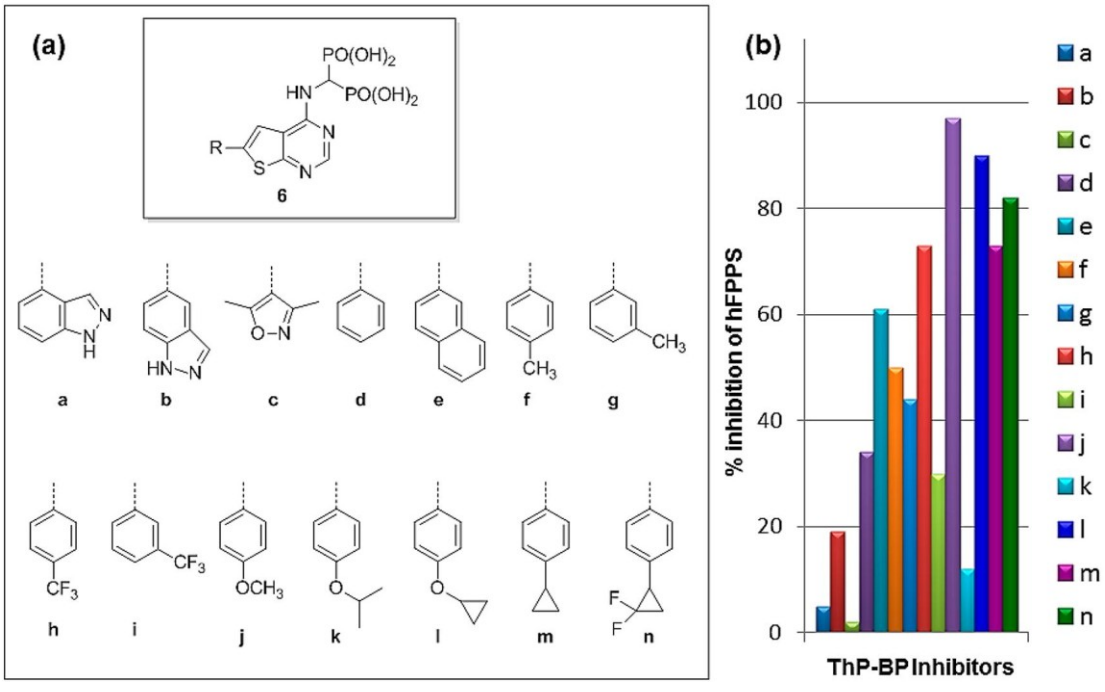

Figure 1. Thienopyrimidine inhibitors of the human FPPS. (a) Representative examples of analogues. (b) Inhibition of hFPPS at 100 nM concentration of each compound using the M2 assay (average of three determinations; standard deviation ≤10%).

privileged in drug discovery due to its inherently favorable biopharmaceutical profile. Thienopyrimidine-based compounds are currently under investigation as therapeutics for the treatment of many diseases, including fungal[27] and viral infections[28] and cancer.[28−36]

At the time of our initial report on ThP-BPs,[26] the mechanism by which these compounds inhibit hFPPS was unclear. Given the significantly larger molecular size of ThP-BPs (e.g., 6d) as compared to the current N-BP drugs (e.g., 1 and 2a), we presumed that their binding interactions with hFPPS may also be different. Mindful of the conformational plasticity of this enzyme that permit the binding of fairly large N-BP molecules (e.g., 4) in the allylic subpocket, we prepared a focused library of ThP-BP derivatives guided by our previous SAR studies (e.g., SAR derived from pyridine analogues such as 4 and 5);[37,38] some representative examples are shown in Figure 1.

The synthesis of the ThP-BP analogues was initiated from the key fragment 6-bromothieno[2,3-d]pyrimidin-4-amine (10), which was prepared via the trimethylsilyl ylidine 9 as previously described (Scheme 1).[26] Intermediate 10 was also prepared starting from 2,5-dihydroxy-1,4-dithiane (12), via the unsubstituted 2-amino-thiophene-3-carbonitrile core, following earlier literature procedures.[39,40] Although the two synthetic protocols (paths A and B) are equivalent in the overall number of steps leading to 10, the average isolated yield via pathway A was significantly higher (Scheme 1; the average overall yield of 10 was 18% vs 8% obtained via pathways A and B, respectively).

Conversion of 10 to the bisphosphonate tetraester 11 was easily achieved upon treatment with triethoxymethane and diethylphosphite. Cross coupling of 11 with a variety of boronate esters, under typical Suzuki conditions, followed by hydrolysis of the tetraethyl bisphosphonate esters 13 with TMSBr/MeOH, resulted in the formation of the final thienopyrimidine bisphosphonic acids of general structure 6 (Scheme 1).

Scheme 1. Synthesis of C-6 Substituted Thieno[2,3-d]pyrimidin-4-amine-Based Bisphosphonate Inhibitors of hFPPS[a]

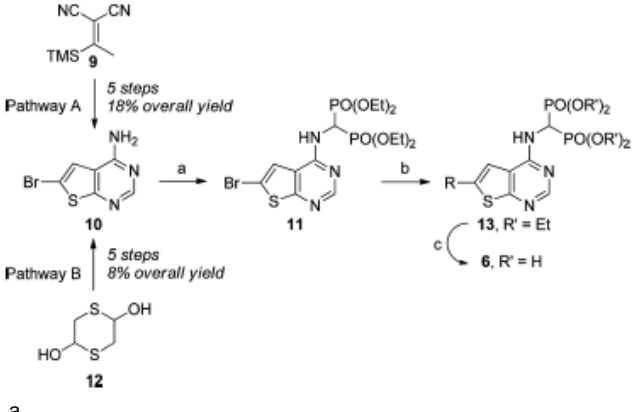

[a]Conditions: (a) $CH(OEt)_3$, diethylphosphite, 130 °C, 24 h (75%); (b) 10 mol % $Pd(PPh_3)_4$, KF, MeOH, 120 °C, μW, 20 min; (c) TMSBr, MeOH, RT, 72 h (overall isolated yield for steps (b) and (c) ranged from ~20% to 80%).

RESULTS AND DISCUSSION

Metabolic disregulation of hFPPS has been implicated in many human diseases, including various cancers (e.g., breast, prostate, and MM) and neurodegenerative diseases such as the Alzheimer's disease.[41,42] However, in vivo investigation of hFPPS as a therapeutic target is hampered by the lack of molecular tools that can selectively inhibit this enzyme and can exhibit significant in vivo distribution into soft tissues. Past efforts toward improving the clinical use of N-BPs have included investigations of pro-drugs,[43,44] improved drug

dx.doi.org/10.1021/jm400946f | J. Med. Chem. 2013, 56, 7939−7950

formulations,[45] and structural modifications that may increase oral bioavailability and decrease the rate of compound clearance from circulation. N-BPs with more lipophilic side chains (e.g., 3,[46,47] 4, 5) than the clinical drugs 1 and 2a, as well as bicyclic heterocyclic side chains, have been explored, including imidazopyridines, benzimidazoles,[48] and azaindoles.[49,50] To the best of our knowledge, none of these efforts have produced an hFPPS inhibitor with superior clinical profile than that of analogues 1 or 2a. We recently identified thienopyrimidine-based bisphosphonates (ThP-BPs) with IC_{50} potency in inhibiting hFPPS in the 0.5−1 μM range. These hits were used for further SAR studies and optimized into low nanomolar inhibitors of hFPPS.

It is noteworthy that several different assays have been reported in the literature for evaluating in vitro hFPPS inhibition. The most commonly used method was originally developed by Reed and Rilling[51] and has been adopted by many researchers with only minor modifications;[13,37,38,53] we refer to these conditions as method 1 (M1). The IC_{50} values of hFPPS inhibitors can vary considerably, depending on the assay method; for example, the reported IC_{50} values of 1 range from approximately 4 nM[11,52,53] to 200 nM,[54] and can be as high as 475 nM if the compound is tested without preincubation with the enzyme.[53] Experimental artifacts in a functional assay can further contribute to the observed potency of a compound and mislead SAR studies. Lipophilicity-dependent aggregation of moderately (or poorly) hydrophilic compounds is the most common factor responsible for false experimental data and can affect both in vitro and cell-based assays.[55] The ability of bisphosphonates to form stable, high-order complexes in solution, particularly in the presence of metal ions, is a well-documented phenomenon, exploited in a number of biomedical applications.[56−58] The high charge density of the magnesium cation may also play a role in augmenting the solvent-induced interaction between the hydrophobic side chains of the ThP-BP inhibitors (as compared to smaller and more polar N-BPs; CLogP values are shown in Table 1).[72] A combination of these effects appear to induce significant aggregation under the M1 assay conditions and lead to artifacts in characterizing hFPPS inhibition. A number of assay modifications were investigated, including lowering the concentration of Mg^{2+} ions and adding Triton X-100 (0.01%) in the assay buffer. The addition of Triton X-100 in the buffer was previously reported for testing nonbisphosphonate inhibitors of hFPPS.[59,60] The ratio of hFPPS protein, IPP/GPP substrates, and Mg^{2+} ion concentrations were also optimized in order to achieve maximum catalytic turnover and highest sensitivity in detecting weakly active compounds; we refer to these conditions as assay method 2 (M2).

The IC_{50} values of several known hFPPS inhibitors were determined using both the M1 and M2 assay conditions. Little variability (≤2-fold) was observed in the observed potency of pyridine-based N-BP molecules (Table 1; analogue 2a and 5). In contrast, the IC_{50} of the hFPPS allosteric inhibitor 7 was approximately 22-fold lower in the M2 assay than the M1 assay and ~100-fold lower than the value reported using yet another assay protocol;[61] the IC_{50} values of 7 were determined to be ~20 and 0.92 μM in the M1 and M2 assay, respectively (Table 1). The IC_{50} values for our initial hits, 6e and 6f, were also lower in the M2 assay as compared to the M1 assay (Figure 1a, Table 1). A defining characteristic of molecular aggregation is the formation of higher-order soluble particles on the submicrometer scale that are disrupted (to some degree) by the presence of a detergent such as Triton X-100, Tween-20, or Tween-80.[55] The higher propensity of ThP-BPs to aggregate in the assay buffer, as compared to the N-BP analogue 2a, was confirmed by dynamic light scattering (DLS); aggregation was particularly pronounced in the presence of high Mg^{2+} concentrations (an example is shown in Supporting Informa-tion Figure 1).

The optimized M2 assay was subsequently adopted for our routine biological screening of all ThP-BP inhibitors. All analogues were initially tested at a concentration of 1.0 and 0.1 μM; representative examples are shown in Figure 1. The general potency profile for these compounds was similar to the SAR previously observed with 2-amino- and 3-aminopyridine libraries.[37,38] For example, analogues with polar heterocyclic side chains, such as 6a, 6b, and 6c, exhibited weak activity in inhibiting hFPPS (<20% inhibition was observed at 100 nM), and meta-substituted phenyls were less potent than their corresponding para-analogues (e.g., analogues 3h and 3i exhibited 73% vs 30% inhibition at 100 nM, respectively). Full dose−response inhibition curves were obtained only for analogues deemed critical to our SAR studies and analogues exhibiting >50% inhibition at 100 nM. A number of novel thienopyrimidine-based inhibitors of hFPPS were identified with IC_{50} values in the 10−50 nM range; representative examples are shown in Table 1. In addition, all analogues with an IC_{50} <100 nM were tested in our in vitro hGGPPS inhibition assay, using compound 8 as the positive control, as previously reported;[37] none of these compounds were active at concentration up to 10 μM; the buffer of our hGGPPS inhibition assay contained 0.2% Tween-20 (i.e., 20-fold higher concentration of detergent than our M2 hFPPS inhibition assay), which should minimize or eliminate any effects due to aggregation.

It has been shown that N-BPs such as 1, that bind very strongly to bone and get rapidly eliminated from plasma, achieve extremely low concentrations in most noncalcified tissues.[21] Consequently, their therapeutic efficacy as antitumor agents for non-bone-related cancers is greatly compromised. The Cα-hydroxy bisphosphonate moiety of the current drugs

Table 1. Inhibition Data for Key Compounds

	hFPPS IC_{50} (nM)[a]		
compd	M1 assay	M2 assay	CLogP of side chain moiety
1	4.1[b]	nd[c]	−0.84
2a	11	5.2	−0.16
5	16	18	3.6
7	~20000	920	nd
6e	250	63	5.0
6f	390	22	4.3
6j	440	15	3.7
6h	nd	21	4.7
6k	nd	200	4.6
6l	nd	14	4.3
6m	115	39	4.8
6n	140	11	4.1

[a]Average IC_{50} values of a minimum of three determinations (standard deviation ≤10). All compounds were also tested in our hGGPPS inhibition assay, and none were active at concentration up to 10 μM. [b]IC_{50} value reported by Kavanagh et al.[53] CLogP values were estimated without the two phosphonate groups in order to simplify the calculations. [c]Value was not determined (nd).

dx.doi.org/10.1021/jm400946f | J. Med. Chem. 2013, 56, 7939−7950

(1 and 2a) is generally believed to enhance bone affinity by allowing a tridentate interaction with Ca^{2+} ions and the bone mineral hydroxyapatite. Consistent with this assumption, replacement of the Cα-hydroxy group with a proton (e.g., 2b) or a halogen (e.g., 2c) was shown to decrease both the affinity for the bone mineral hydroxyapatite and the ability of the compounds to inhibit hFPPS.[13] The in vitro affinity of bisphosphonates for hydroxyapatite is known to correlate well with the in vivo affinity of the N-BP drugs for bone.[13,62] We compared the relative binding affinity of ThP-BPs 6m and N-BP 2a for hydroxyapatite (HAP) using the NMR protocol reported by Jahnke and Henry.[62] After incubation with HAP, changes in the relative intensity of the aromatic proton signals were observed for both compounds. However, a much more significant decrease in the intensity of the aromatic signals of analogue 6m was observed as compared to 2a, consistent with a higher portion of 6m binding to HAP and removed from the solution (Figure 2). Similar results were also obtained with

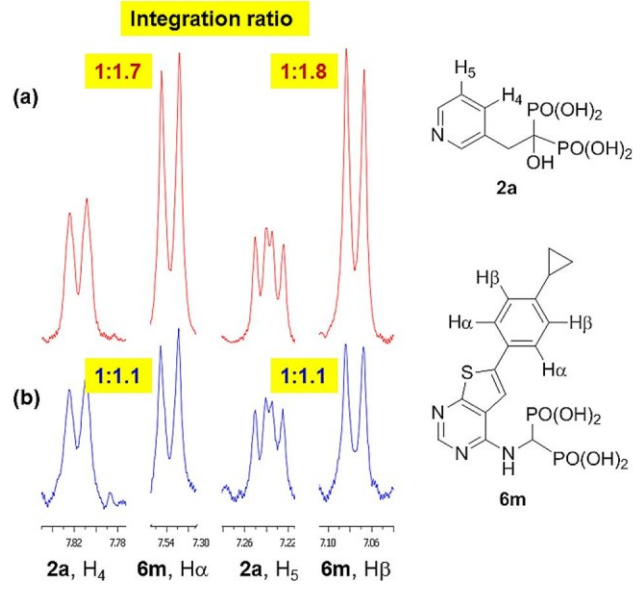

Figure 2. Differentiation of 2a and 6m in their competitive binding to HAP (for clarity, only select regions of the ^{1}H NMR spectra are shown). (a) ^{1}H NMR spectra of 2a and 6m at approximately 1:1 molar ratio (~50 μM of each compound) in Tris buffer before any treatment. (b) ^{1}H NMR spectrum of the same solution of 2a and 6m as that used to acquire the spectrum shown in (a) after incubation with 0.8 mg of HAP at room temperature for 5 min.

analogues 6h and 6l, suggesting that this high affinity for hydroxyapatite is likely structure-dependent. These results are somewhat surprising because it is generally believed that the Cα-hydroxyl substituent of N-BPs provides the optimal "bone hook" and contributes to the antiresorptive efficacy of the current N-BP drugs. Differences in lipophilicity and bone affinity can potentially affect the pharmacokinetic and pharmacodynamics properties of these compounds, thus contributing to a unique therapeutic profile.

Clinical evidence is rapidly accumulating which implicates inhibitors of hFPPS as antineoplastic and specifically antimyeloma therapeutic agents.[22,23] Antiproliferation and cytotoxic effects were observed with inhibitor 6m that compared favorably to the effects of 1 and 2a (Table 1). Treatment of human MM cell line RPMI-8226 with each of the three compounds resulted in reductions of cell proliferation with median effective concentrations for 50% growth inhibition (EC_{50}) of 11, 13, and 8.5 μM, for 1, 2a, and 6m, respectively (Table 2); values represent the average of n ≥ 8 determinations with R^2 in the range of 0.90−0.98.

Table 2. Antiproliferation Effects in the Multiple Myeloma Cells

compd	hFPPS IC_{50} (nM) M2 assay	EC_{50} (μM)[a] cell line RPMI-8226
1	nd[b]	11
2a	5.2	13
6m	39	8.5

[a]Average EC_{50} values of n ≥ 8 determinations; R^2 values in the range of 0.90-0.98. [b]Value was not determined (nd).

Finally, two representative ThP-BP inhibitors, 6f and 6m, were also cocrystallized with hFPPS (Table 2). Both compounds were found to bind in the allylic subpocket of the active site in the same manner without causing major conformational strain to the protein despite their bulky and rigid side chains. However, unlike 1 and 2a (which bind to only a small portion of the allylic subpocket), the interactions of 6f and 6m with the active site cavity extend through the capping phenyls (Phe 98/99) and toward the hFPPS dimer interface. Some of the key features of these binding interactions are illustrated with the hFPPS−6m−PPi ternary complex (PDB 4L2X) in Figure 3. The simulated annealing omit map clearly demonstrates the presence of bound 6m, as well as three magnesium ions and water molecules, which mediate the interaction between the bisphosphonate moiety and the two DDXXD motifs of the protein (Figure 3a). Some of the metal-mediated interactions between the bisphosphonate and aspartic acid residues of the DDXXD motifs are direct, whereas others are water mediated. There are three additional interactions between the positively charged residues Arg 112, Lys 200, and Lys 257, which make direct contacts with the bisphosphonate moiety of the inhibitor, which are not shown in Figure 3a for clarity. The side chain of 6m fills the lipophilic cavity of the allylic subpocket completely, with its cyclopropyl tail extending to the end of the cavity at the dimerization interface (Figure 3b). The phenyl ring of the 6m side chain is engaged in stacking interactions with the side chains of Phe 99 and Gln 171, similarly to what was previously observed with inhibitor 4 (Figure 3c).[37,63]

The thienopyrimidine scaffold also displaces the side chain hydroxyl of Thr 201 and the main chain carbonyl of Lys 200 by ~0.65 Å; these residues are presumed to participate in a bifurcated H-bond interaction with the protonated side chain of 1 (Figure 3c). The hFPPS−6m−PPi complex adopts a fully closed conformation, similar to that observed in the hFPPS− 1−IPP ternary complex (PDB 1ZW5).[10] Superposition of our hFPPS−6m−PPi structure with the structure of the hFPPS− 1−IPP ternary complex (Figure 3d) revealed the same folding of the ^{350}KRRK^{353} C-terminal tail over the IPP subpocket. These data are consistent with our earlier observations indicating that following occupancy of the allylic subpocket, inorganic pyrophosphate (PPi) can play the same role as IPP in inducing the closing of the hFPPS active site cavity.[63] Previous investigations suggested that this secondary ligand-induced conformational change of the C-terminal basic residues (^{350}KRRK^{353}) leads to a nearly irreversible inhibition of the

dx.doi.org/10.1021/jm400946f | J. Med. Chem. 2013, 56, 7939−7950

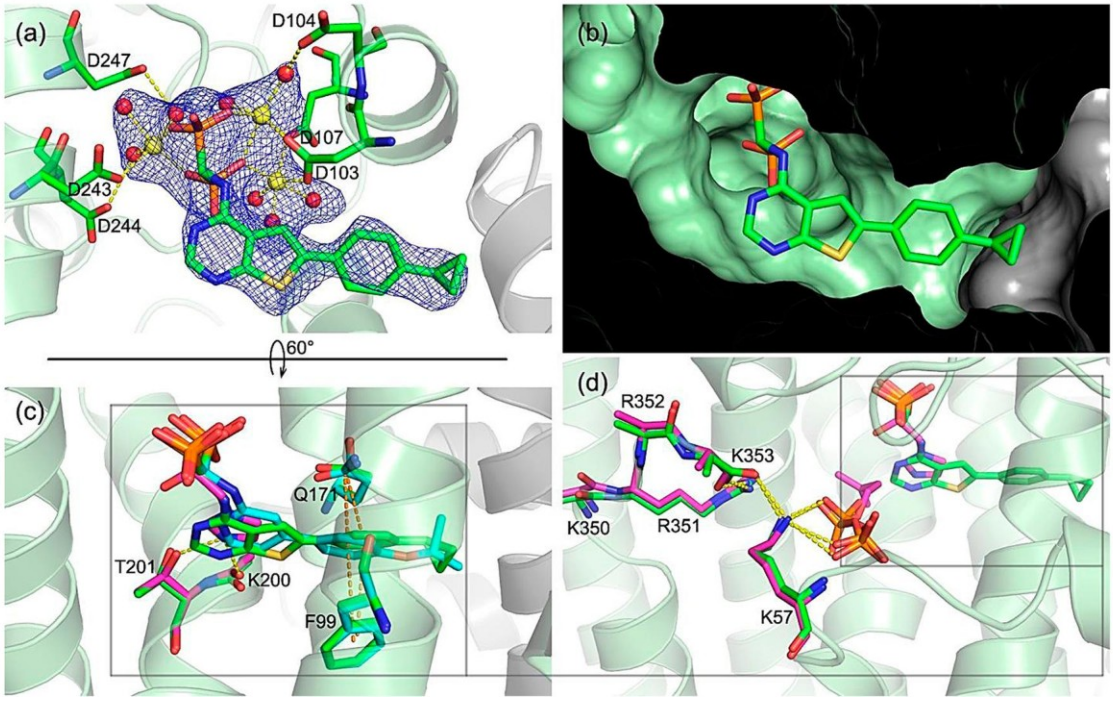

Figure 3. Crystal structure of hFPPS in complex with analogue 6m (PDB 4L2X); key interactions are indicated with dashed yellow lines. (a) The blue mesh represents a simulated annealing omit map ($F_o - F_c$, contoured at 3σ) for the bisphosphonate ligand, magnesium ions (yellow spheres), and coordinated water molecules (red spheres). In addition to the Mg^{2+}-mediated bisphosphonate interactions with the aspartic acid residues (some direct and others via water molecules), there are three direct interactions between the bisphosphonate and Arg 112, Lys 200, and Lys 257, which are not shown for clarity. (b) A cross section view of the allylic (GPP) subpocket rendered in a surface representation. The allylic pocket is blocked at one end by the adjacent monomer (hFPPS exists as a homodimer with an active site in each monomer), which is shown in gray. (c) Superimposition of the N-BP inhibitors 1, 4, and the ThPBP analogue 6m in three cocrystal structures. Carbon atoms are represented in green, cyan, and magenta for the hFPPS−1−IPP (PDB 1ZW5), hFPPS−4−PPi (PDB 4H5D), and hFPPS−6m−PPi (PDB 4L2X) ternary complexes, respectively. The color representation for heteroatoms is: blue for nitrogen, red for oxygen, orange for phosphorus, and yellow for sulfur. The secondary ligands (i.e., PPi or IPP) are omitted for clarity. (d) Closing of the active site in the presence of bound IPP or PPi. The ^{350}KRRK^{353} tail and Lys 57 are rigidified in both the hFPPS−1−IPP and hFPPS−6m−PPi complexes. The side chains of Arg 352 and Lys 353 are not shown for clarity. The potential steric clash between the thienopyrimidine core of 6m and the prenyl side chain of IPP is evident (closest carbon-to-carbon contact is less than 2.7 Å).

enzyme and is partly responsible for the excellent in vivo efficacy of the bisphosphonate compounds.[64]

In addition, our crystal structure suggested that cobinding of IPP and inhibitor 6m was unlikely due to a potential steric clash between the thienopyrimidine core of 6m and the prenyl side chain of IPP (Figure 3d). This prediction was confirmed by determining the thermal stability of the hFPPS complexes using differential scanning fluorimetry (DSF).[65] A substantial differ-ence in thermal stability was observed for the hFPPS−2a and hFPPS−4 complexes in the presence or absence of IPP (T_m) of approximately +8 °C and +14 °C, respectively (Figure 4a,b). The thermal stability difference observed between the hFPPS−2a and hFPPS−2a−IPP complexes is consistent with a T_m of +8.3 °C, measured using differential scanning calorimetry (DSC) under the same ratio of ligands (i.e., 2a:IPP in 1:1 ratio).[10] In contrast, parallel titration of hFPPS with 6m and IPP showed no significant difference in the thermal stability of these complexes (Figure 4c; $T_m \leq 1$ °C), suggesting that cobinding of 6m and IPP was prohibited.

CONCLUSIONS

Herein we disclose the hit-to-lead optimization of a new series of thienopyrimidine-based bisphosphonate (ThP-BP) inhibitors of hFPPS, which led to the identification of compounds with low nanomolar potency. The crystal structures of the hFPPS−6f−SO_4 and hFPPS−6m−PPi ternary complexes revealed that the inhibitors bind to the allylic subpocket of the active site and their side chain extends through the capping phenyls and toward the protein dimer interface. The side chain of these inhibitors engages in stacking interactions with both Phe 99 and Gln 171, as we previously observed with inhibitor 4.[37,63] A number of other conformational changes within the active site were also observed, including the closing of the C-terminal tail over the IPP subpocket, which was induced by inorganic pyrophosphate (PPi). Our X-ray structures and the DSF thermal stability data of the hFPPS−6m complex also suggest that the ThP-BP inhibitors compete for binding with both natural substrates of hFPPS (i.e., DMAPP/GPP and IPP) and occupy (in part) both subpockets of the active site cavity. Significant physicochemical differences between the ThP-BP compounds and the current N-BP drugs include higher lipophilicity and higher affinity for the bone mineral hydroxyapatite. Analogue 6m, which exhibits good in vitro potency and a high lipophilicity, was also shown to inhibit proliferation of human multiple myeloma cells (RPMI 8226) with equivalent potency to N-BPs 1 and 2a. Thus further lead optimization of the ThP-BP analogues is warranted and currently in progress. The higher lipophilicity of these compounds could result in lower rate of elimination from plasma, higher volume of distribution into nonskeletal tissue, and better therapeutic value for treating multiple myeloma and other nonskeletal cancers.

dx.doi.org/10.1021/jm400946f | J. Med. Chem. 2013, 56, 7939−7950

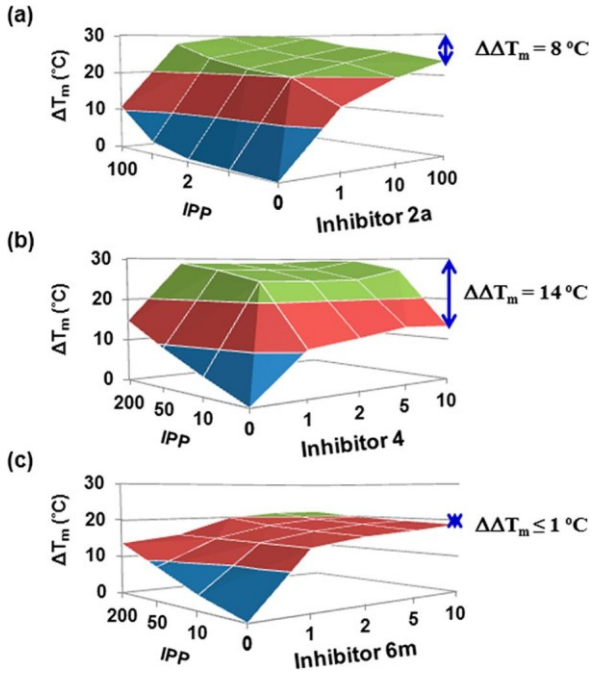

Figure 4. Differential scanning fluorimetry (DSF) surface plots showing concentration-dependent increase in thermal stability of hFPPS−inhibitor−IPP complexes; hFPPS concentration fixed at 4 μM; the x/y axis indicates IPP:inhibitor molar ratios relative to the concentration of hFPPS. (a) Co-binding of inhibitor 2a and IPP to hFPPS. (b) Co-binding of inhibitor 4 and IPP to hFPPS. (c) Co-titration of inhibitor 6m and IPP to a solution of hFPPS; plot suggests the simultaneous binding of 6m and IPP in the hFPPS active site does not occur.

EXPERIMENTAL SECTION

General Procedures for Characterization of Compounds. All analogues 13 were purified by normal phase flash column chromatography using a CombiFlash instrument on silica gel and a solvent gradient from 5% EtOAc in hexanes to 100% EtOAc and then to 20% MeOH in EtOAc unless otherwise indicated. The homogeneity of all analogues 13 was confirmed by reverse-phase HPLC. Only bisphosphonate esters 13 with homogeneity ≥95% were processed further though the hydrolysis step to the final bisphosphonic acid inhibitors 6a−n. IC_{50} values were determined only for final compounds 6a−n with ≥95% homogeneity. HPLC Analysis was performed using a Waters ALLIANCE instrument (e2695 with 2489 UV detector and 3100 mass spectrometer). Each analogue of 13 and 6 was fully characterized by ^{1}H, ^{13}C, and ^{31}P NMR and MS. Chemical shifts (δ) are reported in ppm relative to the internal deuterated solvent (^{1}H, ^{13}C) or external H_3PO_4 (δ 0.00 ^{31}P) unless indicated otherwise. The high-resolution MS spectra of final products 6a−n were recorded using electrospray ionization ($ESI^{\pm}$) and Fourier transform ion cyclotron resonance mass analyzer (FTMS).

Method. (homogeneity analysis using a Waters Atlantis T3 C18 5 μm column): Solvent A: H_2O, 0.1% formic acid. Solvent B: CH_3CN, 0.1% formic acid. Mobile phase: linear gradient from 95%A and 5%B to 5%A and 95%B in 13 min, then 2 min at 100% B. Flow rate: 1 mL/min.

Synthesis of Tetraethyl (((6-Bromothieno[2,3-d]pyrimidin-4-yl)-amino)methylene)bis(phosphonate) (11). A solution of 6-bromothieno[2,3-d]pyrimidin-4-amine (10, 500 mg, 2.173 mmol, 1 equiv) in anhydrous toluene (20 mL) was flushed with argon in a pressure vessel. Diethylphosphite (1.96 mL, 15.2 mmol, 7 equiv) and triethyl orthoformate (0.61 mL, 3.69 mmol, 1.7 equiv) were added to the reaction mixture via syringe, and the reaction mixture was argon flushed, sealed, and stirred at 130 °C in the dark for 48 h. The crude mixture was concentrated to dryness under vacuum. The crude product was purified by normal phase flash column chromatography on silica gel using a CombiFlash instrument and a solvent gradient from 20% EtOAc/hexanes to 100% EtOAc and 100% EtOAc to 20% methanol/EtOAc to give intermediate 11 as a pale-yellow solid (834.2 mg, 74% isolated yield). ^{1}H NMR (400 MHz, CD_3OD): δ 8.44 (s, 1H), 7.85(s, 1H), 5.96 (t, J = 23.7 Hz, 1H), 4.24−4.17 (m, 8H), 1.31−1.25 (m, 12H). ^{13}C NMR (75 MHz, CD_3OD): δ 168.7, 156.2, 154.5, 123.1, 119.1, 113.4, 65.2−65.0 (m), 45.6 (t, J = 150.2 Hz), 16.7−16.6 (m). ^{31}P NMR (81 MHz, D_2O): δ 17.2. MS (ESI−) m/z $[M + H]^+$: 514.1.

Table 3. Data Collection and Refinement Statistics[a]

Data Sets		
PDB ID	4JVJ	4L2X
ligands	inhibitor 6f, SO_4	inhibitor 6m, PPi
Data Collection		
space group	$P4_12_12$	$P4_12_12$
unit cell dimension (Å)	a = b = 111.33, c = 67.46	a = b = 111.34, c = 68.77
resolution range (Å)	50.0−2.80 (2.85−2.80)	50.0−2.55 (2.62−2.55)
redundancy	9.5 (9.6)	9.5 (9.5)
completeness (%)	98.6 (99.6)	98.3 (93.8)
$I/\sigma(I)$	27.3 (6.6)	24.0 (6.1)
R_{merge}	0.073 (0.260)	0.052 (0.382)
Refinement		
no. reflections	10170	13394
no. protein atoms	2648	2687
no. ligand atoms	31	37
no. ion atoms	3	3
no. solvent atoms	14	15
R_{work}/R_{free}	0.236/0.288	0.201/0.257
rms Deviations		
bond length (Å)	0.011	0.013
bond angle (deg)	1.4	1.7

[a]Values in parentheses are for the highest resolution shell.

General Protocol for the Suzuki Cross-Coupling Reactions Using Fragment 11. Suzuki coupling reactions were run in parallel using aliquots of fragment 11 (~40 mg) and various boronate esters (1.4 equiv); examples are shown in Figure 1. All reactions were carried out in MeOH (purged with argon, both before and after the addition of reagents), in an argon flushed microwave reactor vial, at 120 °C for 20 min (120W), catalyzed by $Pd(PPh_3)_4$ (0.1 equiv) and KF (2.5 equiv). The crude mixtures were filtered through Celite, concentrated to dryness under vacuum, and purified using automation as described in the general procedures.

General Protocol for the Hydrolysis of the Esters 13 to Give the Final Inhibitors 6a−n. A solution of the tetraethyl bisphosphonate ester (1 equiv) in CH_2Cl_2 was cooled to 0 °C, and trimethylsilyl bromide (15 equiv) was added via syringe. The reaction mixture was stirred at room temperature for 3−5 days; completion of conversion was monitored by ^{31}P NMR. The mixture was then concentrated under vacuum, diluted with HPLC grade MeOH (~5 mL), and the solvent was evaporated to dryness; this step was repeated four times. The organic solvents were evaporated under vacuum, the residue was suspended in 0.5 mL MeOH, and H_2O (~5 mL Milli-Q grade) was added to induce precipitation of the thienopyrimidine bisphosphonic acid 6. The amorphous powder was collected by filtration, washed with deionized water (2×), HPLC-grade CH_3CN (2×), and with distilled Et_2O or toluene (2×). The residue was then dried under vacuum to give the final compound 6a−n as a solid; it should be noted that although the conversion of 13 to 6 was quantitative (as determined by HPLC and ^{31}P NMR), the isolated yields varied depending on the solubility of each final products.

(((6-(1H-Indazol-4-yl)thieno[2,3-d]pyrimidin-4-yl)amino)-methylene)diphosphonic Acid (6a). Isolated as a yellow solid, 18.5

dx.doi.org/10.1021/jm400946f | J. Med. Chem. 2013, 56, 7939−7950

mg (66% overall isolated yield). ^{1}H NMR (500 MHz, D_2O): δ 8.30 (overlapping singlets, 2H), 7.31−7.29 (m, 2H), 7.15−7.12 (m, 2H); central methylene proton obscured by solvent signal (confirmed by HSQC). ^{13}C NMR (126 MHz, D_2O): δ 162.8, 156.0, 153.3, 140.6, 137.1, 132.5, 126.7, 125.7, 119.7, 118.7, 118.0, 115.6, 110.9, 50.4 (t, J = 124.9 Hz). HSQC (^{1}H−^{13}C): ^{1}H δ 4.57 correlates with ^{13}Cα δ 50.4. ^{31}P NMR (81 MHz, D_2O): δ 13.8. HRMS (ESI−) calculated for $C_{14}H_{12}N_5P_2O_6S$ m/z [M − H]$^-$, 439.99890; found, m/z 439.99914.

(((6-(1H-Indazol-5-yl)thieno[2,3-d]pyrimidin-4-yl)amino)-methylene)diphosphonic Acid (6b). Isolated as a pale-pink solid, 14.9 mg (17% overall isolated yield). ^{1}H NMR (500 MHz, D_2O): δ 8.02 (s, 1H), 7.65 (d, J = 8.2 Hz, 1H), 7.59 (s, 1H), 7.55 (s, 1H), 7.50 (d, J = 8.2 Hz, 1H), 6.94 (s, 1H) ; central methylene proton obscured by solvent signal. ^{13}C NMR (126 MHz, D_2O): δ 161.7, 155.4, 152.8, 139.2, 139.1, 133.3, 125.8, 124.3, 122.1, 118.1, 117.9, 112.9, 111.8, Cα observed by HSQC. HSQC (^{1}H−^{13}C): ^{1}H δ 4.56 correlates with ^{13}C δ 50.8. ^{31}P NMR (81 MHz, D_2O): δ 13.9. HRMS (ESI−) calculated for $C_{14}H_{12}N_5P_2O_6S$ m/z [M − H]$^-$, 439.99890; found, m/z 439.99912.

(((6-(3,5-Dimethylisoxazol-4-yl)thieno[2,3-d]pyrimidin-4-yl)-amino)methylene)diphosphonic Acid (6c). Isolated as a white solid, 18.2 mg (39% overall isolated yield). ^{1}H NMR (500 MHz, D_2O): δ 8.29 (s, 1H), 7.56 (s, 1H), 4.63 (t, J = 18.9 Hz, 1H), 2.56 (s, 3H), 2.40 (s, 3H). ^{13}C NMR (126 MHz, D_2O): δ 167.9, 163.5, 159.8, 156.1, 153.5, 126.6, 118.5, 117.7, 110.1, 50.8 (t, J = 125.9 Hz), 11.4, 10.2. ^{31}P NMR (81 MHz, D_2O): δ 13.6. HRMS (ESI−) calculated for $C_{12}H_{13}N_4P_2O_7S$ m/z [M − H]$^-$, 418.9986; found, m/z 418.9985.

(((6-(m-Tolyl)thieno[2,3-d]pyrimidin-4-yl)amino)methylene)-diphosphonic Acid (6g). Isolated as a pale-yellow solid, 25.5 mg (55% overall isolated yield). ^{1}H NMR (500 MHz, D_2O): δ 8.28 (s, 1H), 7.87 (s, 1H), 7.65 (s, 1H), 7.60 (d, J = 7.8 Hz, 1H), 7.40 (t, J = 7.8 Hz, 1H), 7.27 (d, J = 7.8 Hz, 1H), 4.63 (t, J = 18.8 Hz, 1H), 2.39 (s, 3H). ^{13}C NMR (126 MHz, D_2O): δ 163.2, 156.2, 153.5, 139.5, 139.4, 133.1, 129.3, 129.2, 126.5, 123.0, 118.6, 114.6, 20.3, Cα observed by HSQC. HSQC (^{1}H−^{13}C): ^{1}H δ 4.63 correlates with ^{13}C δ 51.0. ^{31}P NMR (81 MHz, D_2O): δ 13.7. HRMS (ESI−) calculated for $C_{14}H_{14}N_3P_2O_6S$ m/ z [M − H] , 414.00840; found, m/z 414.00848.

(((6-(4-(Trifluoromethyl)phenyl)thieno[2,3-d]pyrimidin-4-yl)-amino)methylene)diphosphonic Acid (6h). Isolated as a yellow solid, 25.4 mg (52% overall isolated yield). ^{1}H NMR (500 MHz, D_2O): δ 8.29 (s, 1H), 8.00 (s, 1H), 7.93 (d, J = 8.2 Hz, 2H), 7.79 (d, J = 8.2 Hz, 2H), 4.63 (t, J = 18.9 Hz, 1H). ^{13}C NMR (126 MHz, D_2O): δ 163.6, 156.3, 153.9, 137.5, 136.7, 129.2 (q, J = 32.4 Hz), 126.2, 126.0 (q, J = 3.8 Hz), 124.1 (q, J = 270.1 Hz), 118.5, 116.5, Cα observed by HSQC. HSQC (^{1}H−^{13}C): ^{1}H δ 4.63 correlates with ^{13}C δ 51.1. ^{31}P NMR (81 MHz, D_2O): δ 13.6. HRMS (ESI−) calculated for $C_{14}H_{11}F_3N_3P_2O_6S$ m/z [M − H]$^-$, 467.97959; found, m/z 467.9783.

(((6-(3-(Trifluoromethyl)phenyl)thieno[2,3-d]pyrimidin-4-yl)-amino)methylene)diphosphonic Acid (6i). Isolated as a white solid, 23.4 mg (44% overall isolated yield). ^{1}H NMR (500 MHz, D_2O): δ 8.29 (s, 1H), 8.08 (s, 1H), 8.00 (d, J = 7.8 Hz, 1H), 7.95 (s, 1H), 7.71 (d, J = 7.8 Hz, 1H), 7.65 (t, J = 7.8 Hz, 1H), 4.64 (t, J = 18.8 Hz, 1H). ^{13}C NMR (126 MHz, D_2O): δ 163.5, 156.3, 153.8, 137.7, 134.0, 130.8 (q, J = 32.9 Hz), 129.7, 129.5, 124.9 (q, J = 3.7 Hz), 123.9 (q, J = 272.3 Hz), 122.7 (q, J = 3.8 Hz), 118.5, 115.9, 50.9. ^{31}P NMR (81 MHz, D_2O): δ 13.7. HRMS (ESI−) calculated for $C_{14}H_{11}F_3N_3P_2O_6S$ m/z [M − H]$^-$, 467.98014; found, m/z 467.978033.

(((6-(4-Methoxyphenyl)thieno[2,3-d]pyrimidin-4-yl)amino)-methylene)diphosphonic Acid (6j). Isolated as a pale-yellow powder; 30.8 mg (71% overall isolated yield). ^{1}H NMR (400 MHz, D_2O): δ 8.11 (s, 1H), 7.58(s, 1H), 7.57 (d, J = 8.0 Hz, 2H), 6.91 (d, J = 8.0 Hz, 2H), 3.70 (s, 3H); central methylene proton obscured by solvent signal. ^{13}C NMR (126 MHz, D_2O): δ 162.7, 159.2, 156.0, 153.2, 139.1, 127.5, 126.3, 118.7, 114.6, 113.4, 55.3, Cα observed by HSQC. HSQC (^{1}H−^{13}C): ^{1}H δ 4.74 correlates with ^{13}C δ 49.0. ^{31}P NMR (81 MHz, D_2O): δ 13.7. HRMS (ESI−) calculated for $C_{14}H_{14}N_3P_2O_7S$ m/z [M − H]$^-$, 430.00332; found, m/z 430.00442.

(((6-(4-Isopropoxyphenyl)thieno[2,3-d]pyrimidin-4-yl)amino)-methylene)diphosphonic Acid (6k). Isolated as a white powder; 21.9 mg (54% overall isolated yield). ^{1}H NMR (500 MHz, D_2O): δ 8.17 (s, 1H), 7.69 (s, 1H), 7.67 (d, J = 8.8 Hz, 2H), 7.02 (d, J = 8.8 Hz, 2H), 1.27 (d, J = 6.1, 6H); central methylene proton and I-Pr-CH obscured by solvent signal. ^{13}C NMR (126 MHz, D_2O): δ 164.4, 158.9, 157.7, 155.0, 140.7, 129.2, 128.2, 120.4, 118.6, 115.3, 73.3, 22.7, Cα observed by HSQC. HSQC (^{1}H−^{13}C): ^{1}H δ 4.60 correlates with ^{13}C δ 73.3 and ^{1}H δ 4.47 correlates with ^{13}C δ 50.4. ^{31}P NMR (81 MHz, D_2O): δ 13.7. HRMS (ESI−) calculated for $C_{16}H_{18}N_3P_2O_7S$ m/z [M − H]$^-$, 458.03462; found, m/z 458.03532.

(((6-(4-Cyclopropoxyphenyl)thieno[2,3-d]pyrimidin-4-yl)amino)-methylene)diphosphonic Acid (6l). Isolated as a beige powder; 16.2 mg (38% overall isolated yield). ^{1}H NMR (500 MHz, D_2O): δ 8.12 (s, 1H), 7.63 (s, 1H), 7.62 (d, J = 8.7 Hz, 2H), 7.10 (d, J = 8.7 Hz, 2H), 4.42 (br s, 1H), 3.82−3.80 (m, 1H), 0.74−0.71 (m, 2H), 0.65−0.62 (m, 2H); central methylene proton obscured by solvent signal. ^{13}C NMR (126 MHz, D_2O): δ 162.7, 158.5, 156.0, 153.3, 139.1, 127.4, 126.7, 118.7, 115.7, 113.6, 51.3, 5.45, Cα observed by HSQC at ~50. ^{31}P NMR (81 MHz, D_2O): δ13.6. HRMS (ESI−) calculated for $C_{16}H_{16}N_3P_2O_7S$ m/z [M − H]$^-$, 456.0190; found, m/z 456.0189.

(((6-(4-Cyclopropylphenyl)thieno[2,3-d]pyrimidin-4-yl)amino)-methylene)diphosphonic Acid (6m). Isolated as a light-brown powder 18.8 mg (47% overall isolated yield). ^{1}H NMR (400 MHz, D_2O): δ 8.13(s, 1H), 7.70 (s, 1H), 7.58 (d, J = 8.3 Hz, 2H), 7.11 (d, J = 8.3 Hz, 2H), 4.46 (t, J = 18.7 Hz, 1H), 1.88−1.84 (m, 1H), 0.93−0.86 (m, 2H), 0.66−0.62 (m, 2H). ^{13}C NMR (75 MHz, D_2O): δ 165.4, 158.7, 156.0, 148.0, 141.8, 132.9, 128.7, 128.6, 121.2, 116.6, 17.1, 11.9, Cα observed by HSQC. HSQC (^{1}H−^{13}C): ^{1}H δ 4.46 correlates with ^{13}C δ 50.9. ^{31}P NMR (81 MHz, D_2O): δ 13.8. HRMS (ESI−) calculated for $C_{16}H_{16}N_3P_2O_6S$ m/z [M − H]$^-$, 440.02405; found, m/z 440.02414.

(((6-(4-(2,2-Difluorocyclopropyl)phenyl)thieno[2,3-d]pyrimidin-4-yl)amino)methylene)diphosphonic Acid (6n). Isolated as a pale-yellow solid 26.7 mg (50% overall isolated yield). ^{1}H NMR (500 MHz, D_2O): δ 8.27 (s, 1H), 7.86 (s, 1H), 7.75 (d, J = 8.4 Hz, 2H), 7.38 (d, J = 8.4 Hz, 2H), 4.63 (t, J = 18.9 Hz, 1H), 2.98−2.91 (m, 1H), 1.96− 1.90 (m, 1H), 1.86−1.78 (m, 1H). ^{13}C NMR (126 MHz, D_2O): δ 163.2, 156.2, 153.4, 138.9, 134.3, 132.0, 128.7, 126.0, 118.5, 115.6, 113.3 (t, J = 285 Hz), 26.38 (t, J = 11.2 Hz), 16.1 (t, J = 10.3 Hz), Cα observed by HSQC. HSQC (^{1}H−^{13}C): ^{1}H δ 4.63 correlates with ^{13}C δ 50.5. ^{31}P NMR (81 MHz, D_2O): δ 13.7. HRMS (ESI−) calculated for $C_{16}H_{14}F_2N_3P_2O_6S$ m/z [M − H]$^-$, 476.0052; found, m/z 476.0046.

In Vitro Inhibition Assays. The in vitro enzymatic assay of method 1 (M1) was carried out as previously described.[11,14,16] The human FPPS in vitro inhibition assay of method 2 (M2) was carried out using 4 ng of the human recombinant FPPS and 0.2 μM of each substrates, GPP and IPP (^{3}H-IPP, 3.33 mCi/mmol) in a final volume of 100 μL of buffer containing 50 mM Tris pH 7.7, 1 mM $MgCl_2$, 0.5 mM TCEP, 20 μg/mL BSA, and 0.01% Triton X-100. All assays were run in triplicate with a 10 min preincubation period; hFPPS and inhibitor were incubated in the assay buffer in a volume of 80 μL at 37 °C for 10 min. After the 10 min preincubation, the substrates were added to the reaction mixture (bringing the inhibitor and substrates to the desired final concentrations). All assays were incubated at 37 °C for 8 min and terminated by the addition of 200 μL of HCl/methanol (1:4), followed by an additional incubation of 10 min at 37 °C. The assay mixture was then extracted with 700 μL of ligroin, dried through a plug of anhydrous $MgSO_4$, and 300 μL of the ligroin phase was combined with 8 mL of scintillation cocktail. The radioactivity was then counted using a Beckman Coulter LS6500 liquid scintillation counter.

Reagents for in Vitro Assay. The hFFPS enzyme was stored at −80 °C as a 2 μg/μL solution in the eluent buffer (50 mM HEPES pH 7.5, 500 mM NaCl, 250 mM imidazole, 5% glycerol, 0.5 mM TCEP). ^{3}H-IPP was purchased from American Radiolabeled Chemicals (ART 0377A: 1mCi/mL, 60 Ci/mmol in 0.1 M Tris pH 7.5) and was diluted with cold IPP to a specific activity of 33 mCi/mmol and 2 μM concentration in 200 mM Tris pH 7.7; the IPP solution was stored at −10 °C, warmed to 0 °C, and kept on ice during assay setup. Unlabeled IPP and GPP were purchased from Isoprenoids, Lc. as their ammonium salts. GPP was dissolved and diluted to a 2 μM concentration in 200 mM Tris pH 7.7. It was stored at −10 °C, warmed to 0 °C, and kept on ice during assay setup. Ligroin was

dx.doi.org/10.1021/jm400946f | J. Med. Chem. 2013, 56, 7939−7950

purchased from Sigma Aldrich, liquid scintillation cocktail was purchased from MP Biomedicals: Ecolite (no. 882475),

Cell Culture and Viability Assays. The RPMI 8226 multiple myeloma cell line was obtained courtesy of Dr. Leif Bergsagel (Mayo Clinic, Scottsdale, AZ) and cultured in RPMI-1640 medium supplemented with 10% fetal bovine serum (Gibco BRL, Gaithesburg, MD) supplemented with 2 mM L-glutamine in a 5% CO_2 atmosphere at 37 °C. A dilution method was used to determine EC_{50} values for inhibition for each target compound; compounds were diluted in culture medium. Cells were seeded in 96-well plates at a density 10000 cells per well incubated for 2 h before the addition of 10 μL of compound at half-logarithmic dilutions from 100 nM to 333 μM with a fixed final volume. Plates were then incubated for 72 h at 37 °C in the presence 5% CO_2, following which an MTT, 4,5-dimethylthiazole-2-yl)-2,5-diphenyltetrazolium bromide reagent was used according to the manufacturers documentation (Promega, Madison, WI). Plates were read at OD490 nM on a Dynex MRX microplate reader (Magellan Biosciences, Chelmsford MA). Results were analyzed to obtain dose−response curves and EC_{50} calculations using GraphPad PRISM version 5 (GraphPad Software, San Diego, CA).

Calculation of CLogP Values. CLogP values were estimated using the CLogP tool in ChemDraw Ultra 12.0; the two phosphonate moieties were deleted from each structure in order to simplify the calculations. For example, the structures of 2a and 6m used for the calculations are shown below as fragment 2a−x and 6m−x, respectively. Good correlation was observed between the CLogP values of known compounds calculated using the same tool and those reported in the literature (predicted by other in silico tools, such as MedChem Studio prediction software; ADMET Predictor 5.5, Simulation Plus Inc.). IC_{50} values not determined (nd).

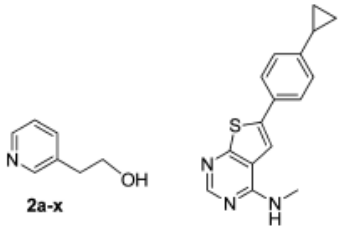

Crystallization of hFPPS in Complex with Inhibitors 6f and 6m. Compounds 6f and 6m were prepared as 20 mM stock solutions in 100 mM TrisHCl (pH 7.5). Each stock solution was added to the concentrated hFPPS sample to give the final concentrations of 1 mM inhibitor and 0.25 mM protein (10 mg/mL). To obtain crystals suitable for X-ray diffraction analysis, microseeding was employed. All crystals were grown at 22 °C by vapor diffusion in sitting drops composed of 1 μL of protein/inhibitor mixture and 1 μL of crystallization solution, and additional 0.5 μL of seed solution when added. Seed solutions were prepared by using Seed Bead kits (Hampton Research). For the hFPPS−CL01−121 complex, the initial crystals formed in a crystallization solution composed of 0.1 M TrisHCl (pH 8.5) and 2 M ammonium dihydrogen phosphate. In the first round of seeding optimization, crystals of improved quality grew in a new crystallization solution containing 0.09 M sodium acetate (pH 4.6), 0.17 M ammonium sulfate, 1.5 mM magnesium chloride, 25.5% (w/v) PEG MME 2000, and 15% (v/v) glycerol. Diffraction quality crystals were identified in the second round of optimization in yet another crystallization condition consisting of 0.1 M TrisHCl (pH 7.0), 0.25 M magnesium chloride, and 7% (w/v) PEG 8000. For the hFPPS−CL02−134 complex, crystals were grown in a solution composed of 0.08 M sodium cacodylate (pH 6.5), 0.16 M magnesium acetate, 16% (w/v) PEG 8000, and 20% glycerol, by using the hFPPS−CL01−121 cocrystals as heterogeneous seeds.

Data Collection, Processing, and Structure Refinement. Diffraction data were collected from single crystals at 100K with synchrotron radiation (Canadian Light Source, Saskatoon, SK) and a Rayonix MX300 CCD detector. The diffraction data were indexed and scaled with either HKL2000[66] or the xia2 package.[67] The initial structure models were built by difference Fourier methods with a ligand/solvent-omitted input model generated from the PDB model 4H5D. The initial models were further improved through iterative rounds of manual and automated refinement with COOT[68] and REFMAC5.[69] The final models have been deposited into the Protein Data Bank. Data collection and refinement statistics, as well as the PDB IDs for these models, are presented in Table 3.

ASSOCIATED CONTENT

* Supporting Information

NMR spectra of final inhibitors 6a−n; examples of homogeneity data for key final inhibitors at (bisphosphonic acids). Some experimental details on the dynamic light scattering (DSL) studies. This material is available free of charge via the Internet at http://pubs.acs.org.

AUTHOR INFORMATION

Corresponding Author

*Phone: 514-398-3638. Fax: 514-398-3797. Email: Youla.tsantrizos@mcgill.ca.

Notes

The authors declare no competing financial interest.

ACKNOWLEDGMENTS

^{1}H NMR experiments to assess HAP binding of our inhibitors were acquired on a 500 MHz NMR instrument at the Quebec/Eastern Canada High Field NMR Facility, supported by the Natural Sciences and Engineering Research Council of Canada (NSERC), the Canada Foundation for Innovation (CFI), the Quebec Ministere de la Recherche en Science et Technologie (FQRNT), and McGill University. We are grateful Xian Fang Huang for assistance with the cell-based assays. We also thank to Jinming Guan for her help with the preparation of some compounds. Financial support for this work was provided by NSERC and FQRNT (research grants to Y. S. Tsantrizos) and the Canadian Institute of Health Research (CIHR; research grants to A. M. Berghuis and M. Sebag).

ABBREVIATIONS USED

hFPPS, human farnesyl pyrophosphate synthase; hGGPPS, human geranylgeranyl pyrophosphate synthase; DMAPP, dimethylallyl pyrophosphate; IPP, isopentenyl pyrophosphate; GPP, geranyl pyrophosphate; FPP, farnesyl pyrophosphate; GGPP, geranylgeranyl pyrophosphate; N-BPs, nitrogen-containing bisphosphonates; MM, multiple myeloma; GTPases, small guanine triphosphate binding proteins; ANT, mitochondrial adenine nucleotide translocase; IFNγ, interferon-γ; TNFα, tumor necrosis factor-α; hSQS, human squalene synthase; ApppI, derivative 1-adenosin-5′-yl ester 3-(3-methylbut-3-enyl) triphosphoric acid; HAP, hydroxyapatite; SAS, structure− activity studies; SAR, structure−activity relationship; DLS, dynamic light scattering

REFERENCES

(1) Dunford, J. E.; Thompson, K.; Coxon, F. P.; Luckma, S. P.; Hahn, F. M.; Poulter, C. D.; Ebetino, F. H.; Rogers, M. J. Structure−Activity Relationship for Inhibition of Farnesyl Diphosphate Synthase in Vitro and Inhibition of Bone Resorption in Vivo by Nitrogen-Containing Bisphosphonates. J. Pharmacol. Exp. Ther. 2001, 296, 235−242.

(2) Coxon, F. P.; Thompson, K.; Rogers, M. J. Recent advances in understanding the mechanism of action of bisphosphonates. Curr. Opin. Pharmacol. 2006, 6, 307−312.

(3) Chapman, M. A.; Lawrence, M. S.; Keats, J. J.; Cibulskis, K.; Sougnez, C.; Schinzel, A. C.; Harview, C. L.; Brunet, J. P.; Ahmann, G. J.; Adli, M.; Anderson, K. C.; Ardlie, K. G.; Auclair, D.; Baker, A.; Bergsagel, P. L.; Bernstein, B. E.; Drier, Y.; Fonseca, R.; Gabriel, S. B.; Hofmeister, C. C.; Jagannath, S.; Jakubowiak, A. J.; Krishnan, A.; Levy, J.; Liefeld, T.; Lonial, S.; Mahan, S.; Mfuko, B.; Monti, S.; Perkins, L. M.; Onofrio, R.; Pugh, T. J.; Rajkumar, S. V.; Ramos, A. H.; Siegel, D. S.; Sivachenko, A.; Stewart, A. K.; Trudel, S.; Vij, R.; Voet, D.; Winckler, W.; Zimmerman, T.; Carpten, J.; Trent, J.; Hahn, W. C.; Garraway, L. A.; Meyerson, M.; Lander, E. S.; Getz, G.; Golub, T. R. Initial genome sequencing and analysis of multiple myeloma. Nature 2011, 471, 467−472.

(4) Coleman, R. E. Clinical Features of Metastatic Bone Disease and Risk of Skeletal Morbidity. Clin. Cancer Res. 2006, 12, 6243s−6249s.

(5) Fournier, P. G.; Stresing, V.; Ebetino, F. H.; Clezardin, P. How do Bisphosphonates Inhibit Bone Metastasis in Vivo. Neoplasia 2010, 12, 571−578.

(6) Mönkkönen, H.; Auriola, S.; Lehenkari, P.; Kellinsalmi, M.; Hassinen, I. E.; Vepsalainen, J.; Mönkkönen, J. A new endogenous ATP analog (ApppI) inhibits the mitochondrial adenine nucleotide translocase (ANT) and is responsible for the apoptosis induced by nitrogen-containing bisphosphonates. Br. J. Pharmacol. 2006, 147, 437−445.

(7) Mitrofan, L. M.; Pelkonen, J.; Mönkkönen, J. The level ofATP analogs and isopentenyl pyrophosphate correlates with zoledronic acid-induced apoptosis in cancer cells in vitro. Bone 2009, 45, 1153− 1160.

(8) Morita, C. T.; Jin, C.; Sarikonda, G.; Wang, H. Nonpeptide antigens, presentation mechanisms, and immunological memory of human Vg2Vg2 T cells: discriminating friends from foe through the recognition of prenyl pyrophosphate antigens. Immunol. Rev. 2007, 215, 59−76.

(9) Tong, H.; Kuder, C. H.; Wasko, B. M.; Hohl, R. J. Quantitative determination of isopentenyl diphosphate in cultured mammalian cells. Anal. Biochem. 2013, 433, 36−42.

(10) Rondeau, J.-M.; Bitsch, F.; Bourgier, E.; Geiser, M.; Hemmig, R.; Kroemer, M.; Lehmann, S.; Ramage, P.; Rieffel, S.; Strauss, A.; Green, J. R.; Jahnke, W. Structural Basis for the Exceptional in vivo Efficacy of Bisphosphonate Drugs. ChemMedChem 2006, 1, 267−273.

(11) Kavanagh, K. L.; Guo, K.; Dunford, J. E.; Wu, X.; Knapp, S.; Ebetino, F. H.; Rogers, M. J.; Russell, R. G. G.; Oppermann, U. The molecular mechanism of nitrogen-containing bisphosphonates as antiosteoporosis drugs. Proc. Natl. Acad. Sci. U. S. A. 2006, 103, 7829−7834.

(12) Martin, M. B.; Arnold, W.; Heath, H. T., III; Urbina, J. A.; Oldfield, E. Nitrogen-Containing Bisphosphonates as Carbocation Transition State Analogs for Isoprenoid Biosynthesis. Biochem. Biophys. Res. Commun. 1999, 263, 754−758.

(13) Marma, M. S.; Xia, Z.; Stewart, C.; Coxon, F.; Dunford, J. E.; Baron, R.; Kashemirov, B. A.; Ebetino, F. H.; Triffitt, J. T.; Russell, G. G.; McKenna, C. E. Synthesis and Biological Evaluation of α-Halogenated Bisphosphonate and Phosphonocarboxylate Analogues of Risedronate. J. Med. Chem. 2007, 50, 5967−5975.

(14) Fournier, P. G.; Stresing, V.; Ebetino, F. H.; Clezardin, P. How Do Bisphosphonates Inhibit Bone Metastasis In Vivo? Neoplasia 2010, 12, 571−578.

(15) Drake, M. T.; Cremers, S. C. L. M. Bisposphonate Therapeutics in Bone Diseases: The Hard and Soft Data on Osteoclast Inhibition. Mol. Interventions 2010, 10, 141−152.

(16) Russell, R. G. G.; Xia, Z.; Dunford, J. E.; Oppermann, U.; Kwaasi, A.; Hulley, P. A.; Kavanagh, K. L.; Triffitt, J. T.; Lundy, M. W.; Phipps, R. J.; Barnett, B. L.; Coxon, F. P.; Rogers, M. J.; Watts, N. B.; Ebetino, F. H. Bisphosphonates. An Update on Mechanism of action and How These Relate to Clinical Efficacy. Ann. N. Y. Acad. Sci. 2007, 1117, 209−257.

(17) Frost, M. L.; Siddique, M.; Blake, G. M.; Moore, A. E.; Marsden, P. K.; Schleyer, P. J.; Eastell, R.; Fogelman, I. Regional bone metabolism at the lumbar spine and hip following discontinuation of alendronate and risedronate treatment in postmenopausal women. Osteoporos Int. 2012, 23, 2107−2116.

(18) Grey, A.; Bolland, M. J.; Wattie, D.; Horne, A.; Gamble, G.; Reid, I. R. The antiresorptive effects of a single dose of zoledronate persists for two years: a randomized placebo-control trial in osteopenic postmenopausal women. J. Clin. Endocrinol. Metab. 2009, 94, 538− 544.

(19) Eastell, R.; Walsh, J. S.; Watts, N. B.; Siris, E. Bisphosphonates for postmenopausal osteoporosis. Bone 2011, 49, 82−88.

(20) Skerjanec, A.; Berenson, J.; Hsu, C.; Major, P.; Miller, W. H., Jr.; Ravera, C.; Schran, H.; Seaman, J.; Waldmeier, F. The pharmacoki-netics and pharmacodynamics of zoledronic acid in cancer patients with varying degrees of renal function. J. Clin. Pharmacol. 2003, 43, 154−162.

(21) Weiss, H. M.; Pfaar, U.; Schweitzer, A.; Wiegand, H.; Skerjanec, A.; Schran, H. Biodistribution and plasma protein binding of zoledronic acid. Drug Metab. Dispos. 2008, 36, 2043−2049.

(22) Morgan, G. J.; Davies, F. E.; Gregory, W. M.; Cocks, K.; Bell, S. E.; Szubert, A. J.; Navarro-Coy, N.; Drayson, M. T.; Owen, R. G.; Feyler, S.; Ashcroft, A. J.; Ross, F.; Byrne, J.; Roddie, H.; Rudin, C.; Cook, G.; Jackson, G. H.; Child, J. A. First-line treatment with zoledronic acid as compared with clodronic acid in multiple myeloma (MRC Myeloma IX): a randomized controlled trial. Lancet 2010, 376, 1989−1999.

(23) Morgan, G. J.; Davies, F. E.; Gregory, W. M.; Szubert, A. J.; Bell, S. E.; Drayson, M. T.; Owen, R. G.; Ashcroft, A. J.; Jackson, G. H.; Child, J. A. Effects of induction and maintenance plus long-term bisphosphonates on bone disease in patients with multiple myeloma: the Medical Research Council Myeloma IX Trial. Blood 2012, 119, 5374−5383.

(24) Gnant, M.; Mlineritsch, B.; Schippinger, W.; Luschin-Ebengreuth, G.; Pöstlberger, S.; Menzel, C.; Jakesz, R.; Seifert, M.; Hubalek, M.; Bjelic-Radisic, V.; Samonigg, H.; Tausch, C.; Eidtmann, H.; Steger, G.; Kwasny, W.; Dubsky, P.; Fridrik, M.; Fitzal, F.; Stierer, M.; Rücklinger, E.; Greil, R. Endocrine Therapy plus Zoledronic Acid in Premenopausal Breast Cancer. New Engl. J. Med. 2009, 360, 679− 691.

(25) Coleman, R. E.; Marshall, H.; Cameron, D.; Dodwell, D.; Burkinshaw, R.; Keane, M.; Gil, M.; Houston, S. J.; Grieve, R. J.; Barrett-Lee, P. J.; Ritchie, D.; Pugh, J.; Gaunt, C.; Rea, U.; Peterson, J.; Davies, C.; Hiley, V.; Gregory, W.; Bell, R. Breast-Cancer Adjuvant Therapy with Zoledronic Acid. New Engl. J. Med. 2011, 365, 1396− 1405.

(26) Leung, C.-Y.; Langille, A. M.; Mancuso, J.; Tsantrizos, Y. S. Discovery of Thienopyrimidine-Based Inhibitors of the Human Farnesyl Pyrophosphate Synthase Parallel Synthesis of Analogs via a Trimethylsilyl Ylidene Intermediate. Bioorg. Med. Chem. Lett. 2013, 21, 2229−2240.

(27) Tani, N.; Rahnasto-Rilla, M.; Wittekindt, C.; Salminen, K. A.; Ritvanen, A.; Ollakka, R.; Koskiranta, J.; Raunio, H.; Juvonen, R. O. Antifungal activity of novel non-azole molecules against S. cerevisiae and C. albicans. Eur. J. Med. Chem. 2012, 47, 270−277.

(28) Babu, Y.; Chand, P.; Wu, M.; Kotian, P. L.; Kumar, V. S.; Lin, T.-H.; El-Kattan, Y.; Ghosh, A. K. Therapeutic Furopyrimidines and Thienopyrimidines. WO 2006/050161, 2006.

(29) McClellan, W. J.; Dai, Y.; Abad-Zapatero, C.; Albert, D. H.; Bouska, J. J.; Glaser, K. B.; Magoc, T. J.; Marcotte, P. A.; Osterling, D. J.; Stewart, K. D.; Davidsen, S. K.; Michaelides, M. R. Discovery of potent and selective thienopyrimidine inhibitors of Aurora kinases. Bioorg. Med. Chem. Lett. 2011, 21, 5620−5624.

(30) Dai, Y.; Guo, Y.; Frey, R. R.; Ji, Z.; Curtin, M. L.; Ahmed, A. A.; Albert, D. H.; Arnold, L.; Arries, S. S.; Barlozzari, T.; Bauch, J. L.; Bouska, J. J.; Bousquet, P. F.; Cunha, G. A.; Glaser, K. B.; Guo, J.; Li, J.; Marcotte, P. A.; Marsh, K. C.; Moskey, M. D.; Pease, L. J.; Stewart, K. D.; Stoll, V. S.; Tapang, P.; Wishart, N.; Davidsen, S. K.; Michaelides, M. R. Thienopyrimidine Ureas as Novel and Potent Multitargeted Receptor Tyrosine Kinase Inhibitors. J. Med. Chem. 2005, 48, 6066−6083.

(31) Luke, R. W.; Ballard, P.; Buttar, D.; Campbell, L.; Curwen, J.; Emery, S. C.; Griffen, A. M.; Hassall, L.; Hayter, B. R.; Jones, C. D.; McCoull, W.; Mellor, M.; Swain, M. L.; Tucker, J. A. Novel thienopyrimidine and thiazolopyrimidine kinase inhibitors with activity against Tie-2 in vitro and in vivo. Bioorg. Med. Chem. Lett. 2009, 19, 6670−6674.

(32) Horiuchi, T.; Chiba, J.; Uoto, K.; Soga, T. Discovery of novel thieno[2,3-d]pyrimidin-4-yl hydrazine-based inhibitors of cyclin D1-CDK4: synthesis, biological evaluation, and structure−activity relation-ship. Bioorg. Med. Chem. Lett. 2009, 19, 305−308.

(33) Axten, J. M.; Grant, S. W.; Heerding, D. A.; Medina, J. R.; Romeril, S. P.; Tang, J. Chemical Compounds. WO 2011/119663, 2011.

(34) Edgar, K. A.; Wallin, J. J.; Berry, M.; Lee, L. B.; Prior, W. W.; Sampath, D.; Friedman, L. S.; Belvin, M. Isoform-Specific Phosphoinositide 3-Kinase Inhibitors Exert Distinct Effects in Solid Tumors. Cancer Res. 2010, 70, 1164−1172.

(35) Heffron, T. P.; Wei, B. Q.; Olivero, A.; Staben, S. T.; Tsui, V.; Do, S.; Dotson, J.; Folkes, A. J.; Goldsmith, P.; Goldsmith, R.; Gunzner, J.; Lesnick, J.; Lewis, C.; Mathieu, S.; Nonomiya, J.; Shuttleworth, S.; Sutherlin, D. P.; Wan, N. C.; Wang, S.; Wiesmann, C.; Zhu, B.-Y. Rational Design of Phosphoinositide 3-Kinase α Inhibitors That Exhibit Selectivity over the Phosphonoinositide 3-Kinase β Isoform. J. Med. Chem. 2011, 54, 7815−7833.

(36) Rheault, T. R.; Ceferro, T. R.; Dickerson, S. H.; Donaldson, K. H.; Gaul, M. D.; Goetz, A. S.; Mullin, R. J.; McDonald, O. B.; Petrov, K. G.; Rusnak, D. W.; Shewchuk, L. M.; Spehar, G. M.; Truesdale, A. T.; Vanderwall, D. E.; Wood, E. R.; Uehling, D. E. Thienopyrimidine-based dual EGFR/ErbB-2 inhibitors. Bioorg. Med. Chem. Lett. 2009, 19, 817−820.

(37) Lin, Y.-S.; Park, J.; De Schutter, J. W.; Huang, X. F.; Berghuis, A. M.; Sebag, M.; Tsantrizos, Y. S. Design and Synthesis of Active Site Inhibitors of the Human Farnesyl Pyrophosphate Synthase Apoptosis and Inhibition of ERK Phosphorylation in Multiple Myeloma Cells. J. Med. Chem. 2012, 55, 3201.

(38) De Schutter, J. W.; Shaw, J.; Lin, Y.-S.; Tsantrizos, Y. S. Design of Potent Bisphosphonate Inhibitors of the Human Farnesyl Pyrophosphate Synthase via Targeted Interactions with the Active Site "Capping" Phenyls. Bioorg. Med. Chem. 2012, 20, 5583−5591.

(39) Hesse, S.; Perspicace, E.; Kirsch, G. Microwave-assisted synthesis of 2-aminothiophene-3-carboxylic acid derivatives, 3H-thieno[2,3-d]pyrimidin-4-one and 4-chlorothieno[2,3-d]pyrimidine. Tetrahedron Lett. 2007, 48, 5261−5264.

(40) Tranberg, C. E.; Zickgraf, A.; Giunta, B. N.; Luetjens, H.; Figler, H.; Murphree, L. J.; Falke, R.; Fleischer, H.; Linden, J.; Scammells, P. J.; Olsson, R. A. 2-Amino-3-aroyl-4,5-alkylthiophenes: Agonist Allosteric Enhancers at Human A_1 Adenosine Receptors. J. Med. Chem. 2002, 45, 382−389.

(41) Eckert, G. P.; Hooff, G. P.; Strandjord, D. M.; Igbavboa, U.; Volmer, D. A.; Müller, W. E.; Wood, W. G. Regulation of the brain isoprenoids farnesyl- and geranylgeranylpyrophosphate is altered in male Alzheimer patients. Neurobiol. Dis. 2009, 35, 251−257.

(42) Hooff, G. P.; Wood, W. G.; Müller, W. E.; Eckert, G. P. Isoprenoids, small GTPases and Alzheimer's diseases. Biochim. Biophys. Acta 2010, 1801, 896−905.

(43) Zhang, Y.; Leon, A.; Song, Y.; Studer, D.; Haase, C.; Koscielski, L. A.; Oldfield, E. Activity of Nitrogen-Containing and Non-Nitrogen-Containing Bisphosphonates on Tumor Cell Lines. J. Med. Chem. 2006, 49, 5804−5814.

(44) Ezra, A.; Hoffma, A.; Breuer, E.; Alferiev, I. S.; Mönkkönen, J.; Hanany-Rozen, N.El; Weiss, G.; Stepensky, D.; Gati, I.; Cohen, H.; Törmä, S.; Amidon, G. L.; Golomb, G. A Peptide Prodrug Approach for Improving Bisphosphonate Oral Absorption. J. Med. Chem. 2000, 43, 3641−3652.

(45) Shmeeda, H.; Amitay, Y.; Gorin, J.; Tsemach, D.; Mak, L.; Ogorka, J.; Kumar, S.; Zhang, J. A.; Gabizon, A. Delivery of zoledronic acid encapsulated in folate-targeted liposome results in potent in vitro cytotoxic activity on tumor cells. J. Controlled Release 2010, 146, 76− 83.

(46) Zhang, Y.; Cao, R.; Yin, F.; Hudock, M. P.; Guo, R.-T.; Krysiak, K.; Mukherjee, S.; Gao, Y.-G.; Robinson, H.; Song, Y.; No, J. H.; Bergan, K.; Leon, A.; Cass, L.; Goddard, A.; Chang, T.-K.; Lin, F.-Y.; Van Beek, E.; Papapoulos, S.; Wang, A.H.-J.; Kubo, T.; Ochi, M.; Mukkamala, D.; Oldfield, E. Lipophilic Bisphosphonates as Dual Farnesyl/Geranylgeranyl Diphosphate Synthase Inhibitors: An X-ray and NMR Investigation. J. Am. Chem. Soc. 2009, 131, 5153−5162.

(47) Zhang, Y.; Cao, R.; Yin, F.; Lin, F.-Y.; Wang, H.; Krysiak, K.; No, J.-H.; Mukkamala, D.; Houlihan, K.; Li, J.; Morita, C. T.; Oldfield, E. Lipophilic Pyridinium Bisphosphonates: Potent gd T Cell Stimulators. Angrew. Chem. Int. Ed. 2010, 49, 1136−1138.

(48) Simoni, D.; Gebbia, N.; Invidiata, F. P.; Eleopra, M.; Marchetti, P.; Rondanin, R.; Baruchello, R.; Provera, S.; Marchioro, C.; Tolomeo, M.; Marinelli, L.; Limongelli, V.; Novellino, E.; Kwaasi, A.; Dunford, J.; Buccheri, S.; Caccamo, N.; Dieli, F. Design, Synthesis, and Biological Evaluation of Novel Aminobisphosphonates Possessing an in Vivo Antitumor Activity Through a gd-T Lymphocyte-Mediated Activation Mechanism. J. Med. Chem. 2008, 51, 6800−6807.

(49) Ebetino, F. H.; Mazur, A.; Lundy, M. W.; Russeli, R. G. G. 4-Azaindole Bisphosphonates. WO 2010/033980 A2, 2010.

(50) Ebetino, F. H.; Mazur, A.; Lundy, M. W.; Russeli, R. G. G. 5-Azaindole Bisphosphonates. WO 2010/033981 A2, 2010.

(51) Reed, B. C.; Rilling, H. C. Crystallization and partial characterization of prenyltransferase from avian liver. Biochemistry 1975, 14, 50−54.

(52) Glickman, J. F.; Schmid, A. Farnesyl Pyrophosphate Synthase: Real-Time Kinetics and Inhibition by Nitrogen-Containing Bi-sphosphonates in a Scintillation Assay. Assay Drug Dev. Technol. 2007, 5, 205−214.

(53) Dunford, J. E.; Kwaasi, A. A.; Rogers, M. J.; Barnett, B. L.; Ebetino, F. H.; Russell, R. G. G.; Oppermann, U.; Kavanagh, K. L. Structure−Activity Relationship Among the Nitrogen Containing Bisphosphonates in Clinical Use and Other Analogues: Time-Dependent Inhibition of Human Farnesyl Pyrophosphate Synthase. J. Med. Chem. 2008, 51, 2187−2195.

(54) Amstutz, R.; Bold, G.; Cotesta, S.; Jahnke, W.; Marzinzik, A.; Mueller-Hartwieg, C.; Ofner, S.; Stauffer, F.; Zimmermann, J. Quinolines as Inhibitors of Farnesyl Pyrophosphate Synthase. WO 2009/106586 A1, 2009.

(55) Owen, S. C.; Doak, A. K.; Wassam, P.; Shoichet, M. S.; Schoichet, B. K. Colloidal Aggregation Affects the Efficacy of Anticancer Drugs in Cell Culture. ACS Chem. Biol. 2012, 7, 1429− 1435.

(56) Giger, E. V.; Castagner, B.; Leroux, J.-C. Biomedical applications of bisphosphonates. J. Controlled Release 2013, 167, 175−188.

(57) Freire, E.; Vega, D. R.; Baggio, R. Zoledronate complexes. III. Two zoledronate complexes with alkaline earth metals: [Mg-$(C_5H_9N_2O_7P_2)_2(H_2O)_2$] and $[Ca(C_5H_8N_2O_7P_2)(H_2O)]_n$. Acta Crystallogr., Sect. C: Cryst. Struct. Commun. 2010, C66, m166−m170.

(58) Kunnas-Hiltunen, S.; Matilainen, M.; Vepsalainen, J. J.; Ahlgren, M. X-ray diffraction study of bisphosphonate metal complexes: Mg, Sr and Ba complexes of (dichloromethylene)bispho-sphonic acid P,P′-dibenzoyl anhydride. Polyhedron 2009, 28, 200−204.

(59) Peukert, S.; Sun, Y.; Zhang, R.; Hurley, B.; Sabio, M.; Shen, X.; Gray, C.; Dzink-Fox, J.; Tao, J.; Cebula, R.; Wattanasin, S. Design and structure−activity relationships of potent and selective inhibitors of undecaprenyl pyrophosphate synthase (UPPS): tetramic, tetronic acids and dihydropyridin-2-ones. Bioorg. Med. Chem. Lett. 2008, 18, 1840−1844.

(60) Lindert, S.; Zhu, W.; Liu, Y.-L.; Pang, R.; Oldfield, E.; McCammon, J. A. Farnesyl Diphosphate Synthase Inhibitors from in Silico Screening. Chem. Biol. Drug Des. 2013, 81, 742−748.

(61) Jahnke, W.; Rondeau, J.-M.; Cotesta, S.; Marzinzik, A.; Pelle, X.; Geiser, M.; Strauss, A.; Götte, M.; Bitsch, F.; Hemmig, R.; Henry, C.; Lehmann, S.; Glickman, J. F.; Roddy, T. P.; Stout, S. J.; Green, J. R. Allosteric non-bisphosphonate FPPS inhibitors identified by fragment-based discovery. Nature Chem. Biol. 2010, 6, 660−666.

(62) Jahnke, W.; Henry, C. An in vitro Assay to Measure Targeted Drug Delivery to Bone Mineral. ChemMedChem 2010, 5, 770−776.

(63) Park, J.; Lin, Y.-S.; Tsantrizos, Y. S.; Berghuis, A. M. Ternary complex structures of human farnesyl pyrophosphate synthase bound with a novel inhibitor and secondary ligands provide insights into the molecular details of the enzyme's active site closure. BMC Struct. Biol. 2012, 12, 32.

(64) Raikkönen, J.; Taskinen, M.; Dunford, J. E.; Mönkkönen, H.; Auriola, S.; Mönkkönen, J. Correlation between time-dependent inhibition of human farnesyl pyrophosphate synthase and blockade of mevalonate pathway by nitrogen-containing bisphosphonate in cultured cells. Biochem. Biophys Res. Commun. 2011, 407, 663−667.

(65) Niesen, F. H.; Berglund, H.; Vedadi, M. The use of differential scanning fluorimetry to detect light interactions that promote protein stability. Nature Protoc. 2007, 2, 2212−2221.

(66) Otwinoski, Z, Minor, W. Processing of X-ray diffraction data collected in oscillation mode. In Methods in Enzymology Macro-molecular Crystallography Part A; Charles, W. C., Ed.; Academic Press: New York, 1997; 307−326.

(67) Winter, G. xia2: an expert system for macromolecular crystallography data reduction. J. Appl. Crystallogr. 2010, 43, 186−190.

(68) Emsley, P.; Cowtan, K. Coot: model-building tools for molecular graphics. Acta Crystallogr., Sect. D: Biol. Crystallogr. 2004, 60, 2126−2132.

(69) Vagin, A. A.; Steiner, R. A.; Lebedev, A. A.; Potterton, L.; McNicholas, S.; Long, F.; Murshudov, G. N. REFMAC5 dictionary: organization of prior chemical knowledge and guidelines for its use. Acta Crystallogr., Sect. D: Biol. Crystallogr. 2004, 60, 2184−2195.

(70) Sparano, J. A.; Moulder, S.; Kazi, A.; Coppola, D.; Negassa, A.; Vahdat, L.; Li, T.; Pellegrino, C.; Fineberg, S.; Munster, P.; Malafa, M.; Lee, D.; Hoschander, S.; Hopkins, U.; Hershman, D.; Wright, J. J.; Kleer, C.; Merajver, S.; Sebti, S. M. Phase II Trial of Tipifarnib plus Neoadjuvant Doxorubicin-Cyclophosphamide in Patients with Clinical Stage IIB-IIC Breast Cancer. Clin. Cancer Res. 2009, 15, 2942−2948.

(71) (a) Yokoyama, K.; Zimmerman, K.; Scholten, J.; Gelb, M. H. Differential Prenyl Pyrophosphate Binding to Mammalian Protein Geranylgeranyltransferase-I and Protein Farnesyltransferase and Its Consequence on the Specificity of Protein Prenylation. J. Biol. Chem. 1997, 272, 3944−3952. (b) Rowinsky, E. K. Lately, It Occurs to Me What a Long, Strange Trip It's Been for the Farnesyltransferase Inhibitors. J. Clin. Oncol. 2006, 24, 2981.

(72) Zangi, R.; Hagen, M.; Berne, B. J. Effect of Ions on the Hydrophobic Interaction between Two Plates. J. Am. Chem. Soc. 2007, 129, 4678−4686.

4. Multistage screening reveals chameleon ligands of the human farnesyl pyrophosphate synthase: implications to drug discovery for neurodegenerative diseases

Reference:

De Schutter, J.W.; Park, J.; Leung, C.Y.; Gormley, P.; Lin, Y.-S.; Hu, Z.; Berghuis, A.M.; Poirier, J.; Tsantrizos, Y.S., Multistage screening reveals chameleon ligands of the human farnesyl pyrophosphate synthase: implications to drug discovery for neurodegenerative diseases. *J. Med. Chem.*, **2014**, *57*, 5764-5776

In the above publication, the synthesis and the *in vitro* activity of the pyridine-based inhibitors was performed by Dr. Joris W. De Schutter and Dr. Yih-Shyan Lin. The differential scan fluorimetry experiments were performed by Dr. Joris W. De Schutter and Zheping Hu. The ^{1}H NMR line broadening studies were performe by Dr. Joris W. De Schutter. Dr. Jaeok Park from Dr. Albert M. Berghuis' lab performed the isothermal titration calorimetry and all the X-ray diffraction acquisition and analysis work. The genetic studies and the analysis of messenger RNA prevalence of hFPPS was performed by Patrick Gormley from Dr. Jude Poirier's lab. Patrick also performed the assay to monitor the level of Tau protein in Alzheimer's brain tissues following treatment with hFPPS inhibitors. I synthesized some of the key compounds and evaluated their ability to inhibit hFPPS and hGGPPS.

Journal of Medicinal Chemistry

Article

pubs.acs.org/jmc

Multistage Screening Reveals Chameleon Ligands of the Human Farnesyl Pyrophosphate Synthase: Implications to Drug Discovery for Neurodegenerative Diseases

Joris W. De Schutter,[†,#] Jaeok Park,[‡,#] Chun Yuen Leung,[†] Patrick Gormley,[§] Yih-Shyan Lin,[†] Zheping Hu,[†,▽] Albert M. Berghuis,[‡,∥,⊥] Judes Poirier,[§] and Youla S. Tsantrizos*[,†,‡,⊥]

[†]Department of Chemistry, McGill University, 801 Sherbrooke Street West, Montreal, Quebec H3A 0B8, Canada

[‡]Department of Biochemistry, McGill University, 3655 Promenade Sir William Osler, Montreal, Quebec H3G 1Y6, Canada

[§]Douglas Mental Health University Institute, 6825 Lasalle, Verdun, Quebec, H4H 1R3, Canada

[∥]Department of Microbiology and Immunology, McGill University, 3775 Rue University, Montreal, Quebec H3A 2B4, Canada

[⊥]Groupe de Recherche Axé sur la Structure des Proteines, McGill University, 3649 Promenade Sir William Osler, Montreal, Quebec H3G 0B1, Canada

*Supporting Information

ABSTRACT: Human farnesyl pyrophosphate synthase (hFPPS) is the gate-keeper of mammalian isoprenoids and the key target of bisphosphonate drugs. Bisphosphonates suffer from poor "drug-like" properties and are mainly effective in treating skeletal diseases. Recent investigations have implicated hFPPS in various nonskeletal diseases, including Alzheimer's disease (AD). Analysis of single nucleotide polymorphisms in the hFPPS gene and mRNA levels in autopsy-confirmed AD subjects was undertaken, and a genetic link between hFPPS and phosphorylated tau (P-Tau) levels in the human brain was identified. Elevated P-Tau levels are strongly implicated in AD progression. The development of nonbisphosphonate inhibitors can provide molecular tools for validating hFPPS as a therapeutic target for tauopathy-associated neurodegeneration. A multistage screening protocol led to the identification of a new monophosphonate chemotype that bind in an allosteric pocket of hFPPS. Optimization of these compounds could lead to human therapeutics that block tau metabolism and arrest the progression of neurodegeneration.

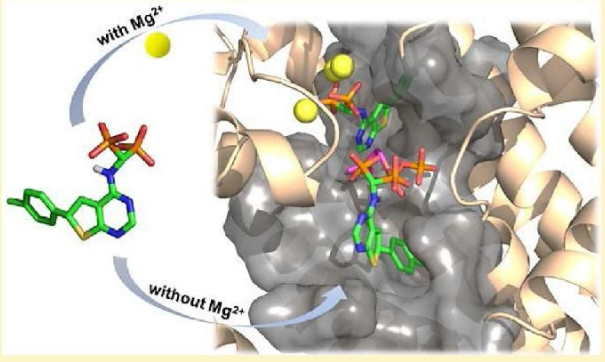

INTRODUCTION

Human farnesyl pyrophosphate synthase (hFPPS) catalyzes the elongation of dimethylallyl pyrophosphate (DMAPP) to geranyl pyrophosphate (GPP) and then to farnesyl pyrophos-phate (FPP) via the sequential condensation of DMAPP and then GPP with an isopentenyl pyrophosphate (IPP) unit. The active site cavity of this enzyme is characterized by two highly charged binding subpockets, making the identification of active site inhibitors, with physicochemical properties appropriate for treating nonskeletal diseases, extremely challenging. The allylic subpocket (DMAPP/GPP binding site) is composed of two aspartate-rich motifs that bind the pyrophosphate moiety of the substrate via metal mediated interactions.[1] The other subpocket is lined with basic residues that engage in direct salt-bridge interactions (K57, R60, R113) or water-mediated interactions (R112, R351) with the pyrophosphate moiety of IPP (Figure 1a).[1] The initial occupancy of the allylic subpocket induces a protein conformational change from the "open" to a "partially-closed" state, which fully defines the shape of the IPP binding site. The subsequent binding of IPP leads to the complete closing of the active site cavity, sequestering its substrates from bulk water.[1a,c]

Currently, nitrogen-containing bisphosphonates (N-BPs) are the only clinically useful inhibitors of hFPPS; the best examples from this class of drugs include zoledronic acid (1) and risedronic acid (2a). These drugs bind exclusively to the allylic subpocket and serve as chemically stable pyrophosphate mimics of DMAPP/GPP (Figure 1a).[1] Because of their highly charged nature and affinity for bone, N-BPs exhibit poor cell-membrane permeability, rapid clearance from the systemic circulation, and almost negligible distribution to nonskeletal tissues.[2] Con-sequently, these drugs are mainly used in treating skeletal disorders such as osteoporosis and tumor-induced osteolytic metastases.[3] However, hFPPS is the gatekeeper for the prenylation and activation of many small GTPases that play an essential role in a plethora of cellular functions including cell signaling,[4] proliferation, and synaptic plasticity.[5] Inhibition of

Received: April 22, 2014
Published: June 9, 2014

dx.doi.org/10.1021/jm500629e | J. Med. Chem. 2014, 57, 5764−5776

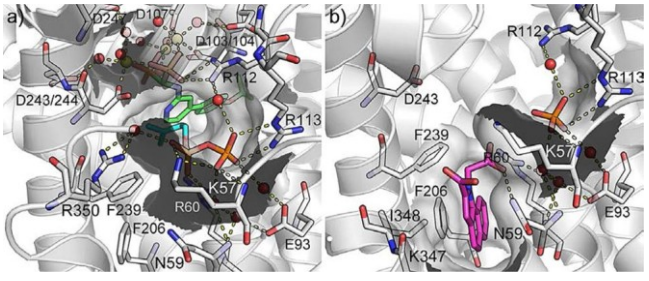

Figure 1. Binding pockets of hFPPS. (a) Structure of the hFPPS/5m/ IPP complex (PDB ID: 4H5E). (b) Structure of the hFPPS/4/Pi complex (PDB ID: 3N6K). The protein surface within 4 Å distance of the bound ligands is rendered semitransparent to indicate the binding pockets. The carbon backbone of IPP, 5m, and 4 are highlighted in cyan, green, and magenta, respectively. Oxygen, nitrogen, and phosphorus atoms are colored in red, blue, and orange, respectively. Yellow and red spheres represent the Mg^{2+} ions and water molecules, respectively.

hFPPS leads to reduction of cell viability and has been implicated in the antitumor clinical benefits of N-BPs.[3,6] Inhibition of hFPPS also induces activation of γδ T cells, providing immunosurveillance against tumors.[7] Additionally, overexpression of hFPPS and high levels of farnesyl pyrophosphate (FPP) in the brain tissue are believed to play a key role in neurodegeneration;[8] the latter is also linked to the metabolism of phosphorylated tau (P-Tau) protein in the human brain. It is indeed possible that the prenylation cascade from FPP → GGPP → RhoA-cdc42 →GSK3-β → P-Tau is largely (or in part) responsible for Alzheimer's-associated tau phosphorylation and tangle formation of neurons. Elevated levels of P-Tau lead to neurofibrillary tangle formation in the brain, a pathological hallmark of neurodegeneration and the Alzheimer's disease (AD). In this study, we report a genetic relationship between hFPPS and P-Tau concentration in the cortical area of the human brain in AD subjects.

The potential value of hFPPS as a therapeutic target (beyond for bone-related diseases) has fuelled efforts toward the identification of nonbisphosphonate inhibitors for this target. Fragment-based screening by NMR and X-ray crystallography led to the first discovery of compounds (e.g. 3) that could bind in an allosteric pocket of hFPPS near the IPP subpocket.[9] Subsequent optimization of these hits provided nonbisphosphonate allosteric inhibitors with nanomolar potency (e.g., 4; Figure 1b). More recently, in silico studies identified bisamidine-type inhibitors with micromolar potency;[10] however, the binding of these molecules in the allosteric pocket has not been confirmed. In this report, we describe the discovery of thienopyrimidine bisphosphonates (ThP-BPs; 6) that exhibit a mixed binding mode and can interact with both the allylic subpocket of the active site and the allosteric pocket of hFPPS. Structural remodeling of these compounds to the mono-phosphonate derivatives (ThP-MP; 7) resulted in a new chemotype of hFPPS inhibitors that bind selectively in the allosteric pocket and exhibit equivalent in vitro potency to compound 4. In a preliminary biological evaluation, we examined the ability of several, structurally diverse hFPPS inhibitors to modulate intracellular P-Tau levels in human immortalized neurons. Our combined medicinal chemistry efforts and genetic analysis data clearly supports a biochemical link between prenylation and the accumulation of P-Tau in neurons and the AD brain that can potentially be alleviated by inhibiting hFPPS.

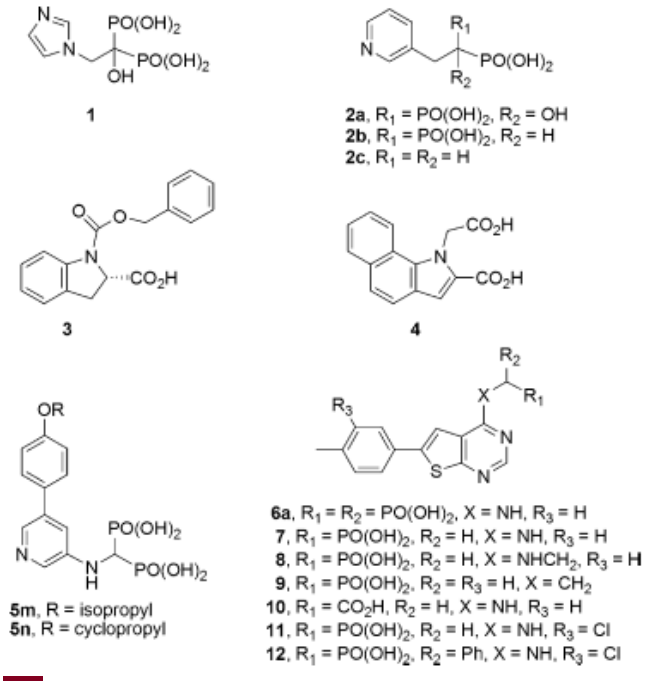

RESULTS AND DISCUSSION

Screening for Allosteric Inhibitors of hFPPS. The bisphosphonate moiety is a chemically stable bioisostere of pyrophosphate. Mindful of the direct interactions that the pyrophosphate moiety of IPP makes with the positively charged residues in its binding pocket (K57, R60, and R113; Figure 1a,b) and the proximity of these residues to the allosteric pocket, we speculated that in the absence of Mg^{2+} ions bisphosphonates may also bind near (or in) the allosteric pocket. The molecular recognition elements surrounding this pocket could conceivably have practical bearings in allowing pyrophosphate-containing metabolites to discriminate between the allylic subpocket and the R/K-rich IPP/allosteric site on the basis of the protein conformation. It is noteworthy that although the biological role of this allosteric pocket is still unknown, on the basis of its amphiphilic nature and proximity to the active site, a regulatory role in feedback inhibition by downstream isoprenoids is plausible and has been proposed.[9] Furthermore, a mixed binding mode of pyrophosphate-containing isoprenoids is not unprecedented; binding of IPP to the allylic subpocket of hFPPS[1b] and of DMAPP in the IPP subpocket of FPPS from Trypanosoma cruzi (PDB ID: 1YHL)[11] have been previously reported.

In earlier studies, we reported the synthesis and in vitro activity of aminopyridine-based bisphosphonate (N-BP; 5) and thienopyrimidine-based bisphosphonate (ThP-BP; 6) inhibitors of hFPPS (Table 1).[12] In this study, we investigated their binding to hFPPS using differential scanning fluorimetry (DSF). The thermal unfolding of hFPPS (T_m) in the presence and absence of these ligands was compared to their in vitro potency (Figures 2 and 3). Initial validation of our DSF assay was carried out with a number of control experiments using known compounds. For example, the DSF data of the hFPPS/2a and hFPPS/2a/IPP complexes (T_m of 22 ± 0.5 and 30 ± 0.5 °C, respectively) were found to be consistent with literature DSC data.[1a] Additionally, the thermal stability of the hFPPS/4 complex (T_m = 8 ± 0.5 °C) was found to be lower than that of hFPPS/2a and invariable by the presence or absence of IPP and Mg^{2+} ions. These observations are in

dx.doi.org/10.1021/jm500629e | J. Med. Chem. 2014, 57, 5764−5776

Table 1. Library of hFPPS Inhibitors Used for Screening: N-BPs and ThP-BPs with General Structure 5 and 6, Respectively (The Synthesis of These Compounds Were Previously Reported[12])

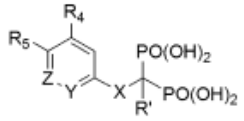

5a, R_4 = **a**, R_5 = H, X = CH_2, Y = CH, Z = N, R' = Fluorine
5b, R_4 = **a**, R_5 = H, X = CH_2, Y = CH, Z = N, R' = H
5c, R_4 = **a**, R_5 = H, X = NH, Y = CH, Z = N, R' = H
5d, R_4 = **a**, R_5 = H, X = NH, Y = N, Z = CH, R' = H
5e, R_4 = H, R_5 = **a**, X = NH, Y = N, Z = CH, R' = H
5f, R_4 = **b**, R_5 = H, X = NH, Y = N, Z = CH, R' = H
5g, R_4 = **c**, R_5 = H, X = NH, Y = CH, Z = N, R' = H
5h, R_4 = **e**, R_5 = H, X = NH, Y = N, Z = CH, R' = H
5i, R_4 = **f**, R_5 = H, X = NH, Y = N, Z = CH, R' = H
5j, R_4 = **h**, R_5 = H, X = NH, Y = N, Z = CH, R' = H
5k, R_4 = **i**, R_5 = H, X = NH, Y = N, Z = CH, R' = H
5l, R_4 = **j**, R_5 = H, X = NH, Y = CH, Z = N, R' = H
5m, R_4 = **j**, R_5 = H, X = NH, Y = N, Z = CH, R' = H
5n, R_4 = **k**, R_5 = H, X = NH, Y = CH, Z = N, R' = H
5o, R_4 = **k**, R_5 = H, X = NH, Y = N, Z = CH, R' = H
5p, R_4 = **l**, R_5 = H, X = NH, Y = N, Z = CH, R' = H
5q, R_4 = **m**, R_5 = H, X = NH, Y = N, Z = CH, R' = H
5r, R_4 = **o**, R_5 = H, X = NH, Y = CH, Z = N, R' = H
5s, R_4 = **p**, R_5 = H, X = NH, Y = CH, Z = N, R' = H
5t, R_4 = **q**, R_5 = H, X = NH, Y = CH, Z = N, R' = H
5u, R_4 = **r**, R_5 = H, X = NH, Y = N, Z = CH, R' = H

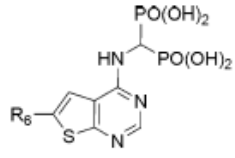

6a, R_6 = **d**
6b, R_6 = **g**
6c, R_6 = **h**
6d, R_6 = **i**
6e, R_6 = **j**
6f, R_6 = **k**
6g, R_6 = **n**
6h, R_6 = **o**

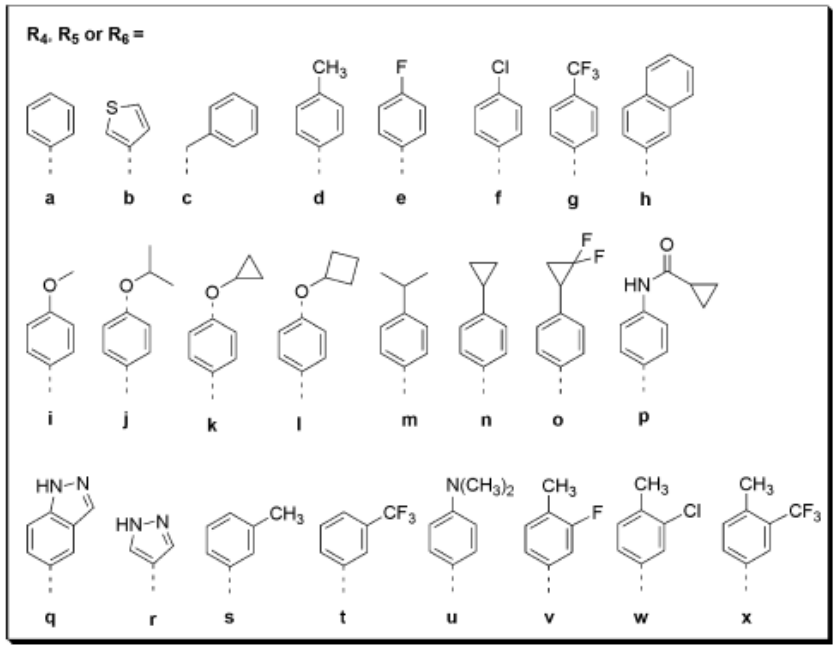

agreement with the lower intrinsic potency of 4 (compared to 2a) and its competitive binding with IPP.[9]

A number of hFPPS/5 and hFPPS/6 complexes were then evaluated by DSF in the presence and absence of the enzyme's Mg^{2+} cofactor (Table 1; Figure 3). To minimize the impact of false positive hits due to nonselective binding, only inhibitors with IC_{50} values below 2 μM and selectivity >100-fold for inhibiting hFPPS vs hGGPPS were included in this screen (Figure 2); N-BPs are known to inhibit related enzymes, such as hGGPPS[13] and hSQS.[14] In the presence of Mg^{2+} ions, a good correlation between the T_m and IC_{50} values for the N-BPs (5) was observed (Figure 3a). Predictably, in the absence of Mg^{2+} ions binding was virtually abolished (T_m <2 °C ± 0.5 °C). Exceptionally, few complexes (e.g. hFPPS/5n), exhibited thermal stability that was 3−4 °C higher than the unliganded enzyme. In general, the hFPPS/6 complexes exhibited higher thermal stability than the hFPPS/5 complexes in both the presence and absence of Mg^{2+} ions (albeit fewer ThP-BPs were tested). Under Mg^{2+}-free conditions, several hFPPS/6 com-plexes exhibited thermal stability equivalent to that of the hFPPS/4 complex (Figure 3b).

To further characterize the binding of our compounds in the presence and absence of Mg^{2+} ions, competitive binding between pairs of ligands was investigated using ^1H line broadening NMR. Broadening of the ^1H resonances of inhibitor 4 was observed in the presence of Mg^{2+} ions and hFPPS (Supporting Information Figure 1), suggesting fast exchange between the free and enzyme-bound state of 4. Addition of 2a

dx.doi.org/10.1021/jm500629e | J. Med. Chem. 2014, 57, 5764−5776

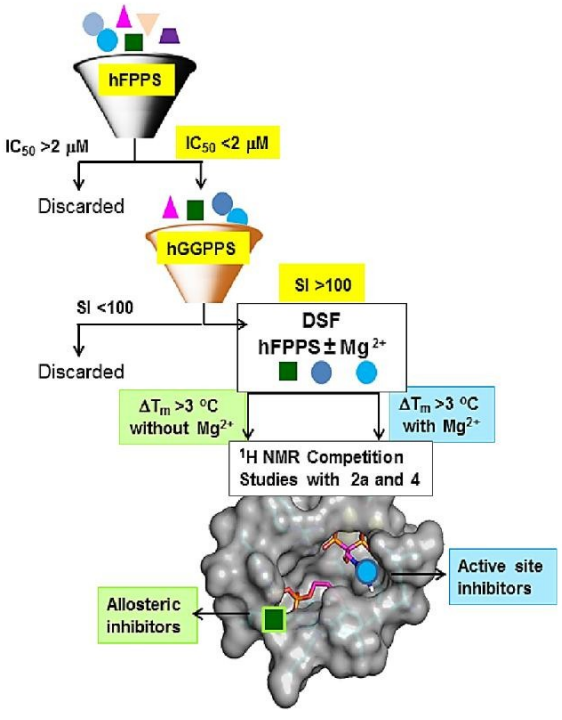

Figure 2. Screening protocol (SI, selectivity index = potency ratio in hFPPS/hGGPPS).

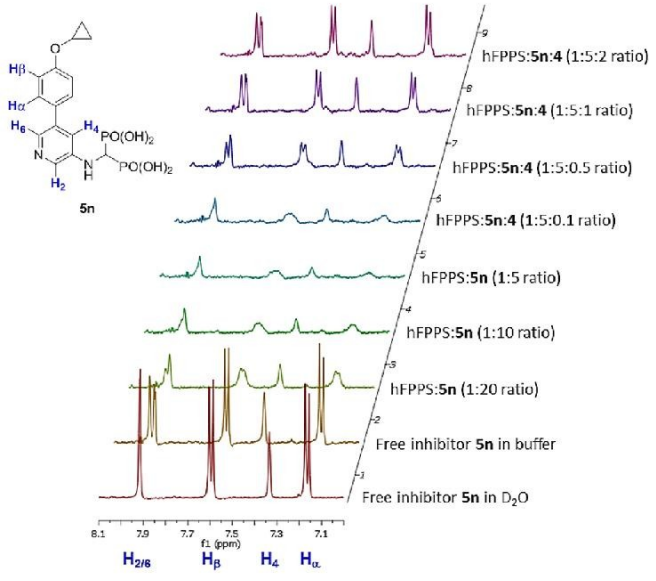

Figure 4. ^{1}H line broadening NMR studies exploring competitive binding of inhibitors 4 and 5n in the absence of Mg^{2+} ions. Stacked spectra of compound 5n free in solution (D_2O and buffer) and in the presence of hFPPS and 4; for clarity, only the aromatic resonances are shown, the molar ratio of ligands and protein are indicated next to each spectra and the proton resonances of 5n are indicated at the bottom of the stacked spectra (in blue).

to the same NMR sample did not restore the ^{1}H resonances of 4 (Supporting Informationm Figure 1), indicating that 2a and 4 do not compete for binding to hFPPS. This is in complete agreement with the structure of the hFPPS/1/3 ternary complex (PDB ID: 3N46), which demonstrated that the allosteric pocket and the allylic subpocket can be simultaneously occupied.[9] In contrast, competitive binding was detected between 4 and IPP (Supporting Information Figure 2), consistent with the expected electrostatic/steric clash between one carboxylic acid moiety of 4 and the pyrophosphate of IPP (PDB ID: 3N6K).[9] In the absence of Mg^{2+} ions, our NMR data clearly showed competitive binding between inhibitors 5n and 4 (Figure 4). However, in the presence of Mg^{2+} ions, the data was inconclusive and we could not rule out that 5n was competing for binding with both 2a and 4; similar observations were made with analogue 6a.

Co-crystallization of 6a bound to hFPPS in both the presence and absence of Mg^{2+} ions provided proof that this compound can bind to both the allylic subpocket of the active site and the allosteric pocket (Figure 5). ThP-BP 6a is the first chemotype to provide conclusive evidence that bisphospho-nates can indeed bind in the allosteric pocket of hFPPS, at least in the absence of the metal cofactor. From here on, we will refer to hFPPS/6 complexes as the hFPPS/$6^{(act)}$ and hFPPS/$6^{(allo)}$ complexes to indicate binding of the ligand in the active site and allosteric pocket, respectively (part a vs part b of Figure 5; PDB IDs 4JVJ vs 4LPG, respectively).

We previously reported the co-crystal structure of the hFPPS/$6a^{(act)}$ complex (PDB ID 4JVJ; Figure 5a).[12d] In the hFPPS/$6a^{(allo)}$ complex, the p-tolyl substituent is buried in the allosteric pocket, engaging in π-stacking interactions with the side chains of N59 and F206 (Figure 5b). The alkyl portions of the L344 and K347 side chains are within van der Waals radius and provide additional hydrophobic interactions. Edge-to-face π-stacking interactions are also observed between the thienopyrimidine core and F239, with the pyrimidine ring partially solvent exposed (Figure 5b). A noteworthy difference in the allosteric bindings of 6a and 4 is that 4 engages in direct

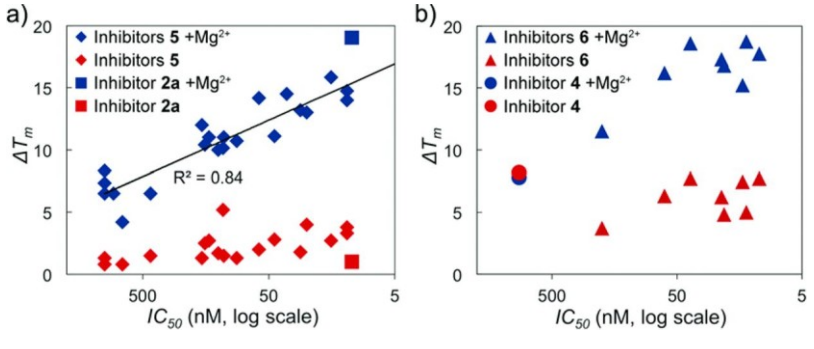

Figure 3. Correlation of in vitro potency in inhibiting hFPPS to the thermal stability of the hFPPS/inhibitor complex in the presence and absence of Mg^{2+} ions. DSF assays were run with 4 mM hFPPS protein and 40 mM inhibitor. (a) IC_{50} vs T_m of hFPPS/N-BP complexes. (b) IC_{50} vs DTm of hFPPS/ThP-BP and hFPPS/4 complexes.

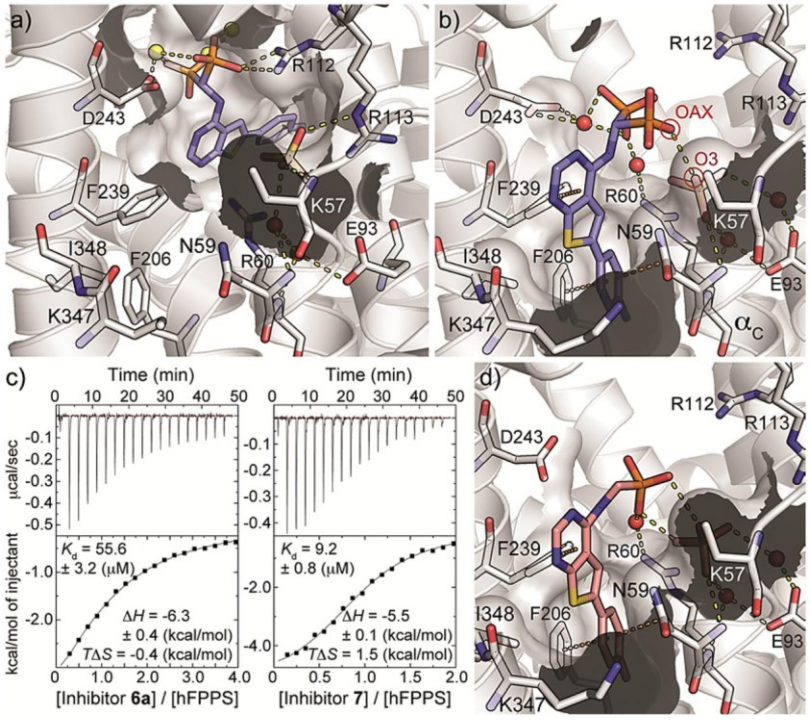

Figure 5. Co-crystal structures of hFPPS/ligand complexes. (a) Complex hFPPS/6a$^{(act)}$/Pi (PDB ID: 4JVJ); metal-coordinated water molecules and some other interactions between the protein and the inhibitor are omitted for clarity. (b) Complex hFPPS/6a$^{(allo)}$/Pi (PDB ID: 4LPG). (c) ITC data for the binding of compounds 6a and 7 in the absence of Mg^{2+} ions. (d) Structure of the hFPPS/7/Pi complex (PDB ID: 4LPH).

interactions with the side chains of K57 and R60 via one of its carboxylic acids, whereas the bisphosphonate of 6a does not form any direct interaction but only water-mediated H-bonds with R60 and D243; the latter residue (D243) is typically involved in metal-mediated interaction with bisphosphonates that are bound in the allylic subpocket (part a vs part b of Figure 5). Surprisingly, the bisphosphonate of 6a is bound very close to an inorganic phosphate ion (Pi) occupying the IPP subpocket (a distance of 2.64 Å between OAX and O3; Figure 5b). Although such proximity between two negatively charged ions is puzzling, the identity and location of both was unambiguously confirmed by anomalous scattering data (Supporting Information Figure 3). Presumably, the negative charge of the Pi is neutralized by the dipole of the α_C helix and/ or R60 (a distance of 3.15 Å was observed between a guanidinium nitrogen and a phosphate oxygen).

The relative contributions of the two binding modes of 6a under biologically relevant conditions are difficult to decipher. Whether they both contribute to the intrinsic potency of 6a (IC_{50} = 22 nM) is equally unclear; in vitro evaluation of hFPPS activity requires Mg^{2+} as the cofactor, which biases the binding of bisphosphonates in favor of the allylic subpocket. Nonethe-less, under Mg^{2+}-free conditions, ITC studies suggested a K_d of ~56 µM for the binding of 6a, presumably in the allosteric pocket only (Figure 5c). The K_d of the corresponding mono-phosphonate analogue 7 was ~9 µM and in close agreement with its IC_{50} value of 4.5 µM (Table 2). More importantly, in the presence of Mg^{2+} ions, competitive binding of 7 was unambiguously observed with compound 4 but not with 2a. These results suggest that under biologically relevant conditions inhibitor 7 binds selectively in the allosteric pocket (Figure 6). It is noteworthy that previous attempts to remove one of the phosphonate moieties of N-BPs led to complete loss of potency (e.g., 2b vs 2c; Table 2).[15]

Table 2. Inhibition Data for Key Compounds

compd	hFPPS[a] IC_{50} (µM)	P-Tau/T-Tau[e] ratio	LDH[f] (%)
control		0.012	0
1	0.003	0.006	+60
2a	0.006	0.004	+60
2b	0.033[b]	nd	nd
2c	>800[b]	nd	nd
4	0.92[c]	0.004	+3
5n	0.018	0.007	0%
6a	0.022	nd	nd
6f	0.014	0.009	−1
7	4.5	nd	nd
8	>20[d]	nd	nd
9	26	nd	nd
10	>20[d]	nd	nd
11	3.3	nd	nd
12	1.2	0.010	−7

[a]The potencies of all analogues of general structure 5 and 6 in inhibiting hFPPS were previously reported.[12] [b]IC_{50} reported by Dunford et al.[15] [c]IC_{50} of 0.2 µM was reported by Jahnke et al. using a different assay protocol.[9] [d]Inhibition of 40% and 27% was observed for 8 and 10, respectively, at 20 µM. [e]P-Tau/T-Tau ratios in human neuroblastoma SH-SY5Y cells were determined at a fixed concentration of 100 nM inhibitor after an incubation period of 24 h; average value of two assays; deviation of <5% was observed. [f]Average % activity of lactate dehydrogenase observed (LDH) compared to the untreated control (set arbitrarily to zero LDH activity); assays run in triplicate and a standard deviation of ~10% was observed.

We subsequently confirmed the binding of 7 in the allosteric pocket by X-ray crystallography (Figure 5d). The overall structures of the hFPPS/7 and hFPPS/6a$^{(allo)}$ complexes are very similar, with the core (Cα) rmsd value of 0.27 Å. Alignment of the two structures showed clear superposition of

dx.doi.org/10.1021/jm500629e | J. Med. Chem. 2014, 57, 5764−5776

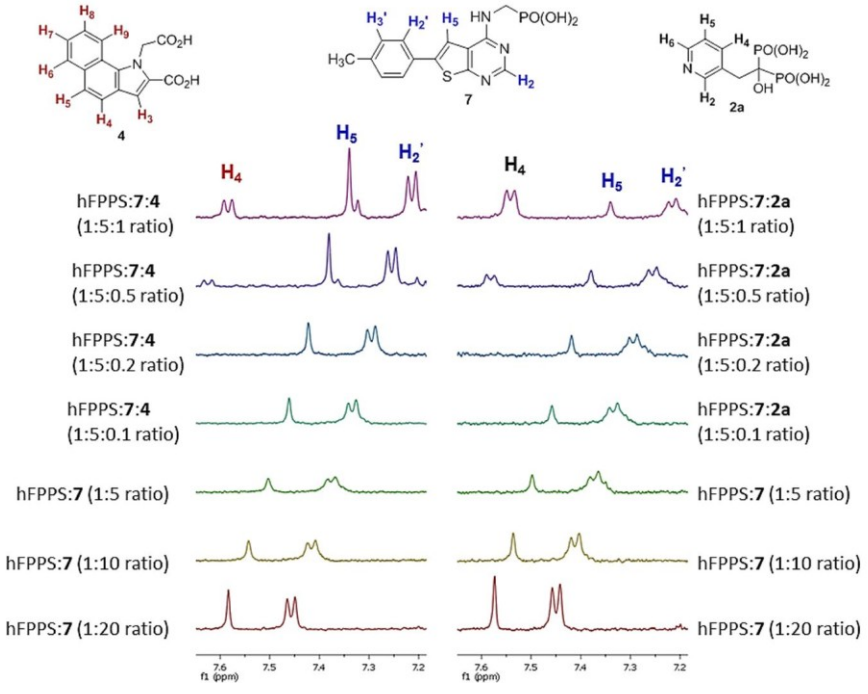

Figure 6. Side-by-side comparison of ^{1}H line broadening NMR studies exploring competitive binding of hFPPS inhibitor 7 with either 4 or 2a in the presence of Mg^{2+} ions. Buffer: BSA 20 mg/mL, Tris 50 mM, pH 7.7, $MgCl_2$ 2 mM, TCEP 0.5 mM. For clarity, only select regions of the spectra are shown; the molar ratio of ligands and protein are indicated next to each spectra. Stacked spectra on the left are those of compound 7 free in solution and in the presence of hFPPS and compound 4; the data clearly shows competitive binding even in the presence of Mg^{2+} ions. Stacked spectra on the right are those of compound 7 free in solution and in the presence of hFPPS and compound 2a, clearly showing that binding of the two compounds is not competitive in the presence of Mg^{2+} ions. All proton resonances are labeled at the top of the spectra in red, blue, and black for compounds 4, 7, and 2a, respectively.

the thienopyrimidine cores, the tolyl side chains and the Pi (part b vs part d of Figure 5). Although the phosphonate moiety of 7 did not overlap with either of the two phosphonates of 6a, it maintained a water-mediated interaction with R60. In an attempt to gain more insight as to the importance of this phosphonate moiety, and possibly allow this moiety to form a direct salt-bridge with R60, we synthesized analogue 8, having a longer linker between the phosphonate and the thienopyrimidine core. A significant drop in potency was observed (Table 2), likely due to the increased conforma-tional freedom and entropic penalty associated with the binding of 8. We also investigated the impact of decreasing the acidity of this pharmacophore by replacing the exocyclic NH with a methylene linker at C-4 (pK_a of P(O)O$^-$OH of ~6.8 and ~7.7 for analogues 7 and 9, respectively) and by completely replacing the phosphonate with a carboxylic acid moiety (i.e., 10). A correlation between loss in potency and decrease in the acidity of this moiety was clearly observed, confirming the importance of this pharmacophore (Table 2). Finally, minor substitutions on the tolyl side chain (e.g., 11; IC_{50} = 3.3 μM) and the Cα to the phosphonate were well tolerated and appear to be additive in improving the potency of this class of compounds. In the present study, analogue 12 (IC_{50} = 1.2 μM) was the most potent hit identified, exhibiting equivalent potency to compound 4 in inhibiting hFPPS in our in vitro assay (IC_{50} = 0.92 μM). More extensive SAR investigations and further optimizing of these allosteric inhibitors is currently in progress.

Synthesis of Ligands Binding to the Allosteric Pocket. The synthesis of the new compounds 7−12 was initiated from the key intermediate 13, prepared as previously reported.[16] Treatment of 13 first with Br_2 in acetic acid, followed by $POCl_3$, provided the 4-chloro-6-bromo intermediate 14 in moderate overall yield (~40% over the two steps). Analogues 7, 11, and 12 were prepared after sequential S_NAr displacement of the C-4 chloro with an aminodiethylphosphonate (prepared as previously reported[17]), followed by Suzuki cross-coupling with an aryl boronate and final deprotection of the phosphonate esters with TMSBr/MeOH (Scheme 1). Alternatively, the Suzuki reaction could be carried first to obtain the key building block 4-chloro-6-(p-tolyl)thieno[2,3-d]pyrimidine, followed by the S_NAr displacement of the C-4 chloro with diethyl (2-aminoethyl)phosphonate to give the diethyl ester of analogue 8, or the unprotected glycine to obtain directly compound 10, with similar overall yields. These two alternative approaches provide easy access to library synthesis of analogues with structural diversity at both the C-4 and C-6 of the thienopyrimidine scaffold.

Suzuki−Miyaura cross coupling of trifluoro(vinyl) borane with the 4-chlorothienopyrimidine, followed by modified Lemieux−Johnson oxidation,[18] gave the aldehyde 15 in good overall yields (Scheme 1). Horner−Wadsworth−Emmons type condensation of intermediate 15 with the sodium anion of tetraethyl methylenediphosphonate gave the α,β-unsaturated monophosphonate diethyl ester.[19] Attempts to remove the ethyl esters of this intermediate (under the usual condition of TMSBr/MeOH) led to some decomposition, therefore, this intermediate was first hydrogenated before the deprotection step to give compound 9 (Scheme 1).

Relevance of hFPPS in Modulating Phospho-Tau Levels in the Human Brain. Elevated plasma cholesterol levels are known among the vascular risk factors of the

dx.doi.org/10.1021/jm500629e | J. Med. Chem. 2014, 57, 5764−5776

Scheme 1. Synthesis of Allosteric Inhibitors of hFPPS[a]

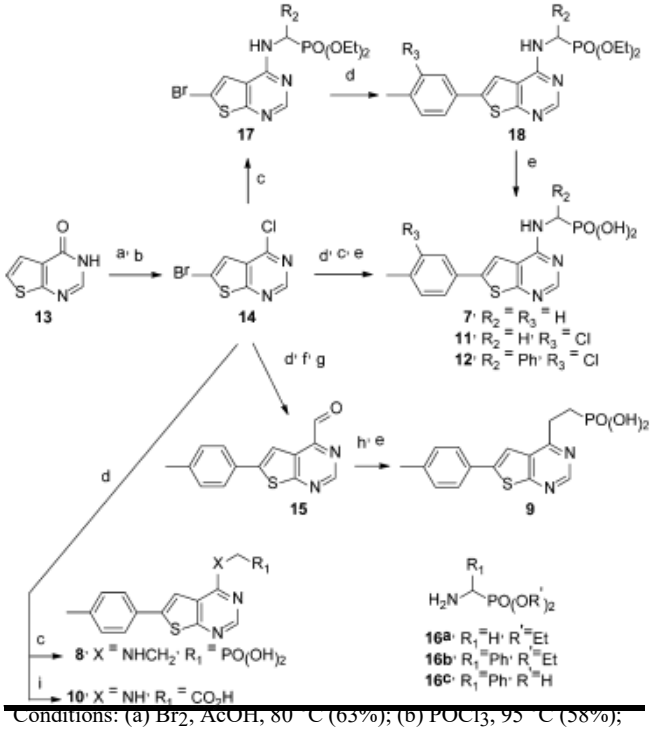

[a] Conditions: (a) Br_2, AcOH, 80 °C (63%); (b) $POCl_3$, 95 °C (58%); (c) $H_2NCHR_1PO(OR')_2$ (16), Et_3N, dioxane, 100 °C, 18−24 h (40−60%); (d) $Pd(PPh_3)_4$, K_2CO_3, dioxane/H_2O (1:1), 100 °C, 1 h (60−70%); (e) TMSBr, MeOH, RT, 72 h (>98% conversion, 50−80% isolated yield); (f) potassium trifluoro(vinyl)borate, $PdCl_2(dppf)$-CH_2Cl_2, Et_3N, i-PrOH/H_2O, 100 °C, 1 h (72%); (g) (i) OsO_4, NMO, 2,6-lutidine, acetone/H_2O, RT, 2 h, (ii) $NaIO_4$, RT, 1 h (64%); (h) (i) tetraethyl methylenediphosphonate, NaH, THF, 0 °C to RT, 1 h, (ii) H_2, Pd/C, RT, 1 h, then step e (45% isolated yield for the 3 steps); (i) $H_2NCH_2CO_2H$, Na_2CO_3, dioxane/H_2O (1:1), 100°C, 3 h (60%).

Alzheimer's disease (AD).[20,21] Although not a universal finding, treatment of middle-aged individuals for hypercholesterolemia with statins has been shown to confer some level of neuroprotection against late-life development of AD.[22] Addi-tionally, statin treatment has been shown to reduce the cerebrospinal fluid phospho-tau content in the human brain.[23] These finding are consistent with the quasi-absence of cortical neurofibrillary tangles in autopsy-confirmed cognitively intact subjects who had used statins for several years as opposed to nonusers.[24]

Phospho-tau production in the brain is regulated by a select number of isoprenoid-activated small G proteins that control the function of the GSK3-β kinase. GSK3-β is believed to be responsible for high levels of tau phosphorylation in neurons.[25] This hypothesis prompted us to carefully examine the relationship between the hFPPS gene and tau metabolism in the Alzheimer's disease (AD).[26] We examined a cohort of 751 pairs of AD and age-matched control subjects to map approximately 535000 polymorphisms in each of the AD cases and control subjects. Five single nucleotide poly-morphisms (SNPs) were examined in the hFPPS gene loci (Supporting Information Figure 4). Frontal cortex brain samples ($n = 116$) from autopsy-confirmed cases of Alzheimer's disease and age-matched control subjects were prepared according to an established protocol[27] prior to ELISA quantification of cortical total tau (T-Tau) and phosphorylated tau (P-Tau) protein levels. While none of the markers were found to exhibit significant association with sporadic AD, a specific and dose dependent genetic association was found between variant rs4971072 (SNP:A/G) in the promoter region of the hFPPS gene and P-Tau protein levels ($p < 0.02$) in the cortical area of the AD brain (Figure 7a). We also examined a subset of AD ($n = 34$) and age-matched control brains ($n = 24$) for the mRNA prevalence of hFPPS using QrtPCR as previously reported.[28] Human FPPS mRNA levels were markedly elevated in the cortical cortices of the AD versus the control subjects (Figure 7b), consistent with a hyper-activation of the isoprenoid pathway in Alzheimer's disease. Although these finding do not imply that hFPPS is causally related to Alzheimer's disease, they support a genetic association between specific genetic variants in hFPPS (rs4971072) and the P-Tau concentrations in the human AD brain. One of the early pathological features of common Alzheimer's disease is the progressive accumulation of ribbon-like intraneuronal tangles made of polymer of the phosphory-lated tau protein (P-Tau), a key cytoskeleton structural component of neurons. Human FPPS clearly affects the accumulation of the pro-toxic P-Tau and may accelerate the progression of AD pathology.[26]

These preliminary results prompted us to also examine the ability of hFPPS inhibitors to block tau metabolism in human neuroblastoma SH-SY5Y cells. Cells were treated with both bisphosphonate and nonbisphophonate inhibitors at concen-trations of 100 and 500 nM for a period of 24 h before they were lysed and their T-Tau and P-Tau levels were quantified using an established ELISA test.[27] Toxicity to the neurons was

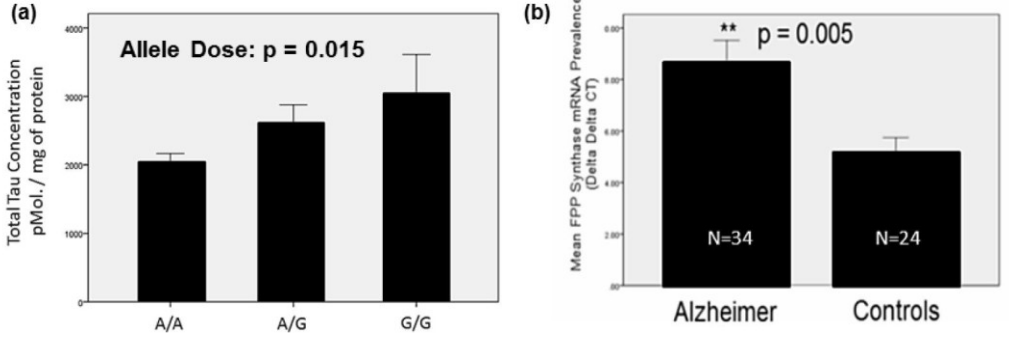

Figure 7. Genetic association between hFPPS and P-Tau metabolism. (a) Effects of rs4971072 variant copy number on P-Tau concentrations in cortical area of the AD brain. (b) Human cortical FPPS mRNA prevalence in the cortical area in AD brain vs control. AD mean Braak stage = 4.9 ± 1.8; age of AD onset = 71 ± 10; age of death = 74 ± 12 and 78 ± 9 for control and AD, respectively.

dx.doi.org/10.1021/jm500629e | J. Med. Chem. 2014, 57, 5764−5776

estimated using a routine lactate dehydrogenase (LDH) assay and found to increase sharply after 48 h of incubation with the inhibitors tested. Similarly, some toxicity was observed with most inhibitors if tested at concentrations of 500 nM or higher, prohibiting a clear determination of P-Tau/T-Tau levels. Although a significant decrease (≥50% decrease) in the P-Tau/T-Tau levels was observed with the most potent N-BP inhibitors 1 and 2a, significant toxicity was also observed (~60% higher LDH activity as compared to the untreated control) even at concentrations of 100 nM (Table 2). In contrast, the bisphosphonate inhibitors 5n and 6f and nonbisphosphonate inhibitor 4 induced a significant decrease in P-Tau/T-Tau ratio without significant toxicity, whereas the monophosphonate inhibitor 12 exhibited only minor effects (Table 2).

CONCLUSIONS

In our search for allosteric inhibitors of hFPPS, we screened a small library of bisphosphonates using a multistage biochemical and structural platform. Mindful of the structural features of the allosteric pocket, we anticipated that binding in this pocket of large lipophilic bisphosphonates may be possible, particularly in the absence of Mg^{2+} ions. These studies led to the identification of thienopyrimidine-based monophosphonate allosteric inhib-itors. Our screening protocol was guided by DSF, ITC, ^{1}H line-broadening NMR, and X-ray crystallography in the presence and absence of the enzyme's metal cofactor. We also characterized the binding interactions between the hFPPS allosteric pocket and the bisphosphonate inhibitor 6a and compared them to those observed with the selective allosteric inhibitor 7. The protein−ligand interactions observed in both complexes were virtually identical, thus validating screening hFPPS under Mg^{2+}-free conditions. Although Mg^{2+}-free conditions are not biologically relevant, this approach proved to be useful for screening hFPPS and may be applicable to other structurally/functionally related targets. Recently, a similar three-stage biophysical screening method was reported as a general tool for screening in fragment-based drug discovery.[29]

In addition, analysis of our collective X-ray data on thienopyrimidine-based inhibitor bound in the allylic subpocket and the allosteric pocket (e.g., $6a^{(act)}$ vs $6a^{(allo)}$; PDB codes 4JVJ and 4LPG, respectively) revealed very similar interactions involved in both binding sites. For example, the π-stacking interactions between the tolyl side chain of 6a and Phe99/Gln171 in the hFPPS/$6a^{(act)}$ complex are analogous to those observed in the hFPPS/$6a^{(allo)}$ complex with Phe206/Asn59 (Figure 5b). This finding is intriguing and supports the hypothesis that the allosteric pocket plays a regulatory role in product feedback inhibition that is sensitive to the concen-tration of isoprenoids and independent of the Mg^{2+} cofactor concentration.

We identified thienopyrimidine-based monophosphonates (ThP-MP) as a new chemotype of hFPPS allosteric inhibitors. These compounds are amenable to further optimization and may provide tools for validating hFPPS as a therapeutic target for nonskeletal diseases such as various cancers and neuro-degenerative diseases. A relationship between the latter and the levels of FPP/GGPP in the human brain has been previously reported.[8] Herein we provide further evidence of a genetic link between hFPPS and the levels of phosphorylated tau (P-Tau) in the human AD brain. The accumulation of P-Tau in the brain is associated with the pathological accumulation of neurotoxic neurofibrillary tangles, an established hallmark of AD brain pathology. Preliminary evaluation of hFPPS inhibitors in neuroblastoma cells suggested that hFPPS can modulate tau metabolism; confirmation of these results is pending the identification of more potent/less toxic inhibitors of hFPPS with good cell-membrane permeability. Nonetheless, our collective data supports further investigation of hFPPS as a potential therapeutic target for decelerating the progression of AD and other tauopathy-related neurodegenerative diseases.

EXPERIMENTAL SECTION

General Procedures for Characterization of Compounds. All compounds were purified by normal phase flash column chromatography on silica gel using a CombiFlash instrument and a solvent gradient from 5% EtOAc in hexanes to 100% EtOAc and then to 20% MeOH in EtOAc, unless otherwise indicated. The homogeneity of all final compounds (7−12) was confirmed to ≥95% by reverse-phase HPLC. Only phosphonate esters with homogeneity ≥95% were processed further to the final phosphonic acid inhibitors 7−9, 11, and 12. HPLC analysis was performed using a Waters ALLIANCE instrument (e2695 with 2489 UV detector and 3100 mass spectrometer). Each final compound was fully characterized by ^{1}H, ^{13}C, and ^{31}P NMR and HRMS. Chemical shifts (δ) are reported in ppm relative to the internal deuterated solvent (^{1}H, ^{13}C) or external H_3PO_4 (δ 0.00 ^{31}P), unless indicated otherwise. The high-resolution MS spectra of final products were recorded using electrospray ionization ($ESI^{\pm}$) and Fourier transform ion cyclotron resonance mass analyzer (FTMS). Method (homogeneity analysis using a Waters Atlantis T3 C18 5 μm column): solvent A, H_2O, 0.1% formic acid; solvent B, CH_3CN, 0.1% formic acid; mobile phase, linear gradient from 95%A and 5%B to 5%A and 95%B in 13 min, then 2 min at 100% B; flow rate, 1 mL/min.

General Synthetic Protocols. Suzuki cross-coupling reactions and deprotection of the diethyl phosphonates to the phophonic acids were carried out using the general protocols previously reported.[12]

General Protocol for S_NAr displacement of the C-4 Chloro. For the preparation of inhibitors 7, 11, and 12, this reaction was carried out using the 4-cholo intermediate 14, whereas for the synthesis of inhibitors 8 and 10, this reaction was carried out using the common building block 4-chloro-6-(p-tolyl)thieno[2,3-d]pyrimidine (formed after Suzuki cross-coupling of the 4-tolylboronic acid with 14). In a pressure vessel, the 4-chlorothienopyrimidine was dissolved in dioxane, the amine reagent (aminophosphonate; 1.5 equiv) and Et_3N (5 equiv) were added, and the pressure vessel was sealed. The reaction mixture was stirred at 100 °C for 15−24 h; completion of the reaction was monitored by HPLC. The reaction mixture was cooled to RT and diluted with ethyl acetate (50 mL). The organic layer was washed with an aqueous solution of saturated $NaHCO_3$ (15 mL), water (45 mL), and brine (15 mL) and dried over anhydrous $MgSO_4$. The crude was purified by column chromatography to give the desired products. The same procedure was used for the synthesis of compound 10, however, the solvent was changed to dioxane:H_2O (1:1) and Na_2CO_3 (1.5 equiv) was used as the base; the reaction was completed in 3 h.

(((6-(p-Tolyl)thieno[2,3-d]pyrimidin-4-yl)amino)methyl)-phosphonic Acid (7). The final compound 7 was isolated as a white powder (7.4 mg, 50% isolated yield). ^{1}H NMR (500 MHz, D_2O, 5% ND_4OD) δ 7.92 (s, 1H), 7.35 (s, 1H), 7.21 (d, J = 8.0 Hz, 2H), 6.90 (d, J = 8.0 Hz, 2H), 3.29 (d, J = 13.3, 2H), 2.10 (s, 3H). ^{13}C NMR (126 MHz, D_2O, 5% ND_4OD) δ 162.5, 156.4 (d, J = 9 Hz), 152.4, 140.0, 138.8, 129.6, 129.3, 125.2, 118.3, 113.2, 40.4 (d, J = 135 Hz), 20.4. ^{31}P NMR (202 MHz, D_2O, 5% ND_4OD): δ 12.96. HRMS (ESI^-) m/z 334.0415 calculated for $C_{14}H_{13}N_3O_3PS$; found m/z 334.0420 $[M - H]^-$.

(2-((6-(p-Tolyl)thieno[2,3-d]pyrimidin-4-yl)amino)ethyl)-phosphonic Acid (8). The diethyl ester of inhibitor 8 was isolated as a brown solid (45.8 mg, 59% yields). ^{1}H NMR (500 MHz, CD_3OD) δ 8.29 (s, 1H), 7.57 (s, 1H), 7.51 (d, J = 8.0 Hz, 2H), 7.21 (d, J = 8.0 Hz, 2H), 4.13−4.09 (m, 4H), 3.83−3.77 (m, 2H), 2.34 (s, 3H), 2.31−

dx.doi.org/10.1021/jm500629e | J. Med. Chem. 2014, 57, 5764−5776

2.24 (m, 2H), 1.31 (t, J = 7.1 Hz, 3H). ^{13}C NMR (126 MHz, CD_3OD) δ 164.0, 156.5, 153.0, 140.4, 138.6, 130.5, 129.4, 125.5, 118.1, 112.7, 62.0 (d, J = 6.5 Hz), 34.6 (d, J = 2.1 Hz), 24.6 (d, J = 138.0 Hz), 19.8, 15.3 (d, J = 6.1 Hz). ^{31}P NMR (81 MHz, CD_3OD) δ 30.33. MS (ESI +) m/z 405.90 $[M + H]^+$ for $C_{19}H_{25}N_3O_3PS$. The final inhibitor 8 was obtained as a light-brown solid (26.2 mg, near quantitative yield). ^{1}H NMR (500 MHz, D_2O, 5% ND_4OD) δ 7.92 (s, 1H), 7.14 (d, J = 8.0 Hz, 2H), 7.09 (s, 1H), 6.88 (d, J = 8.0 Hz, 2H), 3.50−3.45 (m, 2H), 2.13 (s, 3H), 1.76−1.73 (m, 2H). ^{13}C NMR (126 MHz, D_2O, 5% ND_4OD) δ 162.4, 155.6, 152.2, 139.9, 138.6, 129.4, 129.2, 124.9, 118.0, 112.9, 37.7, 29.2 (d, J = 126 Hz), 20.4. ^{31}P NMR (202 MHz, D_2O, 5% ND_4OD): δ 18.5. HRMS (ESI−) m/z 348.0577 calculated for $C_{15}H_{15}N_3O_3PS$; found m/z 348.0569 $[M - H]^-$.

(2-(6-(p-Tolyl)thieno[2,3-d]pyrimidin-4-yl)ethyl)phosphonic Acid (9). A solution of tetraethyl methylenediphosphonate (26 μL, 0.104 mmol) in THF (3 mL) was cooled to 0 °C, and NaH (60%, 5 mg, 0.125 mmol) was added in a portion and then stirred at 0 °C for 15 min. A solution of aldehyde 15 (29 mg, 0.114 mmol) in THF (1 mL) was added, and the reaction mixture was stirred at RT for 1 h. The reaction was quenched with H_2O, diluted with EtOAc (100 mL), and extracted with 1 N HCl solution (50 mL) and brine (100 mL). The organic layer was collected, dried over $MgSO_4$, concentrated, and purified by chromatography on silica gel (solvent gradient from 0% to 100% EtOAc in Hex). The isolated product was dissolved in EtOH (3 mL), 10% Pd/C (5 mg) was added, and the reaction mixture was stirred under an atmosphere of H_2 for 1 h. The reaction mixture was filtered through Celite and washed with MeOH. The filtrate was concentrated to isolate the product. The isolated product was redissolved in DCM (3 mL) and TMSBr (150 μL, 0.127 mmol) was added dropwise. The reaction mixture was stirred at RT overnight. Subsequently, MeOH (2 mL) was added to the reaction mixture, and stirring was continued for an additional 1 h. The solvent was evaporated under vacuum, and the residue was redissolved in MeOH and triturated with DCM to precipitate the final product. After filtration, compound 9 was isolated as white solid (45% overall yield for the three steps). ^{1}H NMR (500 MHz, D_2O, 5% ND_4OD) δ 8.50 (s, 1H), 7.63 (s, 1H), 7.30 (d, J = 8.6 Hz, 2H), 6.89 (d, J = 8.6 Hz, 2H), 3.07−3.12 (m, 1H), 2.15 (s, 3H), 1.60−1.80 (m, 2H). ^{13}C NMR (125 MHz, D_2O, 5% ND_4OD) δ 166.46, 165.63, 150.84, 144.05, 139.43, 130.99, 129.17, 128.89, 125.61, 114.32, 30.81, 28.93 (d, J = 129.6 Hz), 20.36. ^{31}P NMR (162 MHz, D_2O, 5% ND_4OD) δ 19.53. HRMS (ESI−) m/z 333.0541 calculated for $C_{15}H_{14}N_2O_3PS$; found m/z 333.0473 $[M - H]^-$.

2-((6-(p-Tolyl)thieno[2,3-d]pyrimidin-4-yl)amino)acetic Acid (10). The compound was isolated as a white solid (13.8 mg, 60% yield). ^{1}H NMR (500 MHz, DMSO-d_6) δ 8.34 (s, 1H), 7.99 (s, 1H), 7.58 (d, J = 8.1 Hz, 2H), 7.32 (d, J = 8.1 Hz, 2H), 5.76 (s, 1H), 4.18 (d, J = 4.7 Hz, 2H), 2.35 (s, 3H). ^{13}C NMR (75 MHz, DMSO-d_6) δ 171.5, 164.8, 156.5, 153.6, 138.8, 138.3, 130.4, 130.0, 125.6, 117.7, 114.4, 55.0, 20.8. HRMS (ESI−) m/z 298.0656 calculated for $C_{15}H_{12}N_3O_2S$; found m/z 298.0654 $[M - H]^-$.

(((6-(3-Chloro-4-methylphenyl)thieno[2,3-d]pyrimidin-4-yl)-amino)methyl)phosphonic Acid (11). Compound 11 was isolated as a pale-yellow powder (8.5 mg, 25% overall isolated yield for the last two steps). ^{1}H NMR (400 MHz, D_2O, 5% ND_4OD) δ 8.05 (s, 1H), 7.42 (s, 1H), 7.28 (s, 1H), 7.23 (d, J = 8.0 Hz, 1H), 7.05 (d, J = 8.0 Hz, 1H), 3.44 (d, J = 13.2 Hz, 2H), 2.19 (s, 3H). ^{13}C NMR (126 MHz, D_2O, 5% ND_4OD) δ 162.6, 156.4, 152.5, 138.2, 136.0, 134.0, 131.5, 131.0, 125.0, 123.5, 118.0, 114.2, 40.3 (d, J = 134 Hz), 19.0. ^{31}P NMR (202 MHz, D_2O, 5% ND_4OD): δ 13.67. HRMS (ESI−) m/z 368.0031 calculated for $C_{14}H_{12}ClN_3O_3PS$; found m/z 368.0030 $[M - H]^-$.

(((6-(3-Chloro-4-methylphenyl)thieno[2,3-d]pyrimidin-4-yl)-amino)(phenyl)methyl)phosphonic Acid (12). Compound 12 was isolated as a white solid (20.8 mg, 48% yield for the last two steps). ^{1}H NMR (500 MHz, D_2O, 5% ND_4OD) δ 7.77 (s, 1H), 7.49 (d, J = 7.7 Hz, 3H), 7.35 (t, J = 7.2 Hz, 2H), 7.25, −7.22 (m, 1H), 7.05 (s, 1H), 6.79 (s, 1H), 6.27 (d, J = 7.2 Hz, 1H), 5.00 (d, J = 19.7 Hz, 1H), 1.75 (s, 3H). ^{13}C NMR (126 MHz, D_2O, 5% ND_4OD) δ 162.8, 155.8, 152.2, 140.9, 138.4, 135.6, 131.2, 128.1, 127.8, 126.6, 124.8, 123.2, 118.1, 114.0, 110.0, 55.5 (d, J = 134 Hz), 18.6. ^{31}P NMR (81 MHz, D_2O, 5% ND_4OD) δ 13.84. HRMS (ESI−) m/z 444.0344 calculated for $C_{20}H_{16}ClN_3O_3PS$; found m/z 444.0352 $[M - H]^-$.

6-Bromo-4-chlorothieno[2,3-d]pyrimidine (14). Thieno[2,3-d]-pyrimidin-4(3H)-one (13) was prepared from 2,5-dihydroxy-1,4-dithiane as previously reported,[16] with the exception that all reactions were carried out under thermal conditions. Conversion of intermediate 13 to 14 was achieved by successive reaction of 13 with Br_2 and $POCl_3$ as previously reported.[30] The 6-bromothieno[2,3-d]pyrimidin-4(3H)-one intermediate was obtained as a light-brown solid in 63% yield. The ^{1}H NMR data was consistent with the literature: ^{1}H NMR (300 MHz, DMSO-d_6) δ 12.64 (bs, 1H), 8.15 (s, 1H), 7.56 (s, 1H)]. The 6-bromo-4-chlorothieno[2,3-d]pyrimidine (14) was obtained as a yellow solid in 58% yield. The ^{1}H NMR data was also consistent with the literature: ^{1}H NMR (500 MHz, $CDCl_3$) δ 8.81 (s, 1H), 7.48 (s, 1H)].

6-(p-Tolyl)thieno[2,3-d]pyrimidine-4-carbaldehyde (15). Step f (Scheme 1). The common building block 4-chloro-6-(p-tolyl)thieno-[2,3-d]pyrimidine (50 mg, 0.19 mmol, 1 equiv) was mixed with potassium vinyltrifluoroborate (28 mg, 0.21 mmol, 1.1 equiv) and $PdCl_2(dppf)CH_2Cl_2$ (8 mg, 0.01 mmol, 0.05 equiv) and purged with argon. i-PrOH/H_2O (2 mL, 2/1 ratio) and Et_3N (58 mg, 0.58 mmol, 3 equiv) were added, and the mixture was purged again with argon. The mixture was sealed in pressure vessel and was heated at 100 °C for 1 h. The reaction mixture was cooled to RT, then filtered through Celite, washed with EtOAc, concentrated, and purified by chromatography (100% Hex to 20% EtOAc in Hex) on silica gel to give the C-4 vinyl intermediate 6-(p-tolyl)-4-vinylthieno[2,3-d]pyrimidine as yellow solid (35 mg; 72% yield). The ^{1}H NMR and MS were consistent with the desired product. ^{1}H NMR ($CDCl_3$): δ 2.40 (s, 3H, $-CH_3$), 5.85 (d, J = 10.70 Hz, 1 H), 6.77 (d, J = 10.70 Hz), 7.16−7.23 (m, 1H), 7.26 (d, J = 8.10 Hz, 2H), 7.57 (s, 1H), 7.60 (d, J = 8.10 Hz, 2H), 8.97 (s, 1H).

MS (ESI+) m/z 255.1 $[M + H]^+$ for $C_{15}H_{14}N_2S$.

Step g (Scheme 1). To a solution of the above 4-vinyl-thienopyrimidine (50 mg, 0.2 mmol) in acetone:H_2O (4 mL; 10:1 ratio), 2,6-lutidine (42 mg, 0.4 mmol, 2 equiv), 4-methylmorpholine-N-oxide (35 mg, 0.3 mmol, 1.5 equiv), and osmium tetroxide (0.1 mL of a 40.4 mM solution in toluene) were added. The mixture was stirred for 2 h at RT (at which point LCMS indicated complete conversion to the desirable diol). Then, 1 mL of H_2O was added followed by $NaIO_4$ in small portions, and the mixture was stirred at RT for 1 h. The reaction was quenched with saturated aqueous solution of sodium thiosulfate (10 mL), and the mixture was extracted with ethyl acetate (3 × 15 mL), washed with saturated aqueous solution of ammonium chloride, dried over anhydrous $MgSO_4$, and concentrated under vacuum. The crude residue was purified by flash column chromatography on silica gel eluted with hexane−ethyl acetate (7:1) to give the aldehyde 15 as a yellow solid (32 mg, 64% yield). ^{1}H NMR ($CDCl_3$) δ: 2.43 (s, 3H), 7.30 (d, J = 8.00 Hz, 2H), 7.70 (d, J = 8.10 Hz, 2H), 8.31 (s, 1H), 9.24 (s, 1H), 10.25 (s, 1H). ^{13}C NMR (125 MHz, $CDCl_3$) δ 194.20, 171.65, 152.77, 150.54, 149.08, 140.65, 129.98, 129.81, 128.84, 127.01, 114.19, 21.40. MS (ESI+) m/z 255.12 $[M + H]^+$ for $C_{14}H_{11}N_2OS$.

Diethyl (Amino(phenyl)methyl)phosphonate (16b). In a round-bottom flask, benzaldehyde (742.79 mg, 7.00 mmol, 1 equiv) was mixed with magnesium perchlorate (156.23 mg, 0.7 mmol, 0.1 equiv) for 15 min. Benzylamine (750 mg, 7.00 mmol, 1 equiv) and diethylphosphite (0.939 mL, 7.28 mmol, 1.04 equiv) were added, and the reaction mixture was heated at 85 °C for 24 h. The crude product was dried under vacuum and purified by column chromatography on silica gel to give the diethyl ((benzylamino)-(phenyl)methyl) phosphonate product as a slightly yellow oil in 81% yield (1.8 g). ^{1}H NMR (300 MHz, $CDCl_3$) 7.43−7.28 (m, 10H), 4.15−3.80 (m, 7H), δ 3.56 (d, J = 13.3 Hz, 1H), 2.12 (s, 1H), 1.29 (t, J = 7.0 Hz, 3H), 1.14 (t, J = 7.0 Hz, 3H).[31] Hydrogenation of the diethyl ((benzylamino)(phenyl)methyl)phosphonate intermediate (200 mg, 0.6 mmol) in 4.4% formic acid in methanol (6 mL) using Pearlman's catalyst (84.25 mg, 0.6 mmol, 0.2 equiv) under argon for 2 h gave the desired crude product,[32] which was purified by column chromatography on silica gel to give the free amine as a transparent oil (145.9 mg, quantitative yield). ^{1}H NMR (500 MHz, $CDCl_3$) δ 7.45 (d, J = 7.7

dx.doi.org/10.1021/jm500629e | J. Med. Chem. 2014, 57, 5764−5776

Hz, 2H), 7.35 (t, J = 7.7 Hz, 2H), 7.30 (dd, J = 7.3, 2.0 Hz, 1H), 4.26 (d, J = 17.1 Hz, 1H),4.08−402 (m, 2H), 4.02−3.94 (m, 1H), 3.90− 3.84 (m, 1H), 1.92 (br s, 2H), 1.27 (t, J = 7.0 Hz, 3H), 1.18 (t, J = 7.0 Hz, 3H).

Diethyl (((6-Bromothieno[2,3-d]pyrimidin-4-yl)amino)methyl)-phosphonate (17a; R_2 = H). The product was isolated as yellow solid (884 mg, 50% yield). ^{1}H NMR (400 MHz, CD_3OD): δ 8.36 (s, 1H), 7.56 (s, 1H), 4.20−4.12 (m, 6H), 1.28 (t, J = 7.1 Hz, 6H). ^{13}C NMR (75 MHz, CD_3OD): δ 167.7, 157.0 (d, J = 1.7 Hz), 154.8, 122.8, 118.8, 112.7, 64.1 (d, J = 6.7 Hz), 36.7 (d, J = 158 Hz), 16.7 (d, J = 5.9 Hz). ^{31}P NMR (81 MHz, CD_3OD): δ 23.91. MS (ESI+) m/z 380.10 $[M + H]^+$ for $C_{11}H_{15}BrN_3O_3PS$.

Diethyl (((6-Bromothieno[2,3-d]pyrimidin-4-yl)amino)(phenyl)-methyl)phosphonate (17b; R_2 = Ph). The product was isolated as a white solid (51 mg, 36% yield). ^{1}H NMR (300 MHz, $CDCl_3$) δ 8.42 (s, 1H), 8.11−8.07 (m, 1H), 7.70−7.67 (m, 3H), 7.27−7.22 (m, 2H), 6.32 (dd, J = 22.4, 9.6 Hz, 1H), 4.31−4.07 (m, 3H), 3.93−3.84 (m, 1H), 1.28−1.19 (s, 6H). ^{13}C NMR (75 MHz, $CDCl_3$) δ 167.7, 155.0 (d, J = 9 Hz), 153.7, 128.49 (d, J = 2 Hz), 128.44 (d, J = 2 Hz), 127.99 (d, J = 3 Hz), 121.7, 117.8, 111.3, 63.5 (d, J = 7 Hz), 50.79 (d, J = 156 Hz), 16.3 (dd, J = 19, 6 Hz). MS (ESI+) m/z 456.14 $[M + H]^+$ for $C_{17}H_{21}BrN_3O_3PS$

Diethyl (((6-(p-Tolyl)thieno[2,3-d]pyrimidin-4-yl)amino)methyl)-phosphonate (18a; R_2 = R_3 = H). The product was isolated as a white solid (25.5 mg, 65% yields). ^{1}H NMR (500 MHz, CD_3OD): δ 8.35 (s, 1H), 7.68 (s, 1H), 7.56 (d, J = 8.1 Hz, 2H), 7.25 (d, J = 8.1 Hz, 2H), 4.20−4.14 (m, 6H), 2.36 (s, 3H), 1.29 (t, J = 7.1 Hz, 6H). ^{13}C NMR (126 MHz, CD_3OD): δ 164.4, 156.4, 152.8, 140.8, 138.8, 130.5, 129.4, 125.6, 118.2, 112.7, 62.7 (d, J = 6.7 Hz), 35.3 (d, J = 158.1 Hz), 19.8, 15.3 (d, J = 5.9 Hz). ^{31}P NMR (81 MHz, CD_3OD): δ 25.16. MS (ESI+) m/z 391.9 $[M + H]^+$ for $C_{18}H_{23}N_3O_3PS$.

Diethyl (((6-(3-Chloro-4-methylphenyl)thieno[2,3-d]pyrimidin-4-yl)amino)methyl)phosphonate (18b; R_2 = H, R_3 = Cl). The product was isolated as a pale-orange solid (9.6 mg, 29% yield). ^{1}H NMR (500 MHz, CD_3OD) δ 8.38 (s, 1H), 7.76 (s, 1H), 7.39 (t, J = 9.4 Hz, 2H), 7.32 (t, J = 7.9 Hz, 1H), 4.21−4.14 (m, 6H), 2.30 (s, 3H), 1.29 (t, J = 7.1 Hz, 6H). ^{31}P NMR (202 MHz, CD_3OD) δ 23.67. MS (ESI+) m/z 426.3 $[M + H]^+$ for $C_{18}H_{22}ClN_3O_3PS$.

Diethyl (((6-(3-Chloro-4-methylphenyl)thieno[2,3-d]pyrimidin-4-yl)amino)(phenyl)methyl)phosphonate (18c; R_2 = Ph, R_3 = Cl). The product was isolated as a pale-yellow solid (27.2 mg, 60% yield). ^{1}H NMR (400 MHz, $CDCl_3$) δ 8.46 (s, 1H), 7.74 (s, 1H), 7.72 (s, 2H), 7.53 (d, J = 1.6 Hz, 1H), 7.31−7.20 (m, 5H), 6.32 (d, J = 22.0 Hz, 1H), 4.31−4.14 (m, 2H), 4.02−3.93 (m, 1H), 3.78−3.68 (m, 1H), 2.39 (s, 3H), 1.23 (t, J = 7.0 Hz, 3H), 1.06 (t, J = 7.0 Hz, 3H). ^{13}C NMR (75 MHz, $CDCl_3$) δ 166.4, 155.9 (d, J = 9 Hz), 153.6, 138.9, 136.3, 135.5, 134.9, 133.0, 131.3, 128.6, 128.6, 128.1 (d, J = 3 Hz), 126.6, 124.6, 118.3, 114.3, 63.5 (d, J = 7 Hz), 51.8 (d, J = 155 Hz), 49.8, 19.9, 16.4 (d, J = 6 Hz), 16.0 (d, J = 6 Hz). ^{31}P NMR (81 MHz, $CDCl_3$) δ 21.64. MS (ESI+) m/z 502.25 $[M + H]^+$ for $C_{24}H_{26}ClN_3O_3PS$.

In Vitro Inhibition Assays. In vitro enzymatic assays were carried out using method 2 (M2) as previously described.[12d]

Differential Scanning Fluorimetry Studies. DSF studies were carried out using the general conditions previously described.[1c] Samples were prepared to a final volume of 25 μL containing 4 μM hFPPS protein, 10 mM HEPES (pH 7.5), 10 mM NaCl, with or without 5 mM $MgCl_2$, and 5× SYPRO Orange dye (diluted from commercial stock solution of 5000×; Invitrogen). All samples were prepared in triplicate. Fluorescence was measured using an iCycler RT-PCR instrument with an iQ5 detector (Bio-Rad) while increasing the temperature gradient from 30 to 90 °C in increments of 0.5 °C/10 s. The midpoint temperature of the unfolding protein transition (T_m) was calculated using the software package from Bio-Rad iQ5. The inhibitor and substrate concentrations for each experiment are indicated in the figures.

Isothermal Titration Calorimetry (ITC) Studies. ITC experiments were carried out at 30 °C with a MicroCal iTC_{200} system from GE Healthcare. The protein and ligand solutions were prepared in the same buffer (10 mM HEPES (pH 7.5), 500 mM $NaCl_2$, 2 mM β-mercaptoethanol, and 5% glycerol) at 50 μM and 1 mM concentrations, respectively. Each experiment consisted of a first 1 μL injection of the ligand followed by 18 2 μL injections into the cell containing 200 μL of the protein sample. Heats of dilution were measured in control titrations and subtracted from the actual data. The data were analyzed with the Origin 7 software provided with the instrument.

Evaluation of Competitive Binding by ^{1}H Line Broadening NMR. Spectra were acquired on a 500 MHz Varian INOVA instrument, with a HCN cold probe and z-axis pulsed-field gradients, at the Quebec/Eastern Canada High Field NMR Facility. ^{1}H NMR spectra were acquired with a 1D presaturation sequence, with a sweep width of 8000 Hz and an acquisition time of 1 s. A low power saturation pulse was applied at the HOD frequency during the 3 s relaxation delay. A 5 mm NMR tube was charged with 540 μL of D_2O and 6 μL of an inhibitor (10 mM stock solution in H_2O), and the tube was briefly mixed using a vortex. The ^{1}H NMR spectrum was acquired and the water-suppression parameters were determined (presatura-tion). Buffer solution (60 μL) was added to the NMR tube and briefly mixed for a final inhibitor concentration of 100 μM in buffer containing 50 mM Tris buffer at pH 7.7, 2 mM $MgCl_2$, 0.5 mM TCEP, and 20 μg/mL BSA. The ^{1}H NMR spectrum was acquired of the free inhibitor. Aliquots of the hFPPS solution in buffer (containing 22.63 μg/μL protein, 50 mM Tris at pH 7.7, 500 mM NaCl, 5% glycerol, and 0.5 mM TCEP) were added, followed by gentle mixing, to bring the inhibitor to hFPPS ratio as indicated on each Figure. Finally, a second inhibitor or IPP (purchased from Isoprenoids, LC, as its ammonium salt; 40 mM solution was prepared in 0.5 mM Tris buffer at pH 7.7) was added in incremental amounts to obtain the indicated ratios and confirm whether binding of the two inhibitors was competitive or not (usually titration with the second inhibitor was continued until the resonances of the first inhibitor were restored, or up to the molar ratio of hFPPS: inhibitor A; inhibitor B indicated on the NMR spectra).

Co-crystallization of hFPPS with Inhibitors 6a and 7 in the Absence of Magnesium Ions. Compounds 6a and 7 were prepared as 100 and 25 mM stock solutions in 100 mM TrisHCl (pH 7.5) buffer, respectively. Each stock solution was added to the purified hFPPS sample to give the final concentrations of 5 mM inhibitor and 0.25 mM protein. A microseeding technique was employed to obtain crystals suitable for X-ray diffraction analysis. Crystals were grown at 22 °C by vapor diffusion in sitting drops composed of 1 μL of protein/ inhibitor mixture and 1 μL of crystallization buffer, and an additional 0.5 μL of seed solution when added. Seed solutions were prepared with Seed Bead kits (Hampton Research). For the hFPPS/6a$^{(allo)}$ complex, the initial crystals formed in a crystallization solution composed of 0.1 M TrisHCl (pH 8.5) and 2 M ammonium dihydrogen phosphate. Diffraction quality crystals were obtained in a seeding optimization trial with a new crystallization buffer composed of 0.085 M HEPES (pH 7.5), 17% (w/v) PEG 10K, 6.8% (v/v) ethylene glycol, and 15% (v/v) glycerol. For the hFPPS/7 complex, a single crystal was obtained under the same condition, but with microseeds prepared from the hFPPS/6a crystals.

X-ray Data Collection, Processing, and Structure Refinement. For structure determination, diffraction data were collected from single crystals at 100 K with synchrotron radiation (Canadian Light Source, Saskatoon, SK) and a Rayonix MX300 CCD detector. The data were processed with the xia2 package.[33] The initial structure models were built by difference Fourier methods with a ligand/ solvent-omitted input model generated from the PDB entry 2F7M. The models were improved through iterative rounds of manual and automated refinement with COOT[34] and REFMAC5.[35] The final models were deposited into the Protein Data Bank. To measure the anomalous signal from the phosphorus and sulfur atoms in the hFPPS/6a$^{(allo)}$ complex, additional data were collected from a single crystal at 100 K with a MicroMax-007 HF generator (Rigaku) and a Saturn 944+ CCD detector (Rigaku). This data set was also processed with the xia2 package but without merging the Friedel mates. An anomalous density map was calculated from the processed data with the programs SHELXC[36] and ANODE.[37] Data collection and

dx.doi.org/10.1021/jm500629e | J. Med. Chem. 2014, 57, 5764−5776

Table 3. Data Collection and Refinement Statistics

	data set 1 (synchrotron) inhibitor 6a, Pi	data set 2 (home source) inhibitor 6a, Pi	data set 3 (synchrotron) inhibitor 7, Pi
PDB ID	4LPG		4LPH
	Data Collection		
wavelength (Å)	0.979 49	1.5418	0.979 49
space group	$P4_12_12$	$P4_12_12$	$P4_12_12$
unit cell (Å)	a = b = 110.87, c = 77.03	a =b = 110.96, c = 76.97	a = b = 111.12, c = 77.19
resolution (Å)[a]	49.58−2.35 (2.41−2.35)	39.23−2.61 (2.67−2.61)	55.06−2.30 (2.36−2.30)
redundancy	14.4 (14.4)	7.2 (4.7)	9.4 (9.5)
completeness (%)	99.7 (98.0)	98.7 (99.0)	98.4 (99.1)
$I/\sigma(I)$	36.7 (5.4)	39.3 (5.5)	22.3 (4.8)
R_{merge}	0.044 (0.527)		0.055 (0.411)
	Refinement		
no. reflections	19406		20290
no. protein atoms	2666		2700
no. ligand atoms	31		27
no. solvent atoms	40		50
R_{work}/R_{free}	0.182/0.230		0.183/0.226
average B factor (Å^2)			
protein atoms	73.9		78.9
ligand atoms	80.4		93.4
rms deviations			
bond length (Å)	0.016		0.017
bond angle (deg)	1.8		1.8

[a]Values in parentheses are for the highest resolution shell.

refinement statistics, as well as the PDB IDs for the structure models, are presented in Table 3.

Studies on Genetic Associations. Using a cohort of 751 pairs of Alzheimer and age-matched control French Canadian subjects from a population isolate from eastern Canada, we performed the mapping of some 535000 polymorphisms in each of our case and control subjects using the Illumina 550k Human Quad genomic beadchip according to methodology reported previously.[38] Five single nucleotide polymorphisms (SNPs) were examined in the human FPPS gene loci. A specific genetic associations between variant rs4971072 (A/G) in the promoter area of hFPPS and Tau protein levels ($p < 0.02$) in the cortical area was found to be significantly associated with phospho-tau concentrations ($p < 0.02$) in the same brain region in the AD cohort.

Analysis of mRNA Prevalence. A subset of AD ($n = 34$) and age-matched control brains ($n = 24$) were used to quantify the mRNA prevalence of hFPPS using real time quantitative polymerase chain reaction (QrtPCR) as adapted from our previous studies.[28]

Total Tau Protein and Phospho-Tau Levels in the Alzheimer's Brain and in Response to hFPPS Inhibitors. Frontal cortex brain samples from autopsy-confirmed cases of Alzheimer's disease and age-matched control subjects were obtained from the Douglas Institute Brain Bank, Montreal, Canada. Frozen brain samples ($n = 116$) were homogenized and prepared according to a previously established protocol[27] prior to ELISA quantification for total cortical tau protein and phospho-tau levels. Human neuroblastoma cell cultures (SH-Sy5y from the ATCC collection) were used to assay the effects of our newly developed hFPPS inhibitors on tau metabolism and general toxicity. Typically, cells were grown in serum condition for 5 days and then exposed to different concentrations (1−500 nM) of our inhibitors for a period of 24 h. Cell were washed and lysed prior to tau and phospho-tau ELISA quantification. Total tau (T-Tau) and phospho-tau (P-Tau) concentrations were measured using a commercial enzyme immunoassay (Innotest Inc., Ghent, Belgium). In this assay, the wells of polystyrene microtiter plates were coated with the solid phase anti-human tau monoclonal antibody (AT120 for tau and AT270 for phospho-tau). The test samples were incubated in these wells along with two separate biotinylated tau monoclonal antibodies (H57 and BT2) that recognize different tau and P-Tau epitopes. Samples were rinsed with an assay buffer and then incubated with peroxidase-labeled streptavidin. Samples were subsequently incubated with tetramethyl-benzidine and 0.006% hydrogen peroxide per manufacturer's instructions. The reaction was stopped with diluted sulfuric acid and optical density measurements read using a Molecular Devices Spectramax Plus plate reader. Intra-assay and interassay variability measures were 5.1% and 9.1%, consistent with manufacturer recommendation.

Lactate Dehydrogenase Assay (LDH). Lactate dehydrogenase activity was measured using a commercial kit. Maximum toxicity was based on % lactic acid dehydrogenase activity observed in the medium of cells treated with an hFPPS inhibitor as compared to the control (untreated cells); activity observed in the untreated control cells was set to 0%.

ASSOCIATED CONTENT

* Supporting Information

NMR spectra and homogeneity data for inhibitors 7−12. ^{1}H NMR competition studies and X-ray data. Genetic analysis on hFPPS polymorphisms. This material is available free of charge via the Internet at http://pubs.acs.org.

Accession Codes

The following codes have been deposited in the Protein Data Bank: 4LPG (hFPPS/6a/Pi complex) and 4LPH (hFPPS/7/Pi complex).

AUTHOR INFORMATION

Corresponding Author

*Phone 514-398-3638. Fax 514-398-3797. E-mail: Youla.tsantrizos@mcgill.ca.

Author Contributions

#J. W. De Schutter and J. Park contributed equally to the work described in this manuscript.

Notes

The authors declare no competing financial interest.

∇Zheping Hu: Undergraduate Research Participant.

ACKNOWLEDGMENTS

We thank Dr. Alexios Matralis for contributing to the synthesis of some key building blocks. ^{1}H NMR experiments were acquired on a 500 MHz NMR instrument at the Quebec/Eastern Canada High Field NMR Facility, supported by the Natural Sciences and Engineering Research Council of Canada (NSERC), the Canada Foundation for Innovation (CFI), the Quebec Ministere de la Recherche en Science et Technologie (FQRNT), and McGill University. Financial support for this work was provided by NSERC and FQRNT (research grants to Y. S. Tsantrizos) and the Canadian Institute of Health Research (CIHR; research grants to A. M. Berghuis, J. Poirier, and Y. S. Tsantrizos).

ABBREVIATIONS USED

hFPPS, human farnesyl pyrophosphate synthase; hGGPPS, human geranylgeranyl pyrophosphate synthase; hSQS, human squalene synthase; DMAPP, dimethylallyl pyrophosphate; IPP, isopentenyl pyrophosphate; GPP, geranyl pyrophosphate; N-BPs, nitrogen-containing bisphosphonates; GTPases, small guanine triphosphate binding proteins; IFNγ, interferon-gamma; SAR, structure−activity relationship; DSF, differential scanning fluorimetry; AD, Alzheimer's disease; P-Tau, phosphorylated tau; phospho-tau, phosphorylated tau; T-Tau, total tau protein; LDH, lactate dehydrogenase

REFERENCES

(1) (a) Rondeau, J.-M.; Bitsch, F.; Bourgier, E.; Geiser, M.; Hemmig, R.; Kroemer, M.; Lehmann, S.; Ramage, P.; Rieffel, S.; Strauss, A.; Green, J. R.; Jahnke, W. Structural basis for the exceptional in vivo efficacy of bisphosphonate drugs. ChemMedChem 2006, 1, 267−273. (b) Kavanagh, K. L.; Guo, K.; Dunford, J. E.; Wu, X.; Knapp, S.; Ebetino, F. H.; Rogers, M. J.; Russell, R. G. G.; Oppermann, U. The molecular mechanism of nitrogen-containing bisphosphonates as antiosteoporosis drugs. Proc. Natl. Acad. Sci. U. S. A. 2006, 103, 7829−7834. (c) Park, J.; Lin, Y.-S.; Tsantrizos, Y. S.; Berghuis, A. M. Ternary complex structures of human farnesyl pyrophosphate synthase bound with a novel inhibitor and secondary ligands provide insights into the molecular details of the enzyme's active site closure. BMC Struct. Biol. 2012, 12, 32.

(2) (a) Skerjanec, A.; Berenson, J.; Hsu, C.; Major, P.; Miller, W. H., Jr.; Ravera, C.; Schran, H.; Seaman, J.; Waldmeier, F. The pharmacokinetics and pharmacodynamics of zoledronic acid in cancer patients with varying degrees of renal function. J. Clin. Pharmacol. 2003, 43, 154−162. (b) Weiss, H. M.; Pfaar, U.; Schweitzer, A.; Wiegand, H.; Skerjanec, A.; Schran, H. Biodistribution and plasma protein binding of zoledronic acid. Drug Metab. Dispos. 2008, 36, 2043−2049.

(3) Morgan, G. J.; Davies, F. E.; Gregory, W. M.; Cocks, K.; Bell, S. E.; Szubert, A. J.; Navarro-Coy, N.; Drayson, M. T.; Owen, R. G.; Feyler, S.; Ashcroft, A. J.; Ross, F.; Byrne, J.; Roddie, H.; Rudin, C.; Cook, G.; Jackson, G. H.; Child, J. A. First-line treatment with zoledronic acid as compared with clodronic acid in multiple myeloma (MRC Myeloma IX): a randomized controlled trial. Lancet 2010, 376, 1989−1999.

(4) Nguyen, U. T. T.; Guo, Z.; Delon, C.; Wu, Y.; Deraeve, C.; Franzel, B.; Bon, R. S.; Blankenfeldt, W.; Goody, R. S.; Waldmann, H.; Wolters, D.; Alexandrov, K. Analysis of the eukaryotic prenylome by isoprenoid affinity tagging. Nature Chem. Biol. 2009, 5, 227−235.

(5) Hottman, D. A.; Li, L. Protein prenylation and synaptic plasticity: implications for Alzheimer's diseases. Mol. Neurobiol. 2014, DOI 10.1007/s12035-013-8627-z.

(6) (a) Morgan, G. J.; Davies, F. E.; Gregory, W. M.; Szubert, A. J.; Bell, S. E.; Drayson, M. T.; Owen, R. G.; Ashcroft, A. J.; Jackson, G. H.; Child, J. A. Effects of induction and maintenance plus long-term bisphosphonates on bone disease in patients with multiple myeloma: the Medical Research Council Myeloma IX Trial. Blood 2012, 119, 5374−5383. (b) Gnant, M.; Mlineritsch, B.; Schippinger, W.; Luschin-Ebengreuth, G.; Postlberger, S.; Menzel, C.; Jakesz, R.; Seifert, M.; Hubalek, M.; Bjelic-Radisic, V.; Samonigg, H.; Tausch, C.; Eidtmann, H.; Steger, G.; Kwasny, W.; Dubsky, P.; Fridrik, M.; Fitzal, F.; Stierer, M.; Rucklinger, E.; Greil, R. Endocrine therapy plus zoledronic acid in premenopaisal breast cancer. New Engl. J. Med. 2009, 360, 679−691. (c) Coleman, R. E.; Marshall, H.; Cameron, D.; Dodwell, D.; Burkinshaw, R.; Keane, M.; Gil, M.; Houston, S. J.; Grieve, R. J.; Barrett-Lee, P. J.; Ritchie, D.; Pugh, J.; Gaunt, C.; Rea, U.; Peterson, J.; Davies, C.; Hiley, V.; Gregory, W.; Bell, R. Breast-cancer adjuvant therapy with zoledronic Acid. New Engl. J. Med. 2011, 365, 1396− 1405.

(7) Morita, C. T.; Jin, C.; Sarikonda, G.; Wang, H. Nonpeptide antigens, presentation mechanisms, and immunological memory of human Vγ2Vδ2 T cells: discriminating friends from foe through the recognition of prenyl pyrophosphate antigens. Immunol. Rev. 2007, 215, 59−76.

(8) (a) Eckert, G. P.; Hooff, G. P.; Strandjord, D. M.; Igbavboa, U.; Volmer, D. A.; Muller, W. E.; Wood, W. G. Regulation of the brain isoprenoids farnesyl- and geranylgeranylpyrophosphate is altered in male Alzheimer patients. Neurobiol. Dis. 2009, 35, 251−257. (b) Hooff, G. P.; Wood, W. G.; Muller, W. E.; Eckert, G. P. Isoprenoids, small GTPases and Alzheimer's diseases. Biochim. Biophys. Acta 2010, 1801, 896−905.

(9) Jahnke, W.; Rondeau, J.-M.; Cotesta, S.; Marzinzik, A.; Pelle, X.; Geiser, M.; Strauss, A.; Gotte, M.; Bitsch, F.; Hemmig, R.; Henry, C.; Lehmann, S.; Glickman, J. F.; Roddy, T. P.; Stout, S. J.; Green, J. R. Allosteric non-bisphosphonate FPPS inhibitors identified by fragment-based discovery. Nature Chem. Biol. 2010, 6, 660−666.

(10) Lindert, S.; Zhu, W.; Liu, Y.-L.; Pang, R.; Oldfield, E.; McCammon, J. A. Farnesyl diphosphate synthase inhibitors from in silico screening. Chem. Biol. Drug Des. 2013, 81, 742−748.

(11) Gabelli, S. B.; McLellan, J. S.; Montalvetti, A.; Oldfield, E.; Docampo, R.; Amzel, L. M. Structure and mechanism of the farnesyl diphosphate synthase from Trypanosoma cruzi: implications for drug design. Protein 2006, 62, 80−88.

(12) (a) Lin, Y.-S.; Park, J.; De Schutter, J. W.; Huang, X. F.; Berghuis, A. M.; Sebag, M.; Tsantrizos, Y. S. Design and synthesis of active site inhibitors of the human farnesyl pyrophosphate synthase apoptosis and inhibition of ERK phosphorylation in multiple myeloma cells. J. Med. Chem. 2012, 55, 3201. (b) De Schutter, J. W.; Shaw, J.; Lin, Y.-S.; Tsantrizos, Y. S. Design of potent bisphosphonate inhibitors of the human farnesyl pyrophosphate synthase via targeted interactions with the active site "capping" phenyls. Bioorg. Med. Chem. 2012, 20, 5583−5591. (c) Leung, C.-Y.; Langille, A. M.; Mancuso, J.; Tsantrizos, Y. S. Discovery of thienopyrimidine-based inhibitors of the human farnesyl pyrophosphate synthase parallel synthesis of analogs via a thrimethylsilyl ylidene intermediate. Bioorg. Med. Chem. Lett. 2013, 21, 2229−2240. (d) Leung, C. Y.; Park, J.; De Schutter, J. W.; Sebag, M.; Berghuis, A. M.; Tsantrizos, Y. S. Thienopyrimidine bisphosphonate (ThPBP) inhibitors of the human farnesyl pyrophosphate synthase: optimization and characterization of the mode of inhibition. J. Med. Chem. 2013, 56, 7939−7950.

(13) Zhang, Y.; Cao, R.; Yin, F.; Hudock, M. P.; Guo, R.-T.; Krysiak, K.; Mukherjee, S.; Gao, Y.-G.; Robinson, H.; Song, Y.; No, J. H.; Bergan, K.; Leon, A.; Cass, L.; Goddard, A.; Chang, T.-K.; Lin, F.-Y.; Van Beek, E.; Papapoulos, S.; Wang, A.H.-J.; Kubo, T.; Ochi, M.; Mukkamala, D.; Oldfield, E. Lipophilic bisphosphonates as dual farnesyl/geranylgeranyl diphosphate synthase inhibitors: an X-ray and NMR investigation. J. Am. Chem. Soc. 2009, 131, 5153−5162.

(14) Ciosek, C. P., Jr.; Magnin, D. R.; Harrity, T. W.; Logan, J. V. H.; Dickson, J. K.; Gordon, E. M.; Hamilton, K. A.; Jolibois, K. G.; Kunselman, L. K.; Lawrence, R. M.; Mookhtiar, K. A.; Rich, L. C.; Slusarchyk, D. A.; Sulsky, R. B.; Biller, S. A. Lipophilic 1,1-bisphosphonates are potent squalene synthase inhibitors and orally active cholesterol lowering agents in vivo. J. Biol. Chem. 1993, 268, 24832−24837.

(15) Dunford, J. E.; Kwaasi, A. A.; Rogers, M. J.; Barnett, B. L.; Ebetino, F. H.; Russell, R. G. G.; Oppermann, U.; Kavanagh, K. L. Structure−activity relationship among the nitrogen containing bi-sphosphonates in clinical use and other analogues: time-dependent inhibition of human farnesyl pyrophosphate synthase. J. Med. Chem. 2008, 51, 2187−2195.

(16) Hesse, S.; Perspicace, E.; Kirsch, G. Microwave-assisted synthesis of 2-aminothiophene-3-carboxylic acid derivatives, 3H-thieno[2,3-d]pyrimidin-4-one and 4-chlorothieno[2,3-d]pyrimidine. Tetrahedron Lett. 2007, 48, 5261−5264.

(17) Kalmán, F. K.; Woods, M.; Caravan, P.; Jurek, P.; Spiller, M.; Tircsó, G.; Kiraly, R.; Brücher, E.; Sherry, A. D. Potentiometric and relaxometric properties of a gadolinium-based MRI contrast agent for sensing tissue pH. Inorg. Chem. 2007, 46, 5260−5270.

(18) Yu, W.; Mei, Y.; Kang, Y.; Hua, Z.; Jin, Z. Improved procedure for the oxidative cleavage of olefins by OsO_4-$NaIO_4$. Org. Lett. 2004, 6, 3217−3219.

(19) (a) Waszkuc, W.; Janecki, T.; Bodaiski, R. A Convenient Synthesis of α-Hydroxyaldehydes and Hydroxymethyl Ketones. Synthesis 1984, 1025−1027. (b) Lahrache, H.; Robin, S.; Rousseau, G. Halodephosphorylation of α,β-unsaturated phosphonic acid monoesters. Tetrahedron Lett. 2005, 46, 1635−1637.

(20) Hoffman, A.; Ott, A.; Breteler, M. M. B.; Bots, M. L.; Slooter, A. J. C.; van Harskamp, F.; van Duijn, C. N.; Broeckhoven, C. V.; Grobbee, D. E. Atherosclerosis, apolipoprotein E, and prevalence of dementia and Alzheimer's disease in the Rotterdam Study. Lancet 1997, 349, 151−154.

(21) Marchant, N. L.; Reed, B. R.; Sanossian, N.; Madison, C. M.; Kriger, S.; Dhada, R.; Mack, W. J.; DeCarli, C. The aging brain and cognition-contribution of vascular injury and Aβ to mild cognitive dysfunction. JAMA Neurol. 2013, 70, 488−495.

(22) (a) Jick, H.; Zornberg, G. L.; Jick, S. S.; Seshadri, S.; Drachman, D. A. Statins and the risk of dementia. Lancet 2000, 356, 1627−1631.

(b) Wolozin, B.; Wang, S. W.; Li, N. C.; Lee, A.; Lee, T. A.; Kazis, L. E. Simvastatin is associated with a reduced incidence of dementia and Parkinson's diseases. BMC Med. 2007, 5, 20.

(23) Riekse, R. G.; Li, G.; Petrie, E. C.; Leverenz, J. B.; Vavrek, D.; Vuletic, S.; Albers, J. J.; Montine, T. J.; Lee, V. M.; Lee, M.; Seubert, P.; Galasko, D.; Schellenberg, G. D.; Hazzard, W. R.; Peskind, E. R. Effect of statins on Alzheimer's disease biomarkers in cerebrospinal fluid. J. Alzheimer's Dis. 2006, 10, 399−406.

(24) Li, G.; Larson, E. B.; Sonnen, J. A.; Shofer, J. B.; Petrie, E. C.; Schantz, A.; Peskind, E. R.; Raskind, M. A.; Breitner, J. C. S.; Montine, T. J. Statin therapy is associated with reduced neuropathologic changes of Alzheimer disease. Neurology 2007, 69, 878−885.

(25) Hooper, C.; Killick, R.; Lovestone, S. The GSK3 hypothesis of Alzheimer's disease. J. Neurochem. 2008, 104, 1433−1439.

(26) Ballatore, C.; Lee, V.M.-Y.; Trojanowski, J. Q. Tau-mediated neurodegeneration in Alzheimer's diseases and related disorders. Nature Rev. Neurosci. 2007, 8, 663−672.

(27) Beffert, U.; Cohn, J. S.; Petit-Turcotte, C.; Tremblay, M.; Aumont, N.; Ramassamy, C.; Davignon, J.; Poirier, J. Apolipoprotein E and beta-amyloid levels in the hippocampus and frontal cortex of Alzheimer's disease subjects are disease-related and apolipoprotein E genotype dependent. Brain Res. 1999, 843, 87−94.

(28) Leduc, V.; Legault, V.; Dea, D.; Poirier, J. Normalization of gene expression using SYBR green qPCR: a case for paraoxonase 1 and 2 in Alzheimer's disease brains. J. Neurosci. Methods 2011, 200, 14−19.

(29) Mashalidis, E. H.; Sledz, P.; Lang, S.; Abell, C. A three-stage biophysical screening cascade for fragment-based drug discovery. Nature Protoc. 2013, 8, 2309−2324.

(30) Bugge, S.; Kaspersen, S. J.; Sundby, E.; Hoff, B. H. Route selection in the synthesis of C-4 and C-6 substituted thienopyrimidines. Tetrahedron 2012, 68, 9226−9233.

(31) Wu, J.; Sun, W.; Xia, H.-G.; Sun, X. A facile and highly efficient route to a-aminophosphonates via three-component reactions catalyzed by $Mg(ClO_4)_2$ or molecular iodine. Org. Biomol. Chem. 2006, 4, 1663−1666.

(32) Gray, B. D.; Jeffs, P. W. Alkylation and condensation reactions of N,N-dibenzylglycine esters: synthesis of a-amino acid derivatives. J. Chem. Soc., Chem. Commun. 1987, 1329−1330.

(33) Winter, G. xia2: an expert system for macromolecular crystallography data reduction. J. Appl. Crystallogr. 2010, 43, 186−190.

(34) Emsley, P.; Cowtan, K. Coot: model-building tools for molecular graphics. Acta Crystallogr., Sect. D: Biol. Crystallogr. 2004, 60, 2126−2132.

(35) Vagin, A. A.; Steiner, R. A.; Lebedev, A. A.; Potterton, L.; McNicholas, S.; Long, F.; Murshudov, G. N. REFMAC5 dictionary: organization of prior chemical knowledge and guidelines for its use. Acta Crystallogr., Sect. D: Biol. Crystallogr. 2004, 60, 2184−2195.

(36) Sheldrick, G. M. Experimental phasing with SHELXC/D/E: combining chain tracing with density modification. Acta Crystallogr., Sect. D: Biol. Crystallogr. 2010, 66, 479−485.

(37) Thorn, A.; Sheldrick, G. M. ANODE: anomalous and heavy-atom density calculation. J. Appl. Crystallogr. 2011, 44, 1285−1287.

(38) Lambert, J.-C.; Heath, S.; Even, G.; Campion, D.; Sleegers, K.; Hiltunen, M.; Combarros, O.; Zelenika, D.; Bullido, M. J.; Tavernier, B.; Letenneur, L.; Bettens, K.; Berr, C.; Pasquier, F.; Fievet, N.; Barberger-Gateau, P.; Engelborghs, S.; De Deyn, P.; Mateo, I.; Franck, A.; Helisalmi, S.; Porcellini, E.; Hanon, O.; The European Alzheimer's Disease Initiative Investigators; de Pancorbo, M. M.; Lendon, C.; Dufouil, C.; Jaillard, C.; Leveillard, T.; Alvarez, V.; Bosco, P.; Mancuso, M.; Panza, F.; Nacmias, B.; Bossù, P.; Piccardi, P.; Annoni, G.; Seripa, D.; Galimberti, D.; Hannequin, D.; Licastro, F.; Soininen, H.; Ritchie, K.; Blanché, H.; Dartigues, J.-F.; Tzourio, C.; Gut, I.; Van Broeckhoven, C.; Alperovitch, A.; Lathrop, M.; Amouyel, P. Genome-wide association study identifies variants at CLU and CR1 associated with Alzheimer's disease. Nature Genet. 2009, 41, 1094− 1099.

5. CONCLUSION

A library of bisphosphonate inhibitors was synthesized containing the thienopyrimidine core and having signfficantly higher overall lipophilicity as compared to the current clinical drugs targeting hFPPS. *In vitro* inhibition assay against hFPPS showed that our novel thienopymidine-based bisphosphonates (ThPBPs) exhibit low nanomolar activity. Using differential scan fluorimetry, the thienopyrimidine bisphosphonates were found to thermally stabilize hFPPS in the absence of magnesium ions, suggesting the possibility that the ThPBPs can have a dual binding mode, where the second binding site is found outside the allylic sub-pocket. Further biophysical studies including ITC and X-ray crystallography confirmed that the ThPBPs can bind in an allosteric pocket and in the absence of magnesium ions. A new series of non-bisphosphonate thienopyrimidine analogs was designed and synthesized to bind in the allosteric pocket. The thienopyrimidine monophosphonate (ThPMP) analogs were found to be low micromolar inhibitors against hFPPS. NMR binding competition studies and X-ray crystallography confirmed that the ThPMP indeed bind to a catalytically relevant allosteric pocket of hFPPS.